A model membrane approach for interrogating membrane morphological responses induced by membrane-active peptides surfactants

Kim, Min Chul

2017

Kim, M. C. (2017). A model membrane approach for interrogating membrane morphological responses induced by membrane-active peptides surfactants. Doctoral thesis, Nanyang Technological University, Singapore.

http://hdl.handle.net/10356/72878

https://doi.org/10.32657/10356/72878

NANYANG TECHNOLOGICAL UNIVERSITY

A MODEL MEMBRANE APPROACH FOR INTERROGATING MEMBRANE MORPHOLOGICAL RESPONSES INDUCED BY MEMBRANE-ACTIVE PEPTIDES AND SURFACTANTS

KIM MIN CHUL

SCHOOL OF MATERIALS SCIENCE AND ENGINEERING

2017

A MODEL MEMBRANE APPROACH FOR INTERROGATING MEMBRANE MORPHOLOGICAL RESPONSES INDUCED BY MEMBRANE-ACTIVE PEPTIDES AND SURFACTANTS

KIM MIN CHUL

SCHOOL OF MATERIALS SCIENCE AND ENGINEERING

A thesis submitted to the Nanyang Technological University in partial fulfilment of the requirement for the degree of Doctor of Philosophy

2017

Statement of Originality

I hereby certify that the work embodied in this thesis is the result of original research and has not been submitted for a higher degree to any other University or Institution.

10 January 2017

…….. ……..

Date **Kim Min Chul**

Abstract

The cellular membrane is a complex, self-assembled biological structure that is responsible for numerous physiological functions and also serves to compartmentalize various cell organelles. There is great interest in understanding how membrane-active agents perturb cellular membranes from diverse origins, *e.g.*, mammalian and bacterial, as well as other biological entities such as much smaller, enveloped viruses. This interest has directed countless efforts to attempt to mimic the complex nature of cellular membranes in order to create different types of model membrane platforms. In this thesis, the main objective is to examine the biophysical interactions between membrane-active agents such as amphipathic peptides, fatty acids, and monoglycerides, and model membrane platforms in order to distinguish the corresponding membrane morphological responses. The overall hypothesis is that probing membrane morphological responses induced in model lipid membrane platforms can distinguish the mechanisms of action of membrane-active peptides and monoglycerides, thereby revealing novel biophysical insights into molecular evolution and anti-infective applications. Within this scope, three main experimental studies were conducted that were aimed at developing more biologically relevant model platforms as well as investigating unexplored monoglyceride molecules of biological importance. In the first study, in order to create a defect-free supported lipid bilayer, an α-helical (AH) peptide derived from nonstructural protein (NS5A) of the hepatitis C virus, was employed to repair the still unruptured vesicles trapped in the initially formed bilayer after the vesicle fusion, revealing a correlation between vesicle size and rupture potency. For the second study, the preparation of giant unilamellar vesicles (GUVs) that include fractions of human liver microsome (HLM) extracts was conducted in order to study the interactions against AH peptide. Based on the experimental results obtained at different HLM fractions and peptide concentrations in a systematic fashion, it was identified that HLM-GUVs were more resistant to peptide-induced disruption in

direct comparison with DOPC-GUVs, which are composed of wholly synthetic lipids. In the third study, the interaction between GUVs and glycerol monolaurate was explored for the first time. Depending on the aggregation state of glycerol monolaurate (monomeric *versus* micellar states), vesicle fission and fusion behaviors were observed in both simple and complex GUV compositions. This is the first example of a single molecule that can induce both vesicle fusion and fission, highlighting the potentially significant role of monoglycerides in evolutionary biology as a more advanced molecular structure going beyond the earliest, primitive cellular membranes composed of fatty acids. In summary, the findings in this thesis contribute to a fundamental understanding of how different classes of molecules – peptides, fatty acids, monoglycerides – induce membrane morphological responses in biologically relevant model membranes and offer insights into the roles in which these morphological responses play in therapeutic applications as well as molecular evolution.

Acknowledgements

I am very grateful to have this great opportunity to pursue my Ph.D. studies under the guidance of Prof. Nam-joon Cho. During the period of deciding my future between applying to medical school and pursuing Ph.D. studies, I met Prof. Cho. during our meeting, I was totally impressed by his vision in both science and educational philosophies. Hence, after the talk, I finally could make my decision. Throughout the last four years, I have learned a lot from him; from a very simple laboratory technique to my life direction not only as a scientist but also even as a one of human beings. I am still learning every aspect of him and I highly appreciate his concrete support for me.

It also has been a great honor to work with a team of extremely talented people coming from different cultural and educational backgrounds. Largely our group is consisted of two different teams, lipid team and tissue engineering tem. In the microscopic viewpoint, the two teams are working on different fields. However, in the large picture, we are all seeking to solve out medical problems from different perspectives. I would like to thank Seong-oh Kim, Josh Jackman, Seyed Tabaei, Hogyun Chin and Saziye Yorulmaz for their great help and support throughout my PhD studies. Most importantly, I would like to especially thank my family who has supported my educational path. Since I was born in Korea, I went up to middle school there. Then, I moved to United States of America, and graduated from Carnegie Mellon University with a bachelor degree in chemistry. Whenever I made those huge decisions to study abroad, my family always fully supported and encouraged me to go outside the country. I would not be completing this thesis.

Table of Contents

Table Captions

Figure Captions

Abbreviations

AFM	Atomic force microscopy
AH	Alpha-helical peptide
AMP	Antimicrobial peptides
BSA	Bovine serum albumin
Chol	Cholesterol
CMC	Critical micelle concentration
DDG	1-O-dodecyl-rac-glycerol
DLS	Dynamic light scattering
DOPC	1,2-Dioleoyl-sn-glycero-3-phosphocholine
DP-NGPE	1,2 Dipalmitoyl-sn-glycero-3-phosphoethanolamine-N-(glutaryl)
DPPC	1,2-dipalmitoyl-sn-glycero-3-phosphocholine
ECM	Extra cellular matrix
EDC	N-(3-Dimethylaminopropyl)-N'-ethylcarbodiimide hydrochloride
FN	Fibronectin
FRAP	Fluorescence recovery after photobleaching
GML	Glycerol monolaurate
GUV	Giant unilamellar vesicle
HLM	Human liver microscome
ITO	Indium tin oxide
LB	Langmuir-blodgett
LUV	Large unilamellar vesicle
Lyso PC	Lyso phosphatidylcholine
MIC	Minimum inhibitory concentration
NNLS	Non-negatively constrained least squares
NS5A	Nonstructural protein
PC	Phosphocholine

PI	Phosphoinositol
POPC	1-palmitoyl-2-oleoyl-*sn*-glycero-3-phosphocholine
QCM-D	Quartz crystal microbalance with dissipation
Rh-DPPE	1,2-dioleoyl-sn-glycero-3-phosphoethanolamine-N-(lissamine rhodamine sulfonyl)
SALB	Solvent assisted lipid bilayer
SDCM	Spinning disc confocal microscopy
SDS	Sodium dodecyl sulfate
SLB	Supported lipid bilayer
SM	Sphingomyelin
sNHS	sulfo-N-hydroxysuccinimide
SUV	Small unilamellar vesicle

Chapter 1

Introduction

This introductory chapter presents a brief overview of model membrane platforms and explains their rich potential for deeply understanding the membrane morphological responses induced by various classes of membrane-active agents, including amphipathic peptides and monoglycerides. The chapter also presents the specific objectives of my thesis work and the main hypothesis to be tested along with an overview of the dissertation layout and the key novelties of the work.

1.1. Problem Statement

Cellular membrane is a very complex structure responsible for numerous features of cell physiological functions including regulation of ion influx and efflux[1-3], cell signaling[4-5], cellular adhesion[6-7] and maintaining overall cell structure[8-9]. It also acts as a physical enclosure for various cell organelles such as golgi apparatus, endoplasmic reticulum, mitochondria, nucleus and more[10-11]. Hence, for the most of cell interacting materials, cellular membrane is the first organelle to contact with. This has directed to countless efforts of mimicking the complex nature of cell phospholipid membrane leading to create various types of model membrane platform. With the model membrane platforms, there have been many attempts to study changes of membrane responses that can be induced by membrane–active agents including peptides[12-17], detergents[18-21] and fatty acids[18, 22-25]. However, because of complex structural features of the biological cell membrane, there have been many approaches to develop simplified model systems which mimic important properties of membranes can enable fundamental characterization of interaction parameters for such processes. For instance, depending on one's experimental purposes, the model membrane platform can be ranged from highly simple to complex regarding its lipid composition (i.e., from single to more complexed multiple components), the structural difference (2-dimensional supported lipid bilayer or 3-dimensional giant unilamellar vesicle system), etc. Also, the inclusion of any real cell-derived materials including membrane protein or lipid extract would add more biologically relevant aspects to the simplified model membrane system. For many cases, where membrane specific agents and lipid interactions are main experimental target, less biologically relevant or highly simplified model membrane platform consisted of synthetic lipids is needed. For instance, based on similarities between lipid vesicles and the lipid envelops of virus particles, experimental findings from simplified model membrane platforms composed of only synthetic lipids led to the prediction that a range of medically important viruses might be susceptible to rupturing treatment with synthetic AH peptide[26]. Therefore,

depending on the experimental purposes, engineering strategies can break down complex biological systems into simplified biomimetic models that recapitulate the most important focused parameters. This approach is particularly advantageous for membrane-associated biological processes because either less or more biologically relevant model membrane systems provide a more direct characterization of target interactions than is possible with other complicated methods.

In addition to the development of biomimetic membrane platforms, there are still many untapped opportunities to obtain mechanistic insights into the interactions between model membrane platforms, including supported lipid bilayers and especially giant unilamellar vesicle (GUV) which allows it to be optically monitored by microscopy measurements[27-28], and single chain amphiphiles, which are derivatized forms of fatty acids that possibly provide a link for the evolution of membrane compartmentation from primitive cell membranes to modern phospholipid-based membranes[29-32]. In result section of this thesis, depending on the target membrane-specific agents, membrane fluctuations can be regulated utilizing a proper combination of peptide and lipid compositions of vesicles, and a single amphiphile modulating both vesicular fusion and fission behaviors can be induced. Specifically, a very high concentration of glycerol monolaurate, one of the known single chain amphiphile molecules showing antibacterial properties[33], can induce such behavior of simple vesicle fission/fusion process (i.e. mimicking the complex nature of cellular division) against the GUV composed of only fluidic-phase lipids which has not been reported with any other amphiphilic molecules inducing such cellular processes.

1.2. Objectives and Scope

Employing GUV model membrane platforms, which possess a very attractive feature of its optically resolvable size, can bring about new insights regarding the membrane responses upon interaction with membrane-active agents. This feature

will be able to show various undiscovered membrane morphological behaviors which are not possible to be observed with other model membrane platforms. However, as mentioned above, there is still lack of studies conducted employing biological relevant GUV model membrane platforms to explore its changes of morphology responses induced by biologically relevant peptide and fatty acid materials. There have been many approaches utilizing GUVs based on only synthetic lipids indicating the need of developing more biologically relevant compositions of GUV constituents and utilize them to study the mechanism of amphipathic peptides with potential therapeutic applications. In addition, one of the key single-chain amphiphiles, glycerol monolaurate, has not been studied with GUV platforms to observe to what extent it can induce any changes on cell-sized membrane compartments.

Along this line, the main objective of this thesis is to examine the biophysical interactions between membrane-active agents such as amphipathic peptides, fatty acids, and monoglycerides. To conduct biophysical studies on the membrane-specific interactions, there are a few challenges or critical steps need to be resolved.

1) When using supported lipid bilayers (SLBs) prepared by the vesicle fusion method, a completely defect-free SLB needs to be utilized, otherwise false positives can be obtained for detecting membrane rupture and other structural transformations. Even though SLBs formed *via* the vesicle fusion method is one of the widely employed conventional lipid membrane model platforms, the current vesicle fusion method still creates defects or unruptured vesicles after the initial vesicle fusion process. This can affect the reliability of the bilayer as a biophysical sensing platform or even for electrical property measurement purposes. A simple method to address this gap would greatly aid SLB applications development.
2) Aside from SLBs, there is great potential for utilizing GUVs as another model membrane platform for studying biophysical interactions with membrane-active agents. However, to date, GUV-based platforms for interaction studies have only been fabricated from synthetic phospholipids and cell-based lipid extracts have never been incorporated. One particularly promising membrane-active agent to

study is the the antiviral α-helical (AH) peptide derived from hepatitis C virus nonstructural protein (NS5A). To further characterize the interactions of the AH peptide with model membranes, it is essential to explore their interactions with more biologically relevant within the GUV platform towards exploring possible applications.

3) The interaction of single-chain amphiphiles, especially glycerol monolaurate (GML) need to be conducted in order to understand other types of biophysical interactions that hold relevance for membrane self-assembly. To date, such interactions have never been studied. Achieving this goal will help to reveal insights into the evolution of cellular membrane components and membrane compartmentation from fatty acid compositions to modern phospholipid-based cell membranes.

In this thesis, the main hypothesis is that probing membrane morphological responses induced in model lipid membrane platforms can distinguish the mechanisms of action of membrane-active peptides and monoglycerides, thereby revealing novel biophysical insights into evolution of membrane structure and anti-infective applications.

To test this hypothesis, the following experimental studies are proposed in this thesis:

First, in order to create the defect-free SLB, AH peptide, which has been known to selectively rupture small unilamellar vesicles, will be employed to repair the defects or still unruptured vesicles trapped in the initially formed bilayer after the vesicle fusion. Experimental analyses of the AH peptide mediated repair efficiency will be assessed by employing epifluorescence microscopy and quartz crystal microbalance with dissipation (QCM-D) measurements.

Secondly, in order to study interactions between AH peptide and biologically relevant GUV cell-sized model platforms, human liver microsome incorporated GUV (HLM-GUV) will be developed. Then, various concentrations of AH peptide will be administered against the HLM-GUV which will be monitored by confocal fluorescence microscopy measurements.

Lastly, effect of single chain amphiphiles including GML, lauric acid and 1-O-dodecyl-rac-glycerol (DDG) against GUV model platforms will be studied. Again, real-time high resolution tracking of membrane morphological changes will be monitored by confocal fluorescence microscopy. These fatty acid and derivatives materials have never been reported to be studied with GUVs. Hence, the presented results can provide important cue for further understanding the molecular evolution of cellular membrane from single-chain fatty acids to modern phospholipids.

1.3. Dissertation Overview

The dissertation is comprised of following chapters:

Chapter 1: "Introduction" presents hypotheses of the presented thesis work and outlines overall significance and impact of the study.

Chapter 2: "Literature Review" briefly introduces various model membrane platforms and applications. It also highlights the need of employing a GUV model membrane platform to study interactions with membrane-active agents including amphipathic (antiviral) peptides and fatty acids and monoglycerides materials, specifically to observe morphological changes of membrane.

Chapter 3: "Experimental Methodology" lists the major utilized materials with its preparations, and employed experimental techniques throughout the thesis.

Chapter 4: "Supported Lipid Bilayer Repair Mediated by Amphipathic, α-Helical Peptide" presents repair capability of AH peptide on lipid bilayer formed via vesicle fusion method. Utilizing the vesicle size-selective rupturing ability of AH peptide, it performed that the new method can even repair SLBs initially formed from large sizes of small unilamellar vesicles. From the QCM-D and epifluorescence microscopy measurements, the ratio of defect or unruptured vesicles was less than 1% by the AH peptide mediated repair.

Chapter 5: “Influence of GUV Membrane Composition on the Morphological Responses Induced by an Amphipathic, α-Helical Peptide” presents morphological changes induced by AH peptide against various compositions of GUVs including human liver microsome (HLM) containing vesicle platforms. Based on the experimental results obtained at different HLM fractions and peptide concentrations in a systematic fashion, it was determined that HLM-GUVs were more resistant to peptide-induced disruption in direct comparison with DOPC-GUVs, which are composed of pure synthetic lipids. Various membrane biophysical responses of GUVs were examined by employing spinning disc confocal microscopy measurements, and numerous quantitative analyses including membrane fluctuation calculation and kinetics of peptide bindings onto non-labeled vesicles were derived from the recorded fluorescence micrographs

Chapter 6: “Regulating Vesicle Fusion and Fission based on the Aggregation Behavior of Glycerol Monolaurate” presents and discusses concentration-dependent effects induced by glycerol monolaurate (GML). For the first time, it presents vesicle fusion and fission behaviors induced by below and above critical micelle concentrations of GML, respectively. In contrast, structurally similar compounds such as 1-O-dodecyl-rac-glycerol (DDG) did not show any fusion or fission behaviors in both high and low concentrations. Since fatty acids are believed to be one of the main constituents for forming early membranes (e.g., origin of life) or primitive cellular structures[22, 34], the presented results will further contribute to the modeling of protocell functions in exploring the plausible role of fatty acid molecules in enabling cellular compartmentalization and the emergence of organelles and other detailed cellular features. Therefore, the presented results highlighting vesicle fission/fusion induced by GML may lead to prevail new insights into how the chemical evolution of self-assembled amphiphiles connect to biological evolution from primitive cells (or protocell systems) to current complex cells.

Chapter 7: “Future Outlook” presents reconnaissance work that is recommended for the future work.

1.4. Finding and Originality

This dissertation thesis work correlated to several novel findings by:

1. Offering a simple technique to improve the completeness of supported lipid bilayers by employing a vesicle-rupturing peptide as a final step in the fabrication process leading to result in the fraction of unruptured vesicles to less than 1%. This new method utilizing antiviral AH peptide can be easily incorporated into existing vesicle fusion method.
2. Stabilizing effect of human liver microsome (HML) incorporated GUV against lipid membrane destabilizing ability of antiviral peptide. It further revealed phase separation behaviors of only 5% amount of HML incorporated GUV immersed in hypotonic environment where previously only liquid-ordered phase lipids containing GUVs undergo the similar phase separation behaviors in the hypotonic solution[35].
3. For the first time observing vesicle fission and fusion behaviors from liquid disordered phase lipid GUV (DOPC) induced by glycerol monolaurate (GML) based on its critical micelle concentration (CMC) effect. Specifically, it was observed that slightly below CMC of GML induced fusion between neighboring GUVs and above CMCs induced vesicle fission into multiple smaller daughter vesicles.

References

1. SKou, J. C., Enzymatic basis for active transport of Na+ and K+ across cell membrane. *Physiological Reviews* **1965,** *45* (3), 596-618.

2. Rothman, J. E., Mechanisms of intracellular protein transport. **1994**.

3. Ikonen, E., Roles of lipid rafts in membrane transport. *Current opinion in cell biology* **2001,** *13* (4), 470-477.

4. Schlessinger, J., Cell signaling by receptor tyrosine kinases. *Cell* **2000,** *103* (2), 211-225.

5. Brown, D. A.; London, E., Structure and function of sphingolipid-and cholesterol-rich membrane rafts. *Journal of Biological Chemistry* **2000,** *275* (23), 17221-17224.

6. Hynes, R. O., Integrins: versatility, modulation, and signaling in cell adhesion. *Cell* **1992,** *69* (1), 11-25.

7. Staehelin, L. A., Structure and function of intercellular junctions. *International review of cytology* **1974,** *39*, 191-283.

8. Singer, S.; Nicolson, G. L., The fluid mosaic model of the structure of cell membranes. *Membranes and Viruses in Immunopathology; Day, SB, Good, RA, Eds* **1972**, 7-47.

9. Sheetz, M. P., Cell control by membrane–cytoskeleton adhesion. *Nature reviews Molecular cell biology* **2001,** *2* (5), 392-396.

10. BRAY, D.; HEATH, J.; MOSS, D., The membrane-associated 'cortex'of animal cells: its structure and mechanical properties. *J Cell Sci* **1986,** *1986* (Supplement 4), 71-88.

11. O'Brien, J. S., Cell membranes—composition: structure: function. *Journal of theoretical biology* **1967,** *15* (3), 307-324.

12. Cho, N.-J.; Cheong, K. H.; Lee, C.; Frank, C. W.; Glenn, J. S., Binding dynamics of hepatitis C virus' NS5A amphipathic peptide to cell and model membranes. *Journal of virology* **2007,** *81* (12), 6682-6689.

13. dos Santos Cabrera, M. P.; Alvares, D. S.; Leite, N. B.; Monson de Souza, B.; Palma, M. S.; Riske, K. A.; Ruggiero Neto, J. o., New insight into the mechanism of action of wasp mastoparan peptides: lytic activity and clustering observed with giant vesicles. *Langmuir* **2011,** *27* (17), 10805-10813.

14. Tabaei, S. R.; Rabe, M.; Zhdanov, V. P.; Cho, N.-J.; Höök, F., Single vesicle analysis reveals nanoscale membrane curvature selective pore formation in lipid membranes by an antiviral α-helical peptide. *Nano Letters* **2012,** *12* (11), 5719-5725.

15. Lee, J.; Hwang, J.-S.; Hwang, B.; Kim, J.-K.; Kim, S. R.; Kim, Y.; Lee, D. G., Influence of the papiliocin peptide derived from Papilio xuthus on the perturbation of fungal cell membranes. *FEMS microbiology letters* **2010,** *311* (1), 70-75.

16. Lee, M.-T.; Hung, W.-C.; Chen, F.-Y.; Huang, H. W., Mechanism and kinetics of pore formation in membranes by water-soluble amphipathic peptides. *Proceedings of the National Academy of Sciences* **2008,** *105* (13), 5087-5092.

17. Nadeem, A.; Sanborn, J.; Gettel, D. L.; James, H. C.; Rydström, A.; Ngassam, V. N.; Klausen, T. K.; Pedersen, S. F.; Lam, M.; Parikh, A. N., Protein receptor-independent plasma membrane remodeling by HAMLET: a tumoricidal protein-lipid complex. *Scientific reports* **2015,** *5*.

18. Yoon, B. K.; Jackman, J. A.; Kim, M. C.; Cho, N.-J., Spectrum of membrane morphological responses to antibacterial fatty acids and related surfactants. *Langmuir* **2015,** *31* (37), 10223-10232.

19. Schuck, S.; Honsho, M.; Ekroos, K.; Shevchenko, A.; Simons, K., Resistance of cell membranes to different detergents. *Proceedings of the National Academy of Sciences* **2003,** *100* (10), 5795-5800.

20. Mally, M.; Peterlin, P.; Svetina, S. a., Partitioning of oleic acid into phosphatidylcholine membranes is amplified by strain. *The Journal of Physical Chemistry B* **2013,** *117* (40), 12086-12094.

21. Peterlin, P.; Arrigler, V.; Kogej, K.; Svetina, S.; Walde, P., Growth and shape transformations of giant phospholipid vesicles upon interaction with an aqueous oleic acid suspension. *Chemistry and physics of lipids* **2009,** *159* (2), 67-76.

22. Arouri, A.; Lauritsen, K. E.; Nielsen, H. L.; Mouritsen, O. G., Effect of fatty acids on the permeability barrier of model and biological membranes. *Chemistry and physics of lipids* **2016,** *200,* 139-146.

23. Inaoka, Y.; Yamazaki, M., Vesicle fission of giant unilamellar vesicles of liquid-ordered-phase membranes induced by amphiphiles with a single long hydrocarbon chain. *Langmuir* **2007,** *23* (2), 720-728.

24. Tamba, Y.; Ohba, S.; Kubota, M.; Yoshioka, H.; Yoshioka, H.; Yamazaki, M., Single GUV method reveals interaction of tea catechin (−)-epigallocatechin gallate with lipid membranes. *Biophysical Journal* **2007,** *92* (9), 3178-3194.

25. Tanaka, T.; Sano, R.; Yamashita, Y.; Yamazaki, M., Shape changes and vesicle fission of giant unilamellar vesicles of liquid-ordered phase membrane induced by lysophosphatidylcholine. *Langmuir* **2004,** *20* (22), 9526-9534.

26. Cho, N.-J.; Dvory-Sobol, H.; Xiong, A.; Cho, S.-J.; Frank, C. W.; Glenn, J. S., Mechanism of an Amphipathic α-Helical Peptide's Antiviral Activity Involves Size-Dependent Virus Particle Lysis. *ACS Chemical Biology* **2009,** *4* (12), 1061-1067.

27. Menger, F. M.; Angelova, M. I., Giant vesicles: imitating the cytological processes of cell membranes. *Accounts of chemical research* **1998,** *31* (12), 789-797.

28. Dimova, R.; Aranda, S.; Bezlyepkina, N.; Nikolov, V.; Riske, K. A.; Lipowsky, R., A practical guide to giant vesicles. Probing the membrane nanoregime via optical microscopy. *Journal of Physics: Condensed Matter* **2006,** *18* (28), S1151.

29. Hargreaves, W.; Mulvihill, S.; Deamer, D., Synthesis of phospholipids and membranes in prebiotic conditions. *Nature* **1977,** *266*, 78-80.

30. Budin, I.; Szostak, J. W., Physical effects underlying the transition from primitive to modern cell membranes. *Proceedings of the National Academy of Sciences* **2011,** *108* (13), 5249-5254.

31. Simoneit, B. R.; Rushdi, A. I.; Deamer, D. W., Abiotic formation of acylglycerols under simulated hydrothermal conditions and self-assembly properties of such lipid products. *Advances in Space Research* **2007,** *40* (11), 1649-1656.

32. Olasagasti, F.; Maurel, M.-C.; Deamer, D. In *Physico-chemical interactions between compartment-forming lipids and other prebiotically relevant biomolecules*, BIO Web of Conferences, EDP Sciences: 2014; p 05001.

33. Conley, A. J.; Kabara, J. J., Antimicrobial action of esters of polyhydric alcohols. *Antimicrobial agents and chemotherapy* **1973,** *4* (5), 501-506.

34. Tang, D.; Rohaida Che Hak, C.; Thompson, A. J.; Kuimova, M. K.; Williams, D.; Perriman, A. W.; Mann, S., Fatty acid membrane assembly on

coacervate microdroplets as a step towards a hybrid protocell model. *Nature chemistry* **2014,** *6* (6).

35. Oglęcka, K.; Rangamani, P.; Liedberg, B.; Kraut, R. S.; Parikh, A. N., Oscillatory phase separation in giant lipid vesicles induced by transmembrane osmotic differentials. *Elife* **2014,** *3*, e03695.

Chapter 2

Literature Review

The cellular membrane is one of the critical cellular structures that not only separates inner cellular compartments from the exterior environments but it also regulates overall passage of various substances in and out of cells. However, because of its highly complex structure hosting main backbone of phospholipids and various membrane proteins, it is quite cumbersome to carry studies using natural cellular membrane samples. Hence, there is a large need of employing model membrane platforms for studying such complex systems. In this chapter of literature review, an overview of various model membrane platforms is presented. In addition to the thorough introduction of model platforms mainly employed in this thesis, another overview of membrane-active agents, specifically amphipathic peptides and fatty acids with monoglycerides, is presented. It highlights one of the monoglycerides materials, glycerol monolaurate, which is one of the critical antimicrobial materials but has never been studied with cell-sized model membrane platforms.

2.1. Model Membrane Platforms

Within biological systems, cellular membrane is in charge of critical functions such as cellular protection[1] and signal transduction[2]. The cell membrane is a highly organized structure as depicted in the following Figure 2.1 which directs and facilitates various cellular responses to specific and non-specific extracellular signal transduction pathways.

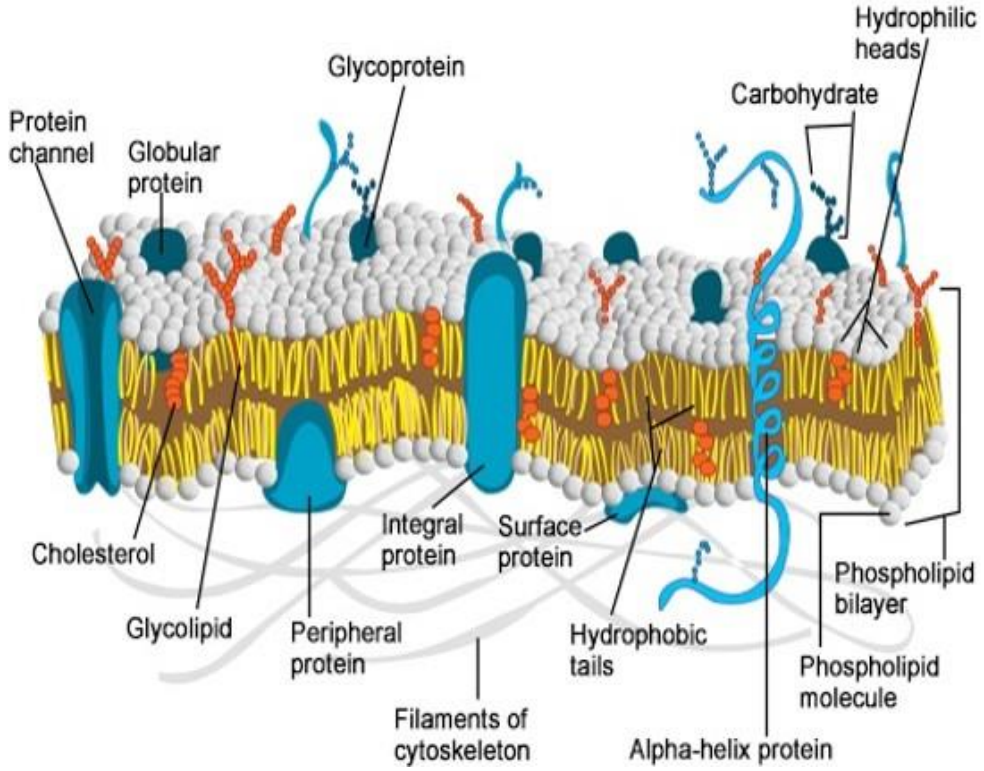

Figure 2. 1 Schematic representation of fluidic mosaic model of a biological cell membrane. Reproduced from Singer et al[3].

Strikingly, within the approximately 4-6 nm of thickness of the phospholipid bilayer, it not only hosts various types of membrane proteins but it also constitutes a regulatory wall between the external cellular environment and internal cellular organelles[3-4]. Hence, in order to mimic such a complex structure of cellular membrane, there have been several different approaches to fabricate simplified experimental model systems using lipid vesicles in aqueous condition such as black

lipid membranes[5], supported lipid bilayer (SLB)[6], tethered lipid bilayer[7], intact vesicle layer[8], hybrid bilayer[9] and giant unilamellar vesicle (GUV)[10]. Following table (Table 2. 1) briefly summarizes each different model membrane platform.

Table 2. 1 Summary of various model membrane platforms.

Model membrane Platform	Summary	Observable Morphological Changes	Surface-sensitive Characterization
Small unilamellar vesicles	Less than 200 nm diameters of diffusing vesicles in aqueous solution	No	No
Black lipid membrane	An open aperture spanning in lipid bilayer	No	No
Supported lipid bilayer	Lipid bilayer formed on solid substrates	Yes	Yes
Tethered lipid bilayer	Immobilized lipid bilayer on solid substrates (larger separation distance between substrate and bilayers compared to SLB)	Yes	Yes
Intact vesicle layer	Layer of intact vesicles adsorbed on solid substrate	In case of vesicle rupture	Yes
Giant unilamellar vesicle	Micron-scale diameters of unilamellar vesicles	Yes	No

Among the various listed lipid-based model platforms, SLB and GUV were mainly employed in this thesis for exploring the membrane morphological changes upon interacting with membrane-active peptides and surfactants.

Lipid vesicles (liposome) can be classified into different types based on its diameter and lamellarity[11]. Specifically, among unilamellar lipid vesicles, liposomes less than 200 nm in diameter are termed as SUV[12], and diameters greater than 200 nm but less than micron size is called large unilamellar vesicle (LUV)[12]. Following schematic diagram (Figure 2. 2) depicts the various types of liposomes classified based on size diameter and lamellarity.

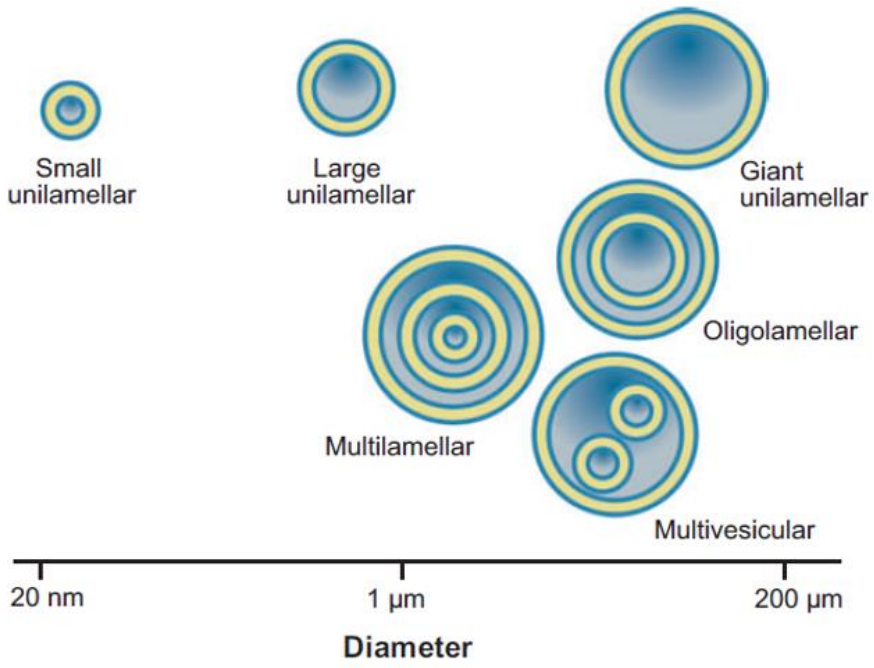

Figure 2. 2 Schematic representation of lipid vesicle classification based on diameter and lamellarity. Schematic is reproduced from Jesorka et al[11].

Following sub-sections will describe more detailed discussion of each different model membrane platform employed in this thesis.

2.1.1. Small Unilamellar Vesicle

As above explained, SUV is a unilamellar lipid vesicle whose diameter is less than 200 nm. It can be produced by two representative methods which are extrusion and sonication methods[13]. Among the two different approaches to form SUVs, extrusion method has been proved to be creating more consistent desired size of vesicles[13]. Further specific mechanism details of extrusion method will be discussed in the Chapter 3.

The SUV platform itself can be used in many different applications including a carrier purpose by encapsulating drug or gene materials inside the vesicle[14], intact vesicle layer to screen the interactions against foreign membrane active materials[15-

[16], and forming supported lipid bilayer (SLB) via vesicle fusion[17-18]. Following figure (Figure 2. 3) depicts schematic diagrams of the intact vesicle layer and supported lipid bilayer platform.

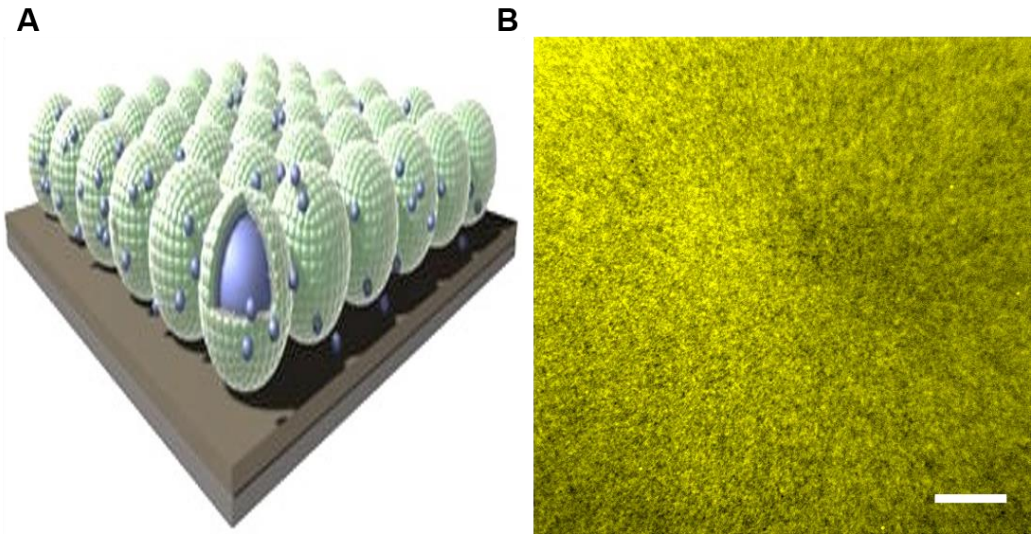

Figure 2. 3 (A) Schematic diagrams and (B) fluorescence micrograph of intact vesicle layer. Herein, SUVs are adsorbed on hydrophobic surfaces of titanium oxide substrates resulting in an intact layer of vesicles. Fluorescence image was taken by epifluorescence microscope using 60x objective lens resulting in 136 µm x 136 µm image size. Scale bar of fluorescence micrograph indicates 20 µm.

As shown in the above Figure 2. 3, SUVs are adsorbed and remained as intact vesicle layer on the solid substrates by injection utilizing mechanical pump or simple pipetting of vesicle solution onto the hydrophobic surfaces of aluminum oxide[19], gold[20] and titanium oxide substrates[8]. This intact vesicle layer platform can be employed for antiviral peptide interaction screening applications by measuring changes of adsorbed mass of vesicles on the substrates via quartz crystal microbalance-dissipation monitoring (QCM-D)[21]. By rupturing interaction with antiviral alpha helical (AH) peptide, the intact vesicle layer can also be transformed into a supported lipid bilayer[15, 20-21].

Unlike with the above discussed intact vesicle layer platform, SUVs can be utilized to spontaneously form supported lipid bilayers via vesicle fusion method on hydrophilic substrates including silicon oxide[22-23], glass[24] and mica[17]. Following figure (Figure 2. 3) presents the schematic diagram and fluorescence micrograph of the supported lipid bilayer platform.

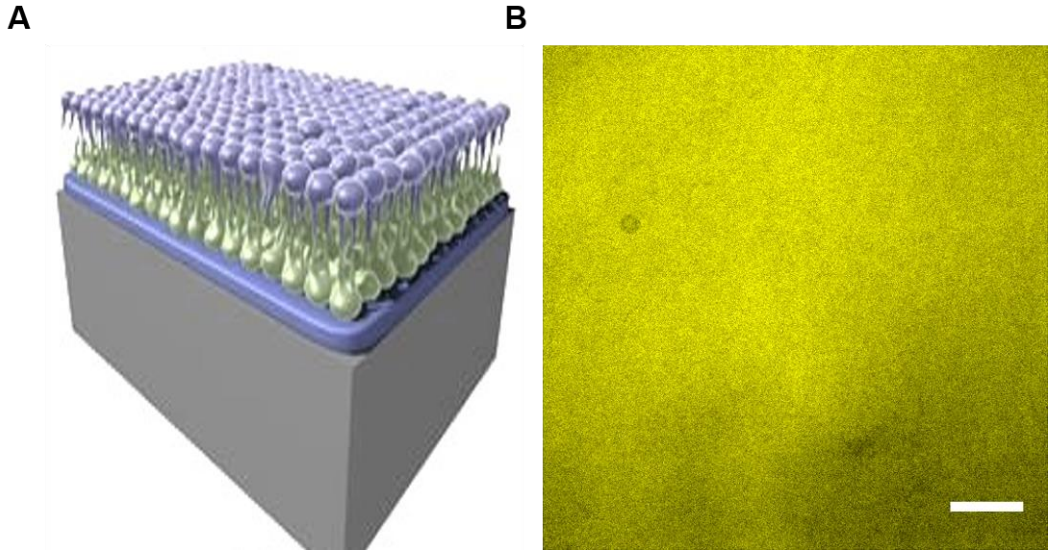

Figure 2. 4 (A) Schematic diagrams and (B) fluorescence micrograph of supported lipid bilayer. Herein, SUVs are adsorbed on hydrophilic surfaces of glass or silicon oxide substrates fusing into a uniform layer of bilayer. Fluorescence image was taken by epifluorescence microscope using 60x objective lens resulting in 136 µm x 136 µm image size. Scale bar indicates 20 µm.

Among different approaches, vesicle fusion method is one of the most robust and consistent methods to create the lipid bilayer on the hydrophilic substrates[17]. Briefly, on the hydrophilic substrates such as glass, mica and silicon oxide, SUVs typically adsorb until reaching a critical coverage and then spontaneous rupture begins. Besides the vesicle-substrate interaction effect, there are various parameters affecting the spontaneous rupture including vesicle size[25], lamellarity[22], vesicle age[13], lipid composition[26],temperature[27] and osmotic pressure[28]. Following

schematic diagram (Figure 2. 5) depicts each step of vesicle fusion method forming a complete lipid bilayer.

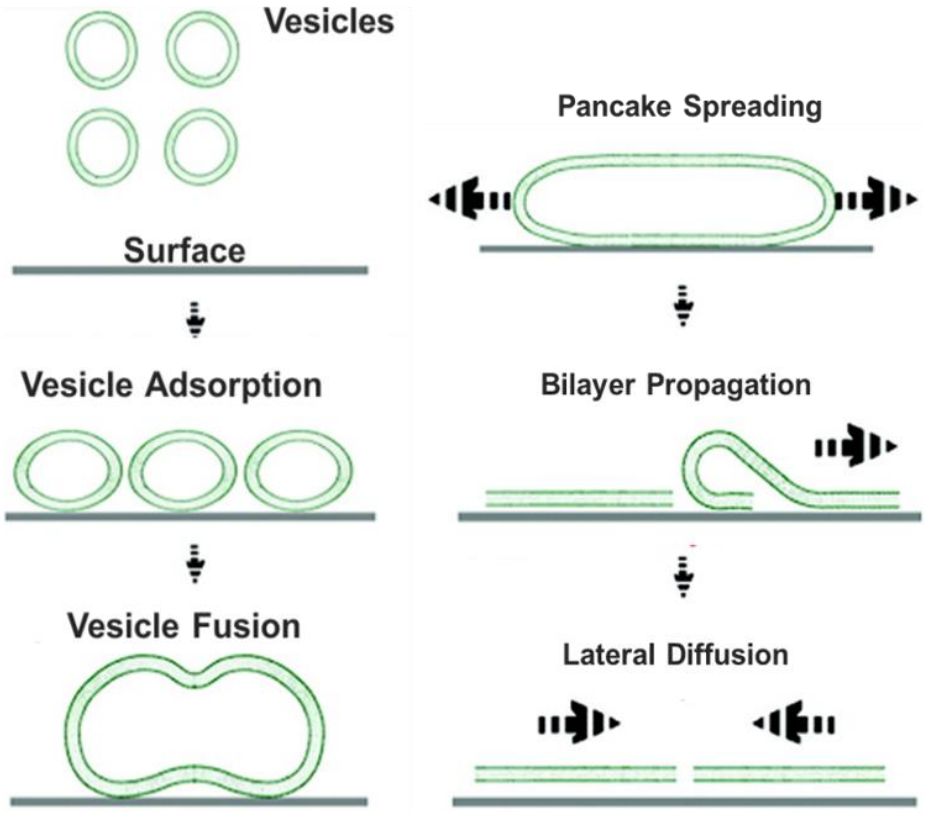

Figure 2. 5 Schematic diagram of supported lipid bilayer formation via vesicle fusion on hydrophilic substrates.

2.1.2. Giant Unilamellar Vesicle

Although the nano-scale sized liposomes can be used for numerous bio-relevant applications, because of their small size, their size is too small to be resolved under microscope for monitoring dynamics of membrane morphological changes. Below figure (Figure 2. 6) of fluorescence micrographs (taken by 60x objective lens) of adsorbed SUVs on the glass surface and settled GUVs on the surface.

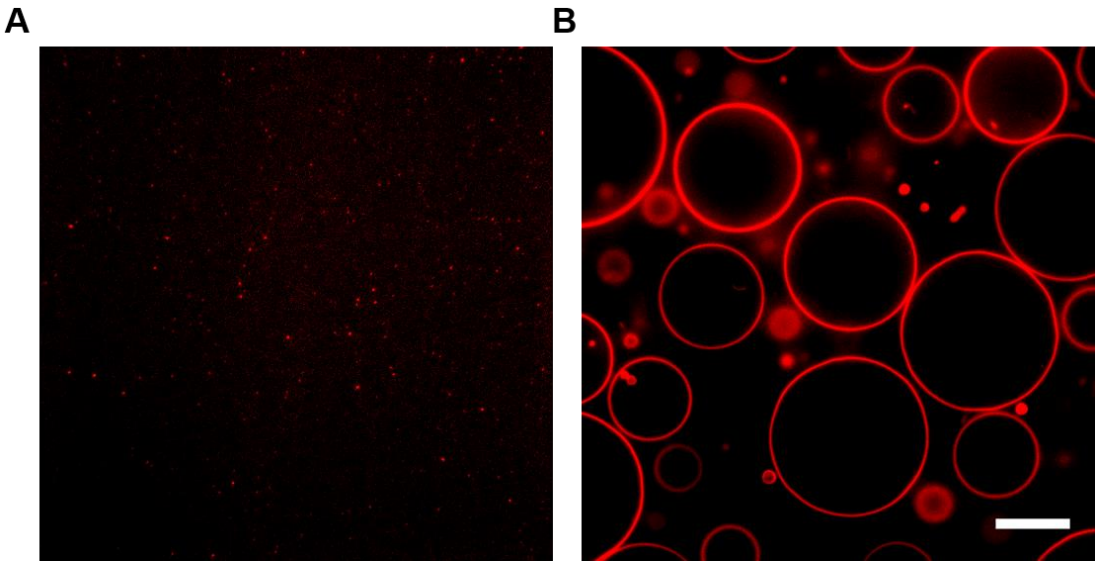

Figure 2. 6 Comparison of fluorescence micrographs of (A) SUV and (B) GUV absorbed and settled on the surface. Both vesicles were mixed with either 0.5 or 1 % of rhodamine labeled DOPC. While fluorescence labeled SUVs are being imaged as red-colored small dots, GUVs are shown as well-recognizable circular structure. Scale bar indicates 20 μm.

As abovementioned, unilamellar lipid vesicles whose diameter is great than 1 μm are classified as GUV. Because of its large size, it can be fully resolved under microscope in both light (phase contrast) and fluorescence imaging modes[29]. Since eukaryotic cell diameters are normally ranged from 10 – 30 μm[10], size feature of GUV makes highly attractive and ideal simple model cell platform for exploring various biophysical properties of such complex biological cell membranes. In summary, GUV platforms offer a simple organizational structure for physically maintaining biological compartmentalization of cells and organelles.

2.1.3. Design Strategies

GUVs can be prepared in various different methods which can affect the relative size distribution and quality (cleanness) of formed vesicles. Historically, "gentle hydration method" was first invented by Reeves et al[30]. Briefly, lipids dissolved in chloroform is dried on the surface of glass flask, and it is hydrated for swelling using aqueous buffer solution for 2 hrs or longer without any agitation which may cause to form multilamellar vesicles and a low number of GUVs[10]. Even though an extreme precaution is given during the gentle hydration process, it is highly difficult to avoid having vesicles of less than micron-sizes and multilamellarity resulting to have a highly diverse population of non-uniform vesicles.

To overcome such issues, Angelova et al[31] further developed the gentle hydration method into "electroformation method" which utilizes AC electric field to efficiently detach the dried lipid film deposited on ITO-coated glass slides. Because of the utilization of electric field throughout the 2 hr or longer duration of hydration, it still has some limitations when it comes to choosing hydration buffer solutions (should contain very low amount of ionic salt and charged lipids). However, it has been reported that the electroformation method has been proved as the most efficient method to form GUV in much more controllable manner in terms of increasing the yield of unilamellar micron-scale sized vesicles[32]. The following table (Table 2. 2) describes details of various GUV formation methods including microfluidic-based formation techniques.

Table 2. 2 Representative GUV formation methods and their advantages/limitations.

Formation Method	Possible Lipid Compositions	Advantage	Limitations
Gentle hydration	1) Zwitterionic lipids (DOPC,POPC, Egg PC and etc.) 2) ~ 40 % negatively charged lipids (PS & PG) 3) Raft compositions (sphingomyelin and cholesterol)	Possible to use physiological buffers and highly charged lipid compositions	1) Low yields of unilamellar vesicles 2) Highly aggregated GUVs
Electroformation	1) Zwitterionic lipids 2) ~ 10 % of negatively charged lipids (PS & PG) 3) DMPC and DPPC 4) Raft compositions	A narrow size distribution and high yield of GUV population can be obtained	1) Greater than 10% of charged lipids cannot be included 2) Sucrose as a hydration buffer should be used instead of physiological buffer
Water-oil two phase emulsion	1) Zwitterionic lipids 2) DPPC, DMPC & DPPE 3) Raft compositions	Depending on microfluidic injecting parameters, uniform size of GUV can be formed	1) Low yields of unilamellar vesicles 2) Charged lipids cannot be included. 3) Non-aqueous solvents (mineral oil, oleic acid, hexane) must be utilized
Lipid/surfactant without emulsion	1) Zwitterionic lipids 2) Raft compositions		

In order to produce consistent population of GUV composed of either DOPC or raft compositions, electroformation method was employed throughout in this thesis.

2.1.4. Applications

As abovementioned, GUV can be fully resolved under microscope measurement allows one to conduct broad range of biophysical and chemical related experiments. The GUV size makes it attractive and efficient cell model platform for exploring membrane dynamics including both microscopic and macroscopic morphological changes upon interacting with foreign membrane-active materials[33-34], and phase separation[5, 35] upon environmental changes, drug delivery system[36-37], constituting compartments for monitoring enzymatic reactions[5, 38], vesicular shape transformations[39], and building up a protocell model to study origin of a cell[40-43]. Following figure (Figure 2. 7) shows several exemplary micrographs of GUV applications which cannot be conducted with other lipid-based membrane model platforms.

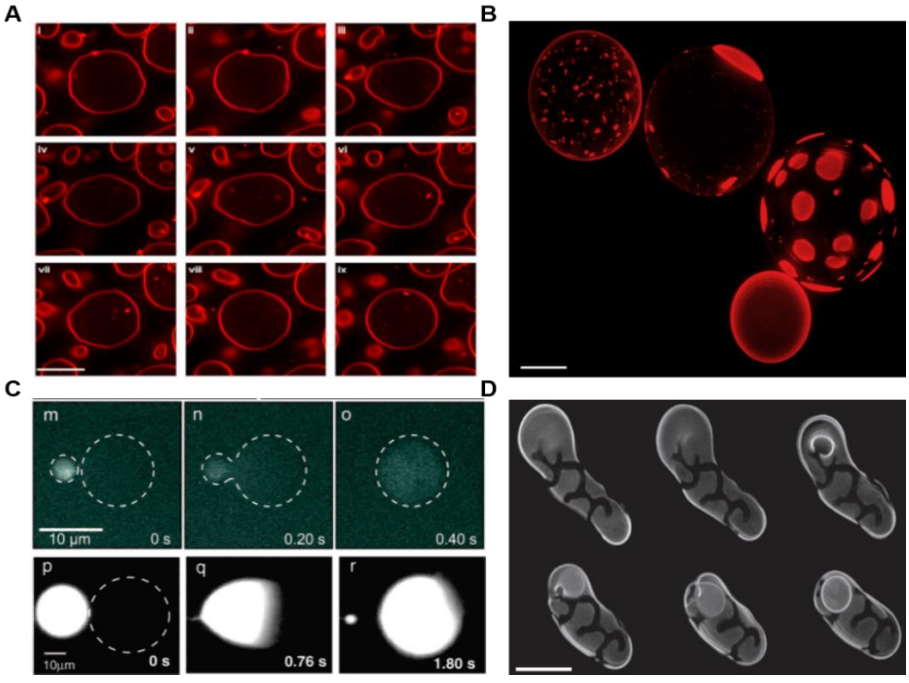

Figure 2. 7 Representative applications of GUV. (A) Membrane softening induced by antiviral peptide interaction Reproduced from Hanson et al[33]. (B) Phase separation between liquid ordered and disordered phases induced by osmotic shock. Reproduced from Oglecka et al[35]. (C) Fusion of GUVs induced by enzymatic reactions. Reproduced from Karlsson et

al[38]. (D) Vesicular shape deformations caused by addition of potassium phosphate buffer. Image reproduced from Oglecka et al[44]. Each scale bare indicates 10 µm.

2.2. Evaluation of Membrane-Active Agents

As stated above, because of its large enough diameter, GUV provides a highly attractive model platform to study membrane dynamics in terms of tracking morphological changes of its bilayers in real-time fashion. Hence, for the direct measurement, microscopy techniques are mainly employed to monitor any changes on GUV upon interacting with membrane-active agents. The size feature of GUV allows it to be monitored even under phase contrast (typically known as light microscopy) imaging microscopy, and it can also be imaged by fluorescence microscopy as long as it contains fluorescence tagged lipids (Figure 2.3).

Both qualitative and quantitative parameters can be obtained from the GUV microscopy images. First, as shown in Figure 2.4 A and D, changes of membrane dynamics including membrane flickering and extreme shape deformations can be recorded at various time points during the course of interaction. Any movements of bilayer of GUVs during or after the interaction with membrane-active agents allows one to measure its changes of bending modulus or rigidity of bilayer[45-46]. The large enough size feature of GUV also allows one to observe the pore formation by interacting with membrane active-agents or in osmotic pressure changes. By encapsulating dye containing glucose solution inside the vesicle, it is possible to observe the dye release phenomenon confirming the formation of pores on the bilayer of GUVs[33]. Then, it is feasible to measure relative percentage of vesicle content leakage throughout the pore formation[33]. As shown in the Figure 2.4B, the phase separation behavior between liquid ordered and disordered phases or in any different phases of lipids constituting GUVs is one of the representative experiment can be monitored using GUV platforms whereas SUVs or LUVs are not possible to be resolved such behavior under microscope. Hence, the phase separation behavior on multiphase-lipids containing GUVs induced by membrane active reagents can be

one of the important parameters to be studied during the vesicle-material or environmental changes interactions. In addition to the above listed various applications of GUV as biophysical tools, the platform can also be served as a biochemical measuring tool for monitoring protein-protein assemblies into clusters on the membranes of GUVs[47] as shown in the below example (Figure 2. 8).

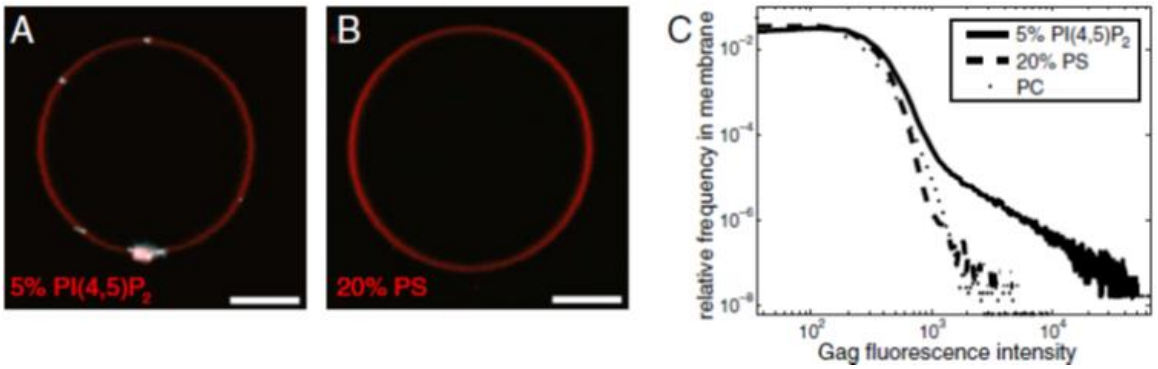

Figure 2. 8 Assembly of binding specific protein on (A) phosphoinositol (PI) lipids and comparison with (B) non-PI containing GUVs. Images reproduced from Carlson et al[47].

Following sub-sections delineates basic scientific background information of membrane-active reagents employed in this thesis work.

2.2.1. Amphipathic Peptides

For understanding underlying numerous biological phenomenon including, cellular life cycles utilizing membrane fusion or lysis, there have been high interests in exploring the working mechanism regarding the interactions between peptides within the lipid-related environments[48-50]. The interactions between phospholipid membranes and the peptides may cause to happen various events such as membrane destabilization[15] and membrane mixing[51-52]. Antimicrobial peptides (AMPs) are one of the essential elements of innate defense systems[50, 53]. It has been reported that the AMPs share a common similar mechanism for interacting against microbial membrane via a specific lipid membrane permeabilization[53-54]. To date, there are hundreds of AMPs have been reported and they are sourced from plants and animals

including humans[53-54]. Since the variety of the peptides is too wide and cumbersome to conduct specific interactions with them, it is inevitable to utilize the cell mimic based model platforms. Hence, GUV platforms provide highly attractive biophysical and biochemical tools to study the effect and working principles of AMPs against the lipid-based artificial cell models.

Based on their killing targets, the AMPs can be simply classified as either antibacterial or antiviral peptides. Herein, we briefly go over some representative antibacterial peptides that have been studied by GUV platforms. Following table (Table 2. 3) briefly presents the summaries of each antibacterial peptide studies that have been conducted with GUV model platforms.

Table 2. 3 Summary of representative antibacterial peptides tested with GUV model platforms. Each antibacterial peptides information is summarized from literatures[55-62].

Antibacterial Peptide	GUV Lipid Composition	Key Observation	Reference
Melittin	di22:1PC & di20:1PC	Pore formation	Lee et al
Magainin	DOPC & DOPG (50 mol %)	Pore formation and vesicular shape changes	Tamba et al
Maculatin	POPC	Pore formation	Ambroggio et al
Aurein		Membrane destabilization with vesicle burst	
Citropin			
Mastoparan	POPC & POPG (10 mol %)	Pore and defect formation on membrane	dos Santo Cabrera et al
Papiliocin	POPC	Pore formation and membrane destabilization into fragments	J. Lee et al
Arenacin-1	PC/PE/PI/ergosterol (5:4:1:2 weight %)	Volume changes leading to vesicle size decrease	Park et al
Psacotheasin	PC/PE/PI/ergosterol (5:4:1:2 weight %)	Pore formation	Hwang et al
Alamethicin	DOPC	Pore formation	Huang et al

As summarized in the above table (Table 2. 2), studies on several antibacterial peptides mainly using GUV cell model platforms have been thoroughly conducted. On the other hand, antiviral peptides, whose main target is viruses as it can be noticed from its name, have not been extensively studied using GUV model platform. Hence, to further reveal the working mechanism of lytic activities induced by antiviral peptides, there is a large need of thorough evaluations employing more cell-close mimic GUV platforms.

An AH peptide, which is derived from the N-terminus of the hepatitis C virus NS5A protein[17], has gained a significant attention to form supported bilayers on certain solid substrates, such as TiO_2 and gold as shown in below schematic figure (Figure 2. 9).

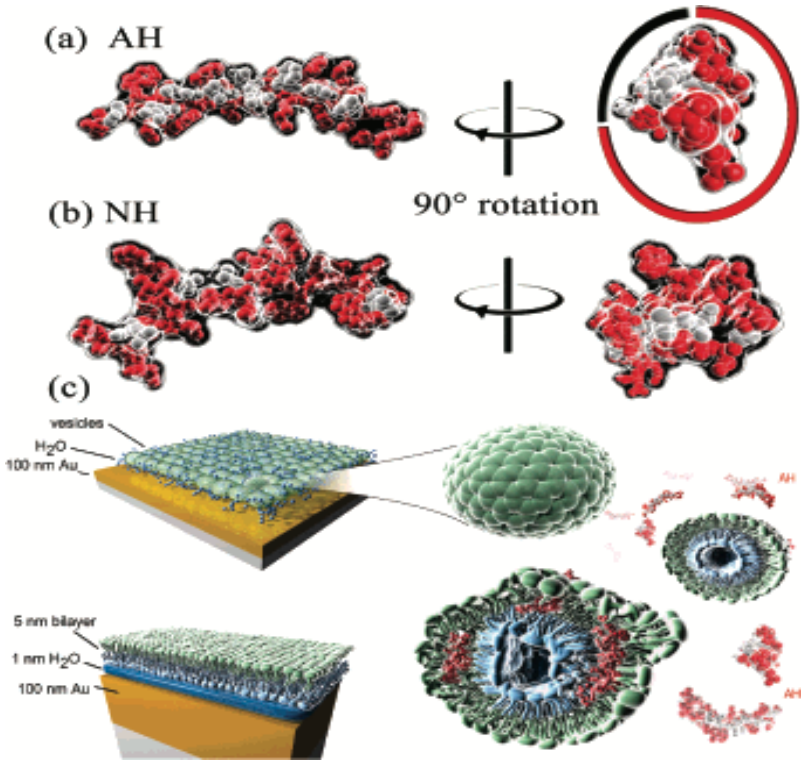

Figure 2. 9 Schematic diagrams of (a) AH peptide (peptide sequence SGSWLRDVWDWICTVLTDFKTWLQSKLDYKD) and (B) NH peptide (sequence: SGSWLRDDW DWECTVLTDDKTWLQSKLDYKD). (C) Speculative diagram of lipid vesicle rupturing process mediated by AH peptide[15].

Recently, AH-mediated bilayer formation was discovered on hitherto intractable substrates by rupturing vesicles, thereby inducing the structural transformation of an intact vesicle layer to a planar bilayer[15]. Cho et al have successfully demonstrated that the AH peptide can destabilize and rupture the leaflets of intact lipid vesicles leading to form a complete bilayer on some substrates which do not allow spontaneous ruptures[15]. Based on a combination of quartz crystal microbalance with dissipation (QCM-D) monitoring experiments and viscoelastic modeling, it was identified that AH peptide first adsorb onto the vesicle surface, before destabilizing the vesicles and causing rupture to form a planar bilayer[17]. Importantly, AH peptide was not found in the planar bilayer after the structural transformation was complete[63].

Hanson et al demonstrated thorough studies on hepatitis C virus derived antiviral peptide, so called amphipathic α-helix (AH) peptide[33]. Following figure (Figure 2. 6) of micrographs showing AH peptide studies employing GUV model platforms deciphering lipid component-specific interaction behaviors. From the experimental findings, it was discovered that the AH peptide selectively induced different results depending on the lipid compositions of GUVs. While on the DOPC-GUVs it induced membrane flickering behavior or fluctuations due to membrane thinning effect by the binding of peptide[64] (Figure 2. 7A), the antiviral peptide induced formation of micro domains of cholesterol and sphingomyelin-enriched regions enabling phase-separated domains to be observed as shown in Figure 2. 7B.

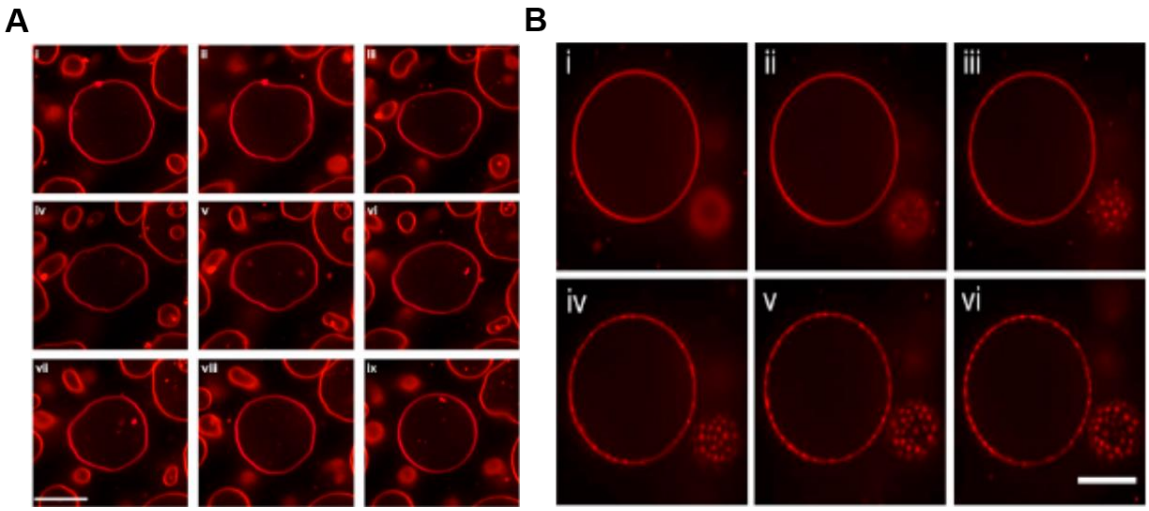

Figure 2. 10 AH peptide induced (A) membrane softening of POPC GUVs and (B) phase separation in raft-components GUVs. 10 µM of AH peptides were injected for both different lipid compositions of GUVs. Both set of fluorescence micrographs were captured by spinning disc confocal microscope. Each scale bar indicates 5 µm. Micrographs were reproduced from Hanson et al[33].

However, this has been the only approach conducted utilizing the GUV model platforms to study the AH peptide interactions against two different lipid compositions of cell-sized vesicles. Hence, there is still a large need of more thorough studies employing more closely cellular membrane mimic GUV experimental platforms. For instance, liver cell membrane extract protein embedded

or containing within bilayers of GUV model will provide more insights on peptide binding mechanism inducing morphological changes on the cell-sized vesicles.

2.2.2. Fatty Acids and Monoglycerides

Several representative antimicrobial lipid-related materials have been gaining attentions on their attractive antibacterial ability[65]. However, most of the studies have been largely focused on the interactions of the antibacterial antimicrobial lipids with actual bacterial strains[66]. Hence, refined insights on working mechanism of inducing membrane morphological changes of target bacterial cells have not been thoroughly explored. Yet, the GUV model platforms as a simplified artificial cell mimic have also been employed for studying interactions against a few fatty acids including detergent materials. Following table (Table 2. 3) summarizes numerous fatty acids and detergent materials that have been investigated against GUV cell model platforms. Following figure (Figure 2. 8) of micrographs presents the exemplary interaction changes of GUVs with the listed agents. Inaoka et al[67] conducted vesicle fission revealing experiments using various phases of GUVs including DPPC, cholesterol (both liquid-ordered phase) and DOPC (liquid-crystalline phase). Herein, they first reported the vesicle fission behaviors of liquid-ordered phase lipids containing GUVs by injection of foreign materials (lyso PC 16:0, lyso PA C18:1, octylglucoside and SDS) as shown in below Figure 2. 8A. Regardless of low and high concentrations of lyso-PC, it all induced the fission when at least 40 mol % of DPPC was included in the GUV lipid composition indicating that fission can only be induced from specific lipid phase. Besides the lyso PC, octylglucoside, SDS, and lyso PA C18:1 all induced the same fission above its threshold concentrations.

Employing oleic acid as a GUV interacting foreign material, Peterlin et al and Mally et al reported pore formations of DOPC-GUV leading to volume changes and burst of vesicle when low concentration was injected. In addition to the pore formations,

it was also observed to be inducing various vesicular morphological changes including budding, invagination and evagination as shown in the Figure 2. 8B at high concentrations of oleic acid.

Another antibacterial material, tea catechin (EGCg), study on egg PC GUVs conducted by Tamba et al[68] showed shape transformations of GUVs into various vesicular shapes such as pearling shapes as several spheres connected by narrow neck at low concentration. At high concentrations of EGCg, the GUVs were burst within approximately 1 min of injection.

Table 2. 4 Summary of representative membrane-active fatty acids and related detergent materials tested with GUV model platforms. Each material information and its interaction results is summarized from Inaoka et al[67], Peterlin et al[69], Mally et al[70], Tamba et al[68] and Tanaka et al[71].

Membrane-active agent	GUV Composition	Concentration	Key Observation	Reference
Lyso PC (16:0)	DPPC/Chol (6/4)	0.5 μM	Vesicle Fission	Inaoka et al
Lyso PC (16:0)	DPPC/DOPC/Chol (5.5/0.5/4)	0.7 μM		
Lyso PC (16:0)	DPPC/DOPC/Chol (5/1/4)	1 μM		
Lyso PC (16:0)	DPPC/DOPC/Chol (4/2/4)	3 μM		
Lyso PC (16:0)	DPPC/DOPC/Chol (3/3/4)	4 μM	Shape Transformation	
Lyso PC (16:0)	DOPC/Chol (6/4)	4 μM		
Lyso PC (16:0)	DOPC	4 μM		
Octylglucoside	DPPC/Chol (6/4)	4 mM	Vesicle Fission	
SDS		50 μM		
Lyso PA (C18:1)		20 μM		
Oleic acid (suspension)	POPC	0.8 mM	Area expansion, Budding, invagination, evagination	Peterlin et al
Oleic acid (suspension with glycerol)		0.1 mM	Growth & burst then reseal	Mally et al
Tea Catechin (EGCg)	Egg PC	100 μM	Burst of GUV & transformation into small lump	Tamba et al
		0.5 μM	Shape Transformation into two spheres connected by narrow neck changed into a dumbbell prolate shape	
Lyso PC (10:0)	DPPC/Chol (6/4)	500 μM / 1 M	Shape changes / Fission	Tanaka et al
Lyso PC (12:0)		20 μM / 4 μM		
Lyso PC (14:0)		0.9 μM / 8 μM		
Lyso PC (16:0)		0.07 μM / 0.5 μM		

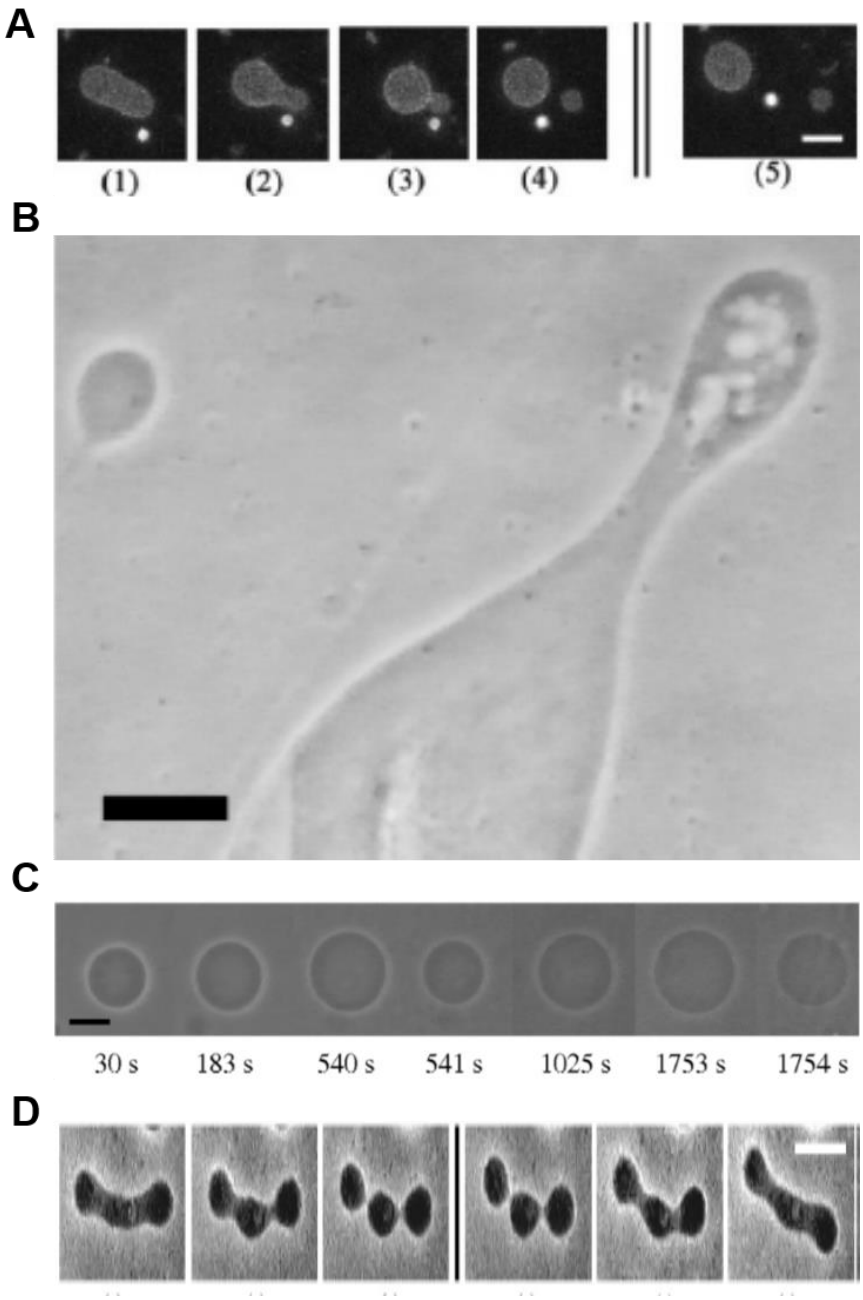

Figure 2. 11 Possible GUV morphological changes upon interacting with antimicrobial lipids. (A) Vesicle fission behavior happening from DPPC/DOPC/cholesterol GUV induced by 2 μM of lyso-PC (16:0). Scale bar represents 10 μm[67]. (B) Vesicle invagination was occurred at the tip of vesicle protrusion (POPC GUV induced by 0.8 mM of oleic acid)[69]. Scale bar indicates 20 μm. (C) Vesicle growth and burst induced by 0.1 mM of oleic acid[70]. Scale bar indicates 10 μm. (D) Vesicular shape

transformation is induced by addition of 1 μM EGCg. Scale bar is 10 μm. Images are reproduced from the listed literatures.

Even though there have been somewhat extensive studies on GUV interactions with some representative antimicrobial lipids as shown in the above table and figure, there are still missing observations on some key fatty acid and monoglyceride materials. One of the key antimicrobial lipids is glycerol monolaurate (GML) which have not been investigated with GUV platforms yet. GML is specifically a 1-monoglyceride derivative of lauric acid as shown in the below molecular structures (Figure 2. 9), and it was reported to show a lower minimum inhibitory (MIC) concentration against S. aureus bacterial strains[72].

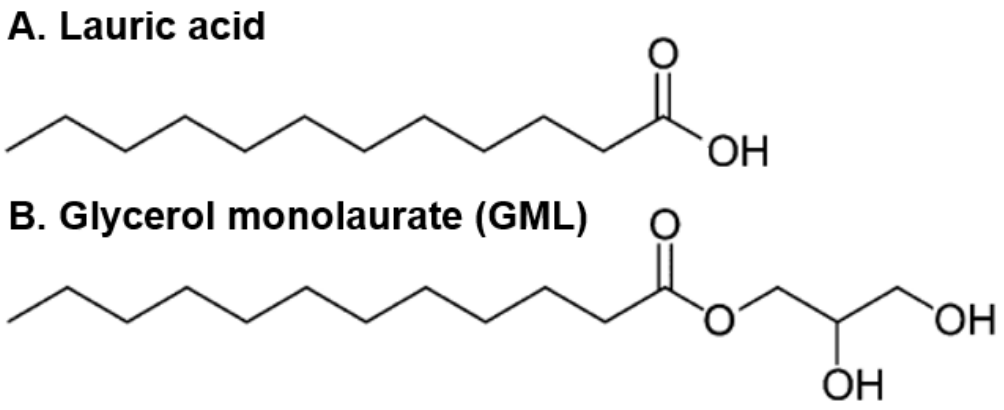

Figure 2. 12 Molecular structures of (A) lauric acid and (B) GML.

There has been a recent thorough study conducted on lauric acid and GML against supported lipid bilayer (SLB) platforms[72]. From the SLB study, it was observed that how membranes were morphologically destabilized when interacting with above and below critical micelle concentration (CMC) of tested antimicrobial lipids. Below fluorescence micrographs (Figure 2. 13) show the extreme morphological changes of lipid bilayer after the addition of GML leading to form growing entangled tubules and result in forming spherical caps at the end of injection.

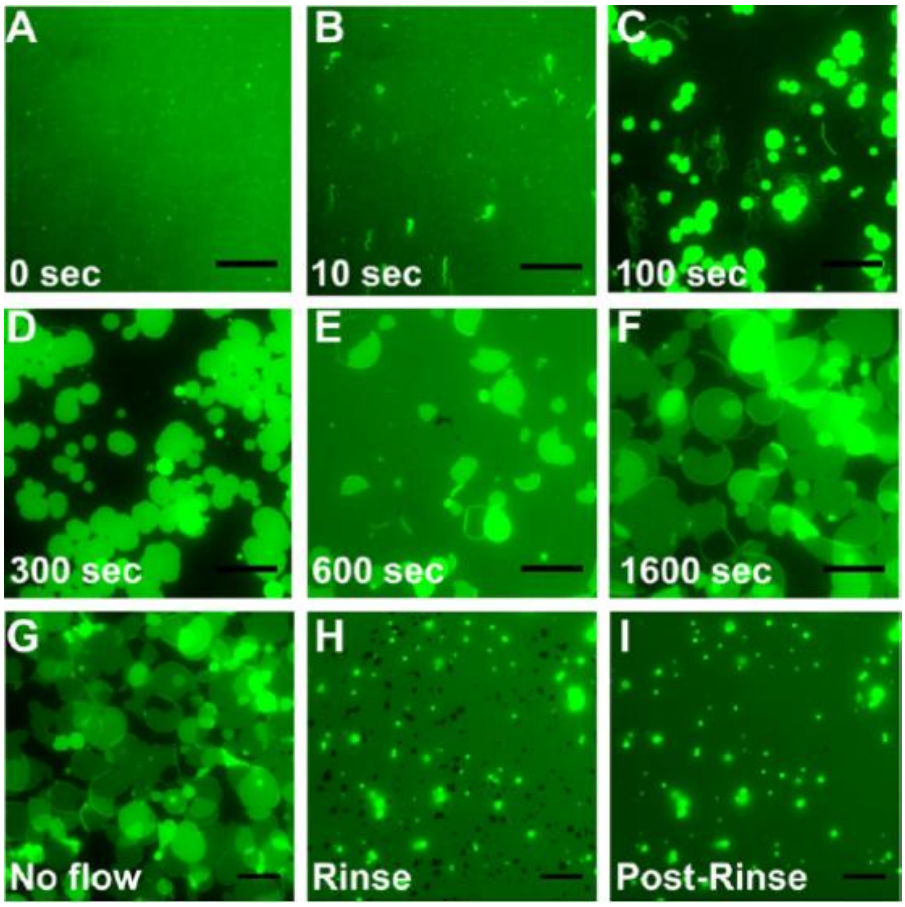

Figure 2. 13 Fluorescence micrographs of morphological changes of supported lipid bilayer after the addition of GML. 0 sec of time point indicates the addition of 500 μM of GML into the fluidic chamber. Scale bars indicate 20 μm. The fluorescence micrographs were re-produced from Yoon et al[72].

As it was stated in work by Giger et al[73], 2-dimensional SLBs have confined structures and a limited ability to freely expand and contract. Hence, creating and observing any three-dimensional structures upon interaction with fatty acids or any other membrane-specific agents are hindered, and the confinement and corresponding membrane-substrate interactions induce artificial morphological responses, in contrast to less constricted GUVs with more degrees of freedom. Also, depending on one's experimental purpose, each platform has different advantages. For example, if one needs to observe small scale changes happening on the surface

of bilayer upon the interaction with membrane-active materials, then employing SLB will be more suitable because there are numerous surface-sensitive measurement techniques that can be employed. While, observing any overall morphological changes of cell structural model is mostly possible with GUV model platforms. Experimentally, there are significantly different results were observed between SLB and GUV models against the same membrane-active agents. While the SLB model platform employed studies against various fatty acids including lauric acid and GML conducted by Yoon et al[72] showed that formation of spherical protrusions with above CMC of GML as shown in the Figure 2. 13 of Chapter 2, the same above CMC of GML induced vesicle fission behaviors were induced from GUV models which were composed of same DOPC zwitterionic lipid as presented in Chapter 6. Hence, the structural difference (2-d vs. 3-d) between SLB and GUV models can induce significantly different morphological transformations against the same membrane-active agent. Also, fission and fusion behaviors derived from GUV, which is a structurally and dimensionally closely mimicking cell model platform, are more biologically relevant findings compared to tubular and budding formations observed from SLB model platform where its structural limitations hinders the freedom of lipid molecules to expand or contract.

References

1. Israelachvili, J.; Marcelja, S.; Horn, R., Physical principles of membrane organization. *Q. Rev. Biophys* **1980,** *13* (2), 121-200.

2. Simons, K.; Toomre, D., Lipid rafts and signal transduction. *Nature reviews Molecular cell biology* **2000,** *1* (1), 31-39.

3. Singer, S.; Nicolson, G. L., The fluid mosaic model of the structure of cell membranes. *Membranes and Viruses in Immunopathology; Day, SB, Good, RA, Eds* **1972**, 7-47.

4. Zagnoni, M., Miniaturised technologies for the development of artificial lipid bilayer systems. *Lab on a Chip* **2012,** *12* (6), 1026-1039.

5. Chan, Y. H.; Boxer, S. G., Model membrane systems and their applications. *Current Opinion in Chemical Biology* **2007,** *11* (6), 581-7.

6. Hardy, G. J.; Nayak, R.; Zauscher, S., Model cell membranes: Techniques to form complex biomimetic supported lipid bilayers via vesicle fusion. *Current opinion in colloid & interface science* **2013,** *18* (5), 448-458.

7. Jackman, J. A.; Knoll, W.; Cho, N.-J., Biotechnology applications of tethered lipid bilayer membranes. *Materials* **2012,** *5* (12), 2637-2657.

8. Cho, N.-J.; Frank, C. W., Fabrication of a planar zwitterionic lipid bilayer on titanium oxide. *Langmuir* **2010,** *26* (20), 15706-15710.

9. Hubbard, J.; Silin, V.; Plant, A. L., Self assembly driven by hydrophobic interactions at alkanethiol monolayers: mechanism of formation of hybrid bilayer membranes. *Biophysical chemistry* **1998,** *75* (3), 163-176.

10. Walde, P.; Cosentino, K.; Engel, H.; Stano, P., Giant vesicles: preparations and applications. *ChemBioChem* **2010,** *11* (7), 848-865.

11. Jesorka, A.; Orwar, O., Liposomes: technologies and analytical applications. *Annu. Rev. Anal. Chem.* **2008,** *1*, 801-832.

12. Maherani, B.; Arab-Tehrany, E.; R Mozafari, M.; Gaiani, C.; Linder, M., Liposomes: a review of manufacturing techniques and targeting strategies. *Current Nanoscience* **2011,** *7* (3), 436-452.

13. Cho, N.-J.; Hwang, L. Y.; Solandt, J. J.; Frank, C. W., Comparison of extruded and sonicated vesicles for planar bilayer self-assembly. *Materials* **2013,** *6* (8), 3294-3308.

14. Maurer, N.; Fenske, D. B.; Cullis, P. R., Developments in liposomal drug delivery systems. *Expert opinion on biological therapy* **2001,** *1* (6), 923-947.

15. Cho, N.-J.; Cho, S.-J.; Cheong, K. H.; Glenn, J. S.; Frank, C. W., Employing an amphipathic viral peptide to create a lipid bilayer on Au and TiO2. *Journal of the American Chemical Society* **2007,** *129* (33), 10050-10051.

16. Cho, N.-J.; Wang, G.; Edvardsson, M.; Glenn, J. S.; Hook, F.; Frank, C. W., Alpha-helical peptide-induced vesicle rupture revealing new insight into the vesicle fusion process as monitored in situ by quartz crystal microbalance-dissipation and reflectometry. *Analytical chemistry* **2009,** *81* (12), 4752-4761.

17. Richter, R. P.; Brisson, A. R., Following the formation of supported lipid bilayers on mica: a study combining AFM, QCM-D, and ellipsometry. *Biophysical Journal* **2005,** *88* (5), 3422-3433.

18. Richter, R. P.; Bérat, R.; Brisson, A. R., Formation of solid-supported lipid bilayers: An integrated view. *Langmuir* **2006,** *22* (8), 3497-3505.

19. Jackman, J. A.; Tabaei, S. R.; Zhao, Z.; Yorulmaz, S.; Cho, N.-J., Self-Assembly Formation of Lipid Bilayer Coatings on Bare Aluminum Oxide: Overcoming the Force of Interfacial Water. *ACS Applied Materials & Interfaces* **2015,** *7* (1), 959-968.

20. Cho, N.-J.; Kanazawa, K. K.; Glenn, J. S.; Frank, C. W., Employing two different quartz crystal microbalance models to study changes in viscoelastic behavior upon transformation of lipid vesicles to a bilayer on a gold surface. *Analytical chemistry* **2007,** *79* (18), 7027-7035.

21. Zan, G. H.; Cho, N.-J., Rupture of zwitterionic lipid vesicles by an amphipathic, α-helical peptide: Indirect effects of sensor surface and implications for experimental analysis. *Colloids and Surfaces B: Biointerfaces* **2014,** *121*, 340-346.

22. Jackman, J. A.; Zhao, Z.; Zhdanov, V. P.; Frank, C. W.; Cho, N.-J., Vesicle adhesion and rupture on silicon oxide: Influence of freeze–thaw pretreatment. *Langmuir* **2014,** *30* (8), 2152-2160.

23. Cho, N.-J.; Jackman, J. A.; Liu, M.; Frank, C. W., pH-Driven assembly of various supported lipid platforms: A comparative study on silicon oxide and titanium oxide. *Langmuir* **2011,** *27* (7), 3739-3748.

24. Cremer, P. S.; Boxer, S. G., Formation and spreading of lipid bilayers on planar glass supports. *Journal of Physical Chemistry B* **1999,** *103* (13), 2554-2559.

25. Jackman, J. A.; Kim, M. C.; Zhdanov, V. P.; Cho, N.-J., Relationship between vesicle size and steric hindrance influences vesicle rupture on solid supports. *Physical Chemistry Chemical Physics* **2016,** *18* (4), 3065-3072.

26. Zan, G. H.; Jackman, J. A.; Cho, N.-J., AH peptide-mediated formation of charged planar lipid bilayers. *Journal of Physical Chemistry B* **2014,** *118* (13), 3616-3621.

27. Reimhult, E.; Höök, F.; Kasemo, B., Temperature dependence of formation of a supported phospholipid bilayer from vesicles on SiO 2. *Physical Review E: Statistical, Nonlinear, and Soft Matter Physics* **2002,** *66* (5), 051905.

28. Jackman, J. A.; Choi, J.-H.; Zhdanov, V. P.; Cho, N.-J., Influence of osmotic pressure on adhesion of lipid vesicles to solid supports. *Langmuir* **2013,** *29* (36), 11375-11384.

29. Terasawa, H.; Nishimura, K.; Suzuki, H.; Matsuura, T.; Yomo, T., Coupling of the fusion and budding of giant phospholipid vesicles containing macromolecules. *Proceedings of the National Academy of Sciences* **2012,** *109* (16), 5942-5947.

30. Reeves, J. P.; Dowben, R. M., Formation and properties of thin-walled phospholipid vesicles. *Journal of cellular physiology* **1969,** *73* (1), 49-60.

31. Angelova, M. I.; Dimitrov, D. S., Liposome electroformation. *Faraday discussions of the Chemical Society* **1986,** *81*, 303-311.

32. Rodriguez, N.; Pincet, F.; Cribier, S., Giant vesicles formed by gentle hydration and electroformation: a comparison by fluorescence microscopy. *Colloids and Surfaces B: Biointerfaces* **2005,** *42* (2), 125-130.

33. Hanson, J. M.; Gettel, D. L.; Tabaei, S. R.; Jackman, J.; Kim, M. C.; Sasaki, D. Y.; Groves, J. T.; Liedberg, B.; Cho, N.-J.; Parikh, A. N., Cholesterol-Enriched Domain Formation Induced by Viral-Encoded, Membrane-Active Amphipathic Peptide. *Biophysical Journal* **2016,** *110* (1), 176-187.

34. Nadeem, A.; Sanborn, J.; Gettel, D. L.; James, H. C.; Rydström, A.; Ngassam, V. N.; Klausen, T. K.; Pedersen, S. F.; Lam, M.; Parikh, A. N., Protein receptor-independent plasma membrane remodeling by HAMLET: a tumoricidal protein-lipid complex. *Scientific reports* **2015,** *5*.

35. Oglęcka, K.; Rangamani, P.; Liedberg, B.; Kraut, R. S.; Parikh, A. N., Oscillatory phase separation in giant lipid vesicles induced by transmembrane osmotic differentials. *Elife* **2014,** *3*, e03695.

36. Moscho, A.; Orwar, O.; Chiu, D. T.; Modi, B. P.; Zare, R. N., Rapid preparation of giant unilamellar vesicles. *Proceedings of the National Academy of Sciences* **1996,** *93* (21), 11443-11447.

37. Menger, F. M.; Keiper, J. S., Chemistry and physics of giant vesicles as biomembrane models. *Current Opinion in Chemical Biology* **1998,** *2* (6), 726-732.

38. Karlsson, A.; Sott, K.; Markström, M.; Davidson, M.; Konkoli, Z.; Orwar, O., Controlled initiation of enzymatic reactions in micrometer-sized biomimetic compartments. *The Journal of Physical Chemistry B* **2005,** *109* (4), 1609-1617.

39. Sanborn, J.; Oglęcka, K.; Kraut, R. S.; Parikh, A. N., Transient pearling and vesiculation of membrane tubes under osmotic gradients. *Faraday discussions* **2013,** *161*, 167-176.

40. Takakura, K.; Toyota, T.; Sugawara, T., A novel system of self-reproducing giant vesicles. *Journal of the American Chemical Society* **2003,** *125* (27), 8134-8140.

41. Monnard, P. A.; DeClue, M. S.; Ziock, H. J., Organic Nano-Compartments as Biomimetic Reactors and Protocells. *Current Nanoscience* **2008,** *4* (1), 71-87.

42. Kurihara, K.; Okura, Y.; Matsuo, M.; Toyota, T.; Suzuki, K.; Sugawara, T., A recursive vesicle-based model protocell with a primitive model cell cycle. *Nature communications* **2015,** *6*.

43. Walde, P., Building artificial cells and protocell models: experimental approaches with lipid vesicles. *Bioessays* **2010,** *32* (4), 296-303.

44. Oglecka, K.; Sanborn, J.; Parikh, A. N.; Kraut, R. S., Osmotic gradients induce bio-reminiscent morphological transformations in giant unilamellar vesicles. *Frontiers in physiology* **2012,** *3*, 120.

45. Henriksen, J.; Rowat, A. C.; Ipsen, J. H., Vesicle fluctuation analysis of the effects of sterols on membrane bending rigidity. *European Biophysics Journal* **2004,** *33* (8), 732-741.

46. Loftus, A. F.; Noreng, S.; Hsieh, V. L.; Parthasarathy, R., Robust measurement of membrane bending moduli using light sheet fluorescence imaging of vesicle fluctuations. *Langmuir* **2013,** *29* (47), 14588-14594.

47. Carlson, L.-A.; Hurley, J. H., In vitro reconstitution of the ordered assembly of the endosomal sorting complex required for transport at membrane-bound HIV-1 Gag clusters. *Proceedings of the National Academy of Sciences* **2012,** *109* (42), 16928-16933.

48. Papo, N.; Shai, Y., A molecular mechanism for lipopolysaccharide protection of Gram-negative bacteria from antimicrobial peptides. *Journal of Biological Chemistry* **2005,** *280* (11), 10378-10387.

49. Papo, N.; Shai, Y., Effect of drastic sequence alteration and D-amino acid incorporation on the membrane binding behavior of lytic peptides. *Biochemistry* **2004,** *43* (21), 6393-6403.

50. Papo, N.; Shai, Y., Can we predict biological activity of antimicrobial peptides from their interactions with model phospholipid membranes? *Peptides* **2003,** *24* (11), 1693-1703.

51. Huang, R.-H.; Xiang, Y.; Liu, X.-Z.; Zhang, Y.; Hu, Z.; Wang, D.-C., Two novel antifungal peptides distinct with a five-disulfide motif from the bark of Eucommia ulmoides Oliv. *FEBS letters* **2002,** *521* (1-3), 87-90.

52. Huang, L. C.; Petkova, T. D.; Reins, R. Y.; Proske, R. J.; McDermott, A. M., Multifunctional roles of human cathelicidin (LL-37) at the ocular surface. *Investigative ophthalmology & visual science* **2006,** *47* (6), 2369-2380.

53. Tossi, A.; Sandri, L.; Giangaspero, A., Amphipathic, α-helical antimicrobial peptides. *Peptide Science* **2000,** *55* (1), 4-30.

54. Tossi, A.; Tarantino, C.; Romeo, D., Design of synthetic antimicrobial peptides based on sequence analogy and amphipathicity. *European Journal of Biochemistry* **1997,** *250* (2), 549-558.

55. Lee, M.-T.; Hung, W.-C.; Chen, F.-Y.; Huang, H. W., Mechanism and kinetics of pore formation in membranes by water-soluble amphipathic peptides. *Proceedings of the National Academy of Sciences* **2008,** *105* (13), 5087-5092.

56. Tamba, Y.; Yamazaki, M., Single giant unilamellar vesicle method reveals effect of antimicrobial peptide magainin 2 on membrane permeability. *Biochemistry* **2005,** *44* (48), 15823-15833.

57. Ambroggio, E. E.; Separovic, F.; Bowie, J. H.; Fidelio, G. D.; Bagatolli, L. A., Direct visualization of membrane leakage induced by the antibiotic peptides: maculatin, citropin, and aurein. *Biophysical Journal* **2005,** *89* (3), 1874-1881.

58. dos Santos Cabrera, M. P.; Alvares, D. S.; Leite, N. B.; Monson de Souza, B.; Palma, M. S.; Riske, K. A.; Ruggiero Neto, J. o., New insight into the mechanism of action of wasp mastoparan peptides: lytic activity and clustering observed with giant vesicles. *Langmuir* **2011,** *27* (17), 10805-10813.

59. Lee, J.; Hwang, J.-S.; Hwang, B.; Kim, J.-K.; Kim, S. R.; Kim, Y.; Lee, D. G., Influence of the papiliocin peptide derived from Papilio xuthus on the perturbation of fungal cell membranes. *FEMS microbiology letters* **2010,** *311* (1), 70-75.

60. Park, C.; Lee, D. G., Fungicidal effect of antimicrobial peptide arenicin-1. *Biochimica et Biophysica Acta (BBA)-Biomembranes* **2009,** *1788* (9), 1790-1796.

61. Hwang, B.; Hwang, J.-S.; Lee, J.; Lee, D. G., Antifungal properties and mode of action of psacotheasin, a novel knottin-type peptide derived from Psacothea hilaris. *Biochemical and biophysical research communications* **2010,** *400* (3), 352-357.

62. Huang, H. W., Free energies of molecular bound states in lipid bilayers: lethal concentrations of antimicrobial peptides. *Biophysical Journal* **2009,** *96* (8), 3263-3272.

63. Huang, C.-J.; Tseng, P.-Y.; Chang, Y.-C., Effects of extracellular matrix protein functionalized fluid membrane on cell adhesion and matrix remodeling. *Biomaterials* **2010,** *31* (27), 7183-7195.

64. Cho, N.-J.; Cho, S.-J.; Hardesty, J. O.; Glenn, J. S.; Frank, C. W., Creation of lipid partitions by deposition of amphipathic viral peptides. *Langmuir* **2007,** *23* (21), 10855-10863.

65. Heerklotz, H., Interactions of surfactants with lipid membranes. *Quarterly reviews of biophysics* **2008,** *41* (3-4), 205-264.

66. Desbois, A. P.; Smith, V. J., Antibacterial free fatty acids: activities, mechanisms of action and biotechnological potential. *Applied microbiology and biotechnology* **2010,** *85* (6), 1629-1642.

67. Inaoka, Y.; Yamazaki, M., Vesicle fission of giant unilamellar vesicles of liquid-ordered-phase membranes induced by amphiphiles with a single long hydrocarbon chain. *Langmuir* **2007,** *23* (2), 720-728.

68. Tamba, Y.; Ohba, S.; Kubota, M.; Yoshioka, H.; Yoshioka, H.; Yamazaki, M., Single GUV method reveals interaction of tea catechin (−)-epigallocatechin gallate with lipid membranes. *Biophysical Journal* **2007,** *92* (9), 3178-3194.

69. Peterlin, P.; Arrigler, V.; Kogej, K.; Svetina, S.; Walde, P., Growth and shape transformations of giant phospholipid vesicles upon interaction with an aqueous oleic acid suspension. *Chemistry and physics of lipids* **2009,** *159* (2), 67-76.

70. Mally, M.; Peterlin, P.; Svetina, S. a., Partitioning of oleic acid into phosphatidylcholine membranes is amplified by strain. *The Journal of Physical Chemistry B* **2013,** *117* (40), 12086-12094.

71. Tanaka, T.; Sano, R.; Yamashita, Y.; Yamazaki, M., Shape changes and vesicle fission of giant unilamellar vesicles of liquid-ordered phase membrane induced by lysophosphatidylcholine. *Langmuir* **2004,** *20* (22), 9526-9534.

72. Yoon, B. K.; Jackman, J. A.; Kim, M. C.; Cho, N.-J., Spectrum of membrane morphological responses to antibacterial fatty acids and related surfactants. *Langmuir* **2015,** *31* (37), 10223-10232.

73. Giger, K.; Lamberson, E. R.; Hovis, J. S., Formation of complex three-dimensional structures in supported lipid bilayers. *Langmuir* **2008,** *25* (1), 71-74.

Chapter 3

Experimental Methodology

As mentioned in the previous chapter, various model membrane platforms have been proposed to utilize as simplified phospholipid membrane platforms to study membrane specific interactions which can possibly induce morphological changes. In this chapter, background theories of various model membrane platform preparations including small and giant sized liposome formations and experimental techniques employed throughout the thesis work including instrumentations and protocols which are necessary to characterize the interactions between model membrane and the foreign agent materials are described in detail.

3.1. Rationale for selection of materials and experimental techniques

In this chapter, the experimental methodologies used throughout the thesis will be explained in detail and presented as three main sections; (i) main employed materials, (ii) lipid vesicle preparations including GUV, small unilamellar vesicle preparations and human liver microsomal containing GUV formation, and (iii) major experimental/characterization techniques used to obtain and analyze the experimental data. The first section describes employed materials including phospholipids and any other lipid-related materials, compositions of prepared and utilized buffer solutions (glucose, sucrose and Tris buffer), antiviral peptide, fatty acids and monoglycerides and human liver microsomes. Lipid and any lipid-related reagents were used to form any necessary lipid-based cell membrane mimetic platforms including various types of liposomes and supported lipid bilayer. For each different lipid-based platform and preparations of foreign interacting materials including peptide, fatty acids-related reagents and human liver microsome for incorporating into GUV, specific buffer reagents were prepared and utilized. The second section explains the main principles of the various lipid-based platform preparations along with detailed protocols. Briefly, extrusion method was used to create SUVs, and commercially available GUV formation instrument providing both formation capacitor and conductors for electroformation was employed to form GUV. Lastly, principles and any details of mainly employed experimental and characterization techniques are explained. Quartz crystal microbalance with dissipation (QCM-D) monitoring measurement was conducted to record any changes of mass and viscoelasticity of SLB formation. Microscopy techniques were mainly utilized for monitoring interactions of SLB, SUV, or GUV against above listed foreign materials. As for exploring and optimizing GUV electroformation parameters, light microscopy was used to monitor and record images and sizes of GUVs. To better capture and track any morphological changes of GUV, fluorescence microscopy techniques including both epifluorescence and spinning disc confocal microscopy were utilized. MATLAB-based GUV bending modulus

analysis was conducted and explained its working theory. Critical micelle concentration values of utilized fatty acids and monoglycerides prepared in glucose solution were measured using fluorescence spectroscopy measurements.

3.2. Materials

3.2.1. Lipid Reagents

1,2-dioleoyl-sn-glycero-3-phosphocholine (DOPC), 1-palmitoyl-2-oleoyl-*sn*-glycero-3-phosphocholine (POPC), cholesterol (ovine) (Chol), sphingomyelin (brain, porcine) (SM), 1,2-dioleoyl-*sn*-glycero-3-phosphoethanolamine-N-(lissamine rhodamine B sulfonyl) (Ammonium salt) (Rh-DPPE) were purchased in chloroform from Avanti Polar Lipids (Alabaster, AL, USA). All lipid related materials were stored at -20 ^{o}C freezer. The chemical structures of the phospholipid molecules employed in this thesis are shown in below **Figure 3.1.**

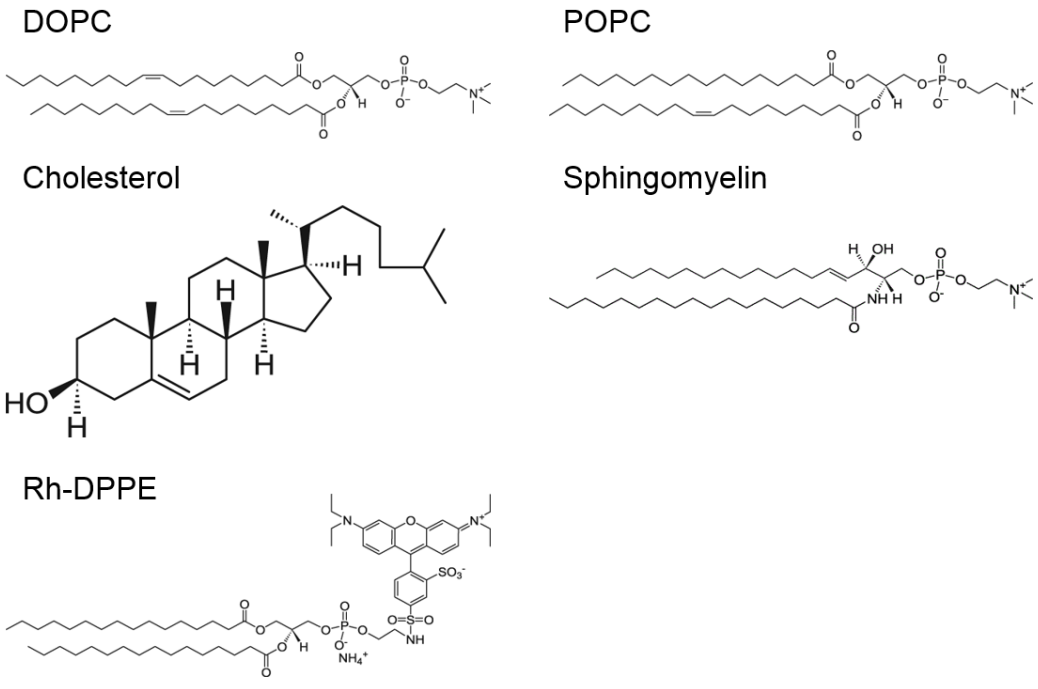

Figure 3. 1 Molecular structures of utilized lipid-related materials

3.2.2. Buffer Reagents

For all aqueous solutions used throughout the conducted experiments, deionized water was obtained from a with using 18.2 MΩ·cm MilliQ water (MilliPore, Oregon, USA). Specified concentrations of glucose and sucrose (both purchased from Sigma-Aldrich, St. Louis, MO, USA) solutions for GUV experiments were prepared. For all SLB-related or SUV formations, Tris buffer (10 mM Tris, 150 mM of NaCl and pH 7.5) was used unless otherwise noted. Tris and NaCl were both obtained from Sigma-Aldrich.

3.2.3. Peptide Reagents

Both amphipathic α-helical peptide (AH) and 5-TAMRA-AH peptide were synthesized by Anaspec Corporation (San Jose, CA, USA). The sequence of AH is H-Ser-Gly-Ser-Trp-Leu-Arg-Asp-Val-Trp-Asp-Trp-Ile-Cys-Thr-Val-Leu-Thr-Asp-Phe-Lys-Thr-Trp-Leu-Gln-Ser-Lys-Leu-Asp-Tyr-Lys-Asp-NH_2, and the sequence of fluorescence labeled TAMRA-AH is 5-TAMRA-Ser-Gly-Ser-Trp-Leu-Arg-Asp-Val-Trp-Asp-Trp-Ile-Cys-Thr-Val-Leu-Thr-Asp-Phe-Lys-Thr-Trp-Leu-Gln-Ser-Lys-Leu-OH. The peptide was prepared and diluted in Tris buffer or desired concentration of glucose solution before conducting the experiments.

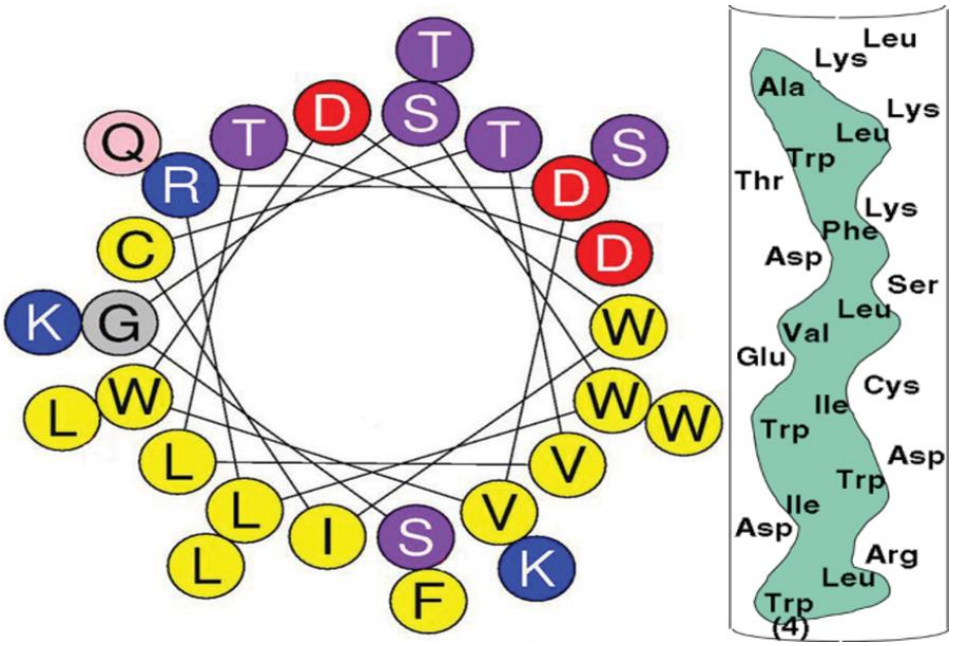

Figure 3. 2 Schematic diagram of AH peptide. (Left) Helical wheel diagram of AH peptide is reproduced from Jackman et al[1]. The projection of AH peptide shows an amphipathic distribution of the hydrophobic (yellow), hydrophilic (purple), positively charged (blue), and negatively charged (red) amino acid residues. (Right) Schematic diagram of AH peptide is depicted, wherein the cylindrical α-helical segment is cut along one direction and then flattened into the plane of the page. The amino acid sequence of NS5A from amino acids 4 to 27 in the N – C terminal direction is shown with the long continuous stretch of hydrophobicity indicated in green color (diagram reproduced from Cho et al[2]).

3.2.4. Fatty Acids and Monoglycerides Preparations

The desired mass of fatty acids and monoglycerides powder were measured and prepared. For each measurement trial, stock solutions (concentrations higher than 200mM) of GML (Abcam, Cambridge, U.K.), monocaprin (Abcam) and 1-O-Dodecyl-rac-glycerol (DDG) (Angene International, U.K.) were prepared by first dissolving the weighed powders in 300 mM glucose solution. As for the lauric acid (Sigma-Aldrich), it was first dissolved in 100% ethanol to a final concentration of

200 mM, and then each diluted aliquot was prepared using 300 mM glucose solution. In order to completely solubilize all stock/diluted samples, the solutions were placed in a 70 °C water bath for 30 min and cooled down for at least 10 min. All sample solutions were prepared immediately before every experiment.

3.2.5. Human Liver Microsomes

Human liver microsomes (HLM) pooled from male human liver was purchased from Sigma-Aldrich. It was kept frozen at -70 °C until conducting experiments. For the actual experiments, the stock sample (10 mg/ml) was quickly thawed using a water bath at 37 °C. The stock was then aliquoted into smaller volume (5 µL).

3.3. Lipid Vesicle Preparations

3.3.1. Small Unilamellar Vesicle Preparations

Liposomes are consisted of closed shell lipid bilayers dispersed in aqueous solution, and among various sizes of lipid vesicles whose diameter is less than 200 nm is considered as Small Unilamellar vesicle (SUV)[3]. There are various methods that enable one to form the SUVs. Among many, sonication and extrusion methods are the most widely utilized methods. In this thesis, since the extrusion method has been reported as one of the most efficient SUV formation techniques that can mechanically produce consistent vesicle diameters[4], the extrusion method was employed to prepare SUVs consisting of POPC or DOPC. For the fluorescence microscopy measurement purposes, the lipids were mixed with 5 mol % of fluorescence labeled Rh-DPPE. The lipids in chloroform solution was dried under a gentle stream of nitrogen gas and will be placed under vacuum for overnight to completely dry the remaining chloroform. The dried lipid film was then hydrated in 1.0 mL of pH 7.5 Tris buffer solution with 10 mM Tris and 150 mM NaCl. In order to create 50±10 nm diameter of SUV, the vesicle solution was extruded through

100-nm, followed by 30-nm Nuclepore^{TM} track-etched polycarbonate membranes (Whatman Schleicher & Schuell, Dassel, Germany) 27 times with using miniextruder (Avanti Polar Lipids). The resulting vesicle size was measured and confirmed by dynamic light scattering (DLS) (Brookhaven Instruments, N.Y., U.S.A.) measurements. SLB formation via vesicle rupture will be conducted on the silicon oxide surface of QCM-D quartz crystal or oxygen plasma treated glass coverslip. Following schematic diagram (**Figure 3.3**) describes each step of SUV formation via extrusion process.

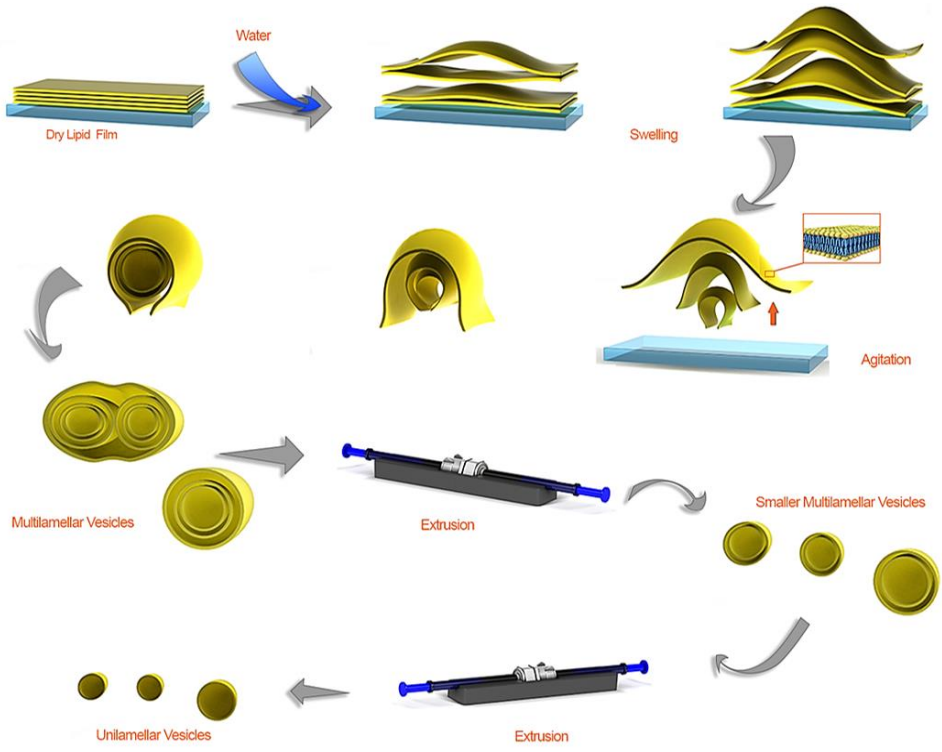

Figure 3. 3 Schematic diagram of overall procedure of extrusion method creating small unilamellar vesicle (SUV) from dried lipid film

3.3.2. Giant Unilamellar Vesicle Preparations

Giant unilamellar vesicles (GUVs) were prepared using the electroformation method[5] which enables one to generate the most defect-free and fairly consistent

diameters of GUVs. Briefly, stock solutions of lipid mixtures (mol:mol) were prepared at 1 mg/ml in chloroform (all lipids were purchased from Avanti Polar Lipids). For subsequent observation with florescence microscopy, GUVs are doped with trace concentrations (1%) of single labeled lipids, which include Rh- DPPE. ~20 μL of the prepared stock solution were spread onto each ITO-coated glass slide (25-30 Ω) within an area delimited by an O-ring and allowed to dry in vacuum desiccator for at least 1 hr. The slides are then put into vacuum desiccators for at least 1 h to completely remove any remaining chloroform residuals. Then, a chamber, acting as a simple capacitor, is formed by bridging the conductive sides of both ITO slides with a 1 mm thick rubber 'O' ring held in place with high vacuum grease from Dow Corning (Midland, MI). Before the 2nd ITO slide is connected to the rubber 'O' ring, the dried film is hydrated using a sucrose buffer solution. Using vacuum grease, the upper ITO-glass slide is placed over the ring with vacuum grease to seal the chamber and ensure that air cannot penetrate. Using a commercial Vesicle Prep Pro (Nanion, Munich, Germany), electroformation was performed with a 300 mM sucrose solution. GUVs utilized in this thesis were electroformed by applying an AC current at 5 Hz and 3 V and at 37 °C (for DOPC-GUV) or 45 °C (cholesterol and sphingomyelin containing GUV) for 120 min. The chamber is kept in a darkened room and covered during formation to protect any fluorescent probes. Lastly, for the confirmation of successful GUV formation or actual measurement imaing, the 5 ~ 10 μL of GUV sample solutions were diluted in a 300 mM glucose solution (normally 300 μL of volume) immediately before microscopy imaging.

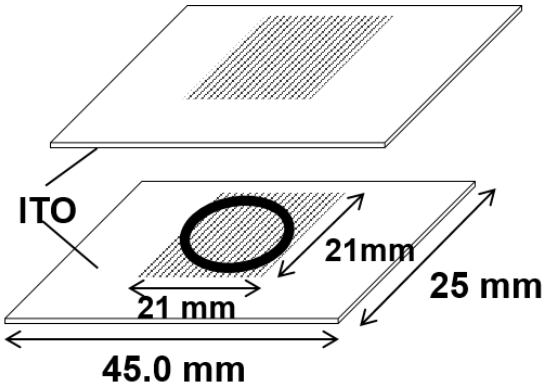

Figure 3. 4 Schematic diagrams of GUV electroformation preparation. Schematic diagram of the assembly of ITO slides in the Veislce Preppro chamber. The stripes represent thin lipid dried films consisting of 20 μg of DOPC, fabricated on each ITO slide conductive surface. An O-ring is sandwiched between the lipid films, encapsulating sucrose solution.

As abovementioned, throughout the thesis 3 V and 5 Hz of AC current were chosen as an optimized GUV electroformation parameter. The parameter was chosen after testing several possible conditions as presented in below figure plots. As shown below plots, either 5 or 10 Hz at 3V gives fairly consistent GUV size ranged from 10-40 μm diameter. However, the largest number of GUVs and most-defect free (data not shown) were found to be formed at 3 V and 5 Hz electroformation condition.

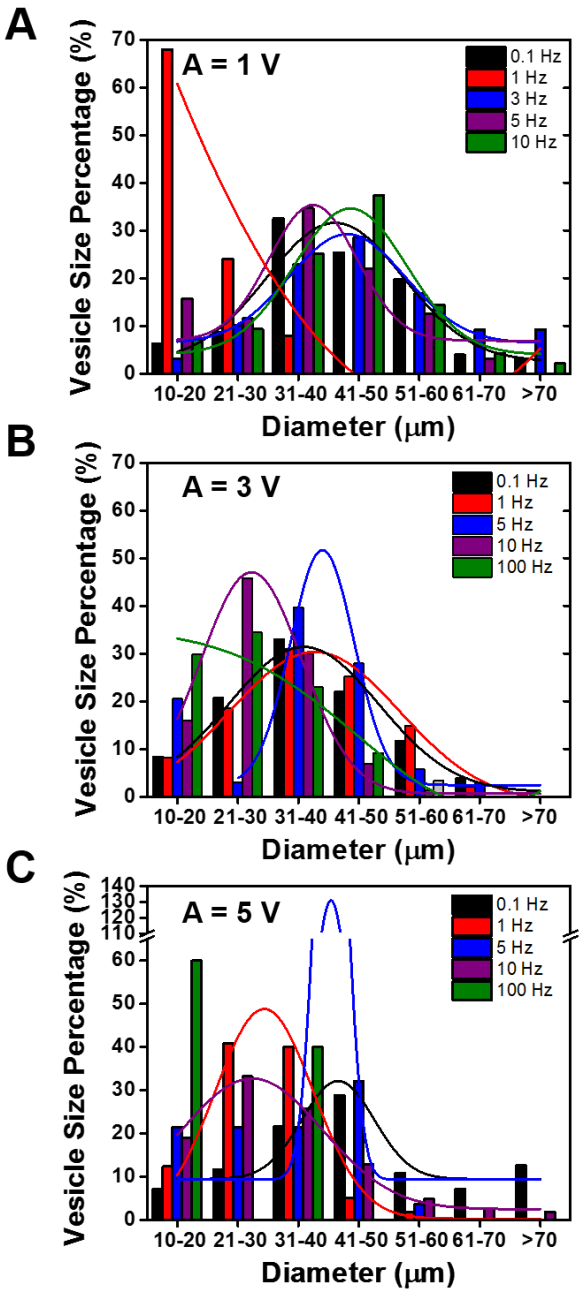

Figure 3. 5 Changes in vesicle size distribution of GUV electroformed at (A) 1 V, (B) 3V and (C) 5V, as a function of frequency.

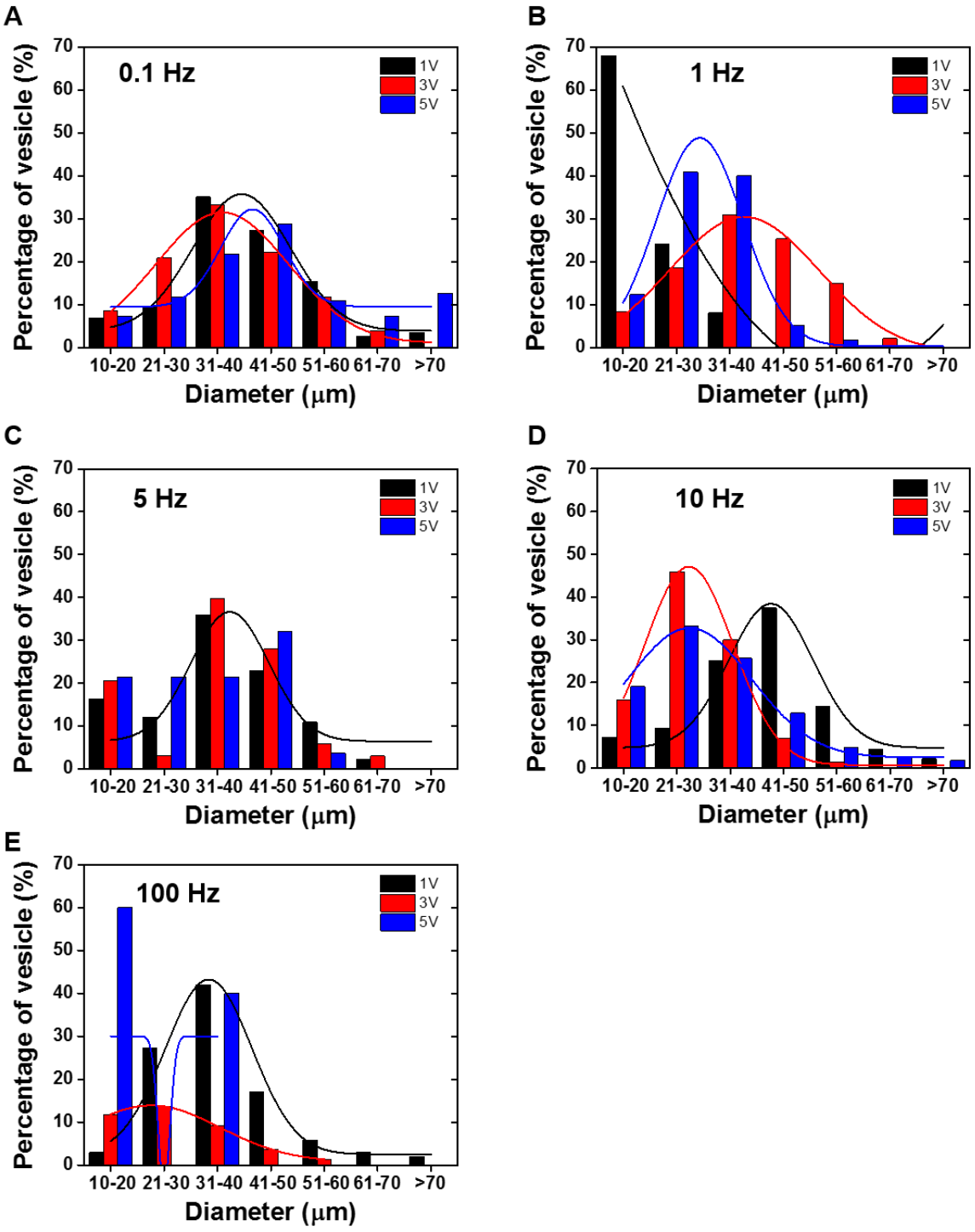

Figure 3. 6 Changes in vesicle size distributions of GUV electroformed at different frequencies, (A) 0.1 (B) 1, (C) 5, (D) 10 and (E) 100 Hz, as a function of peak-to-peak amplitudes.

3.3.3. Human Liver Microsome-Giant Unilamellar Vesicle Formation

In order to incorporate the HLM into bilayers of GUV, membrane protein incorporation method was followed[6]. Regular DOPC lipid drying over ITO coated glass was done for 1 hr for creating dried lipid film. Then, to incorporate desired amount of HLM into GUV bilayers, diluted HLM as 0.5 mg/ml using 300 mM sucrose solution (2 μL of volume) was gently spread over the dried lipid area using a glass syringe needle. It was then stored in vacuum desiccator for additional 6 hours. Lastly, using 300 mM of glucose as a hydration buffer solution, regular electroformation at 5 Hz and 3 V was conducted to generate HLM-DOPC GUVs. Following figure is the comparison micrographs of fluorescence labeled images of HLM containing DOPC GUVs and regular 100% DOPC GUV labeled with Rh-DPPE.

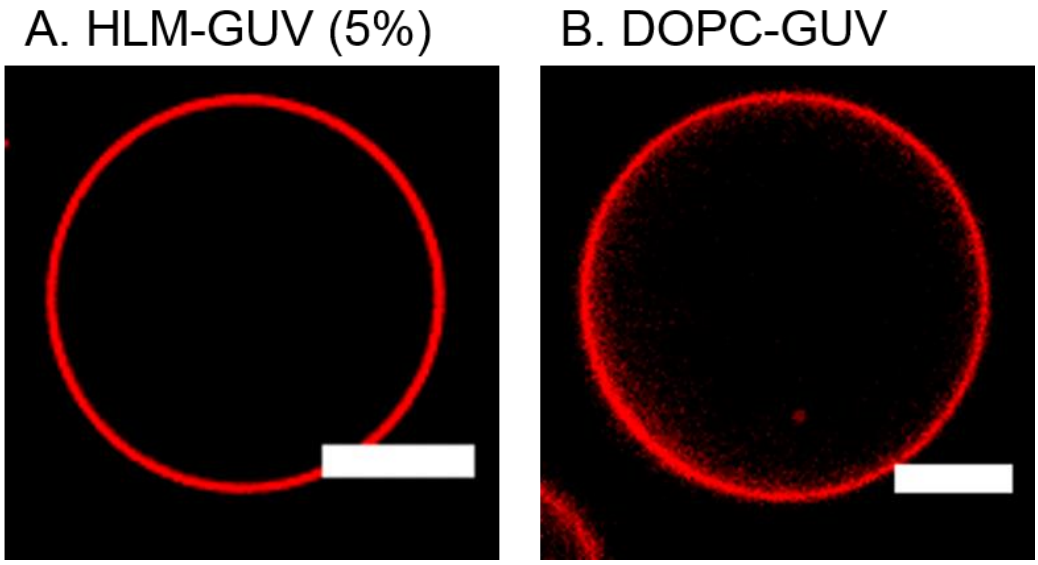

Figure 3. 7 Fluorescence images of (A) HLM-GUV (5% HLM) and (B) regular 100% DOPC GUV. Both fluorescence images were captured using spinning disk confocal microscopy with 60x oil-objective lens. Each scale bar indicates 10 μm.

3.4. Experimental/Characterization Techniques

In this section, the principles and specific analytical methods for each employed experimental techniques used throughout the thesis are explained.

3.4.1. Quartz Crystal Microbalance with Dissipation Measurement

Adsorption kinetics of the SLB formation via vesicle rupture process were measured and analyzed using a QCM-D on a Q-Sense E4 (Q-Sense AB, Gothenburg, Sweden). QCM-D allows to measure resonance frequency and energy dissipation simultaneously[7]. Briefly, providing alternating voltage potential against the quartz crystal placed between two metal electrodes, the crystal undergoes a periodic oscillation with the specific frequency as the set voltage potential. At its resonance frequency (5 MHz) of the quartz crystal, which is directly related to its surface thickness, any adsorbed mass changes on the surface can induce resonance frequency changes. The relationship between resonance frequency and the absorbed mass is formulated by Sauerbrey equation[8],

$$\Delta m = \frac{C}{n} \times \Delta f, \quad \text{(Eq. 3.1)}$$

where Δf is the changes in resonance frequency, n is harmonic number, Δm is the adsorbed mass and C is the sensitivity constant value (-17.7 ng/Hz·cm^2) which is derived from the following equation

$$C = \frac{t_q \times \rho_q}{f_o} \quad \text{(Eq. 3.2)}$$

where t_q is the thickness of the quartz and ρ_q is the density of quartz. QCM-D technique not only measures absorbed mass on the crystal, but it also can measure changes of viscoelastic properties of the adlayer by recording the decay in the free oscillations after the driving potential voltage against the crystal as shown in the schematic diagram (Figure 3.8).

As for the measurement, silicon oxide coated QCM crystal chips (AT-cut quartz crystals) (Q-sense) was utilized for QCM-D measurements for SLB formation as shown in the following schematic figure describing brief working principle.

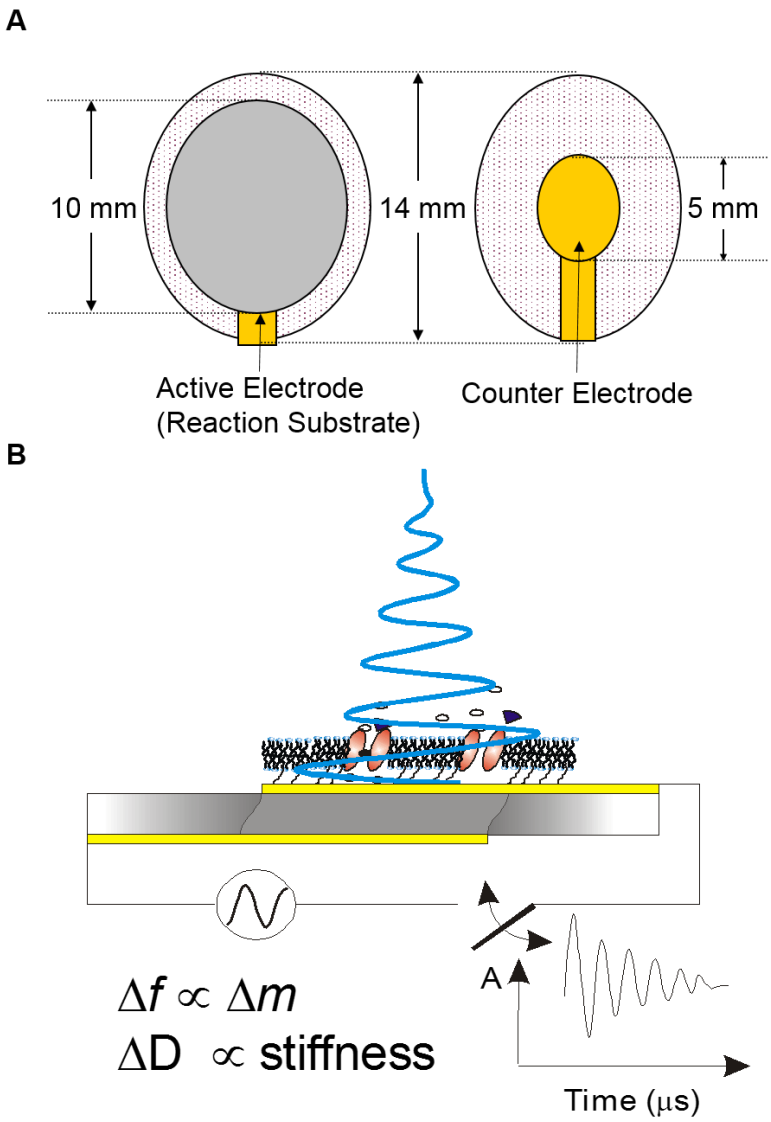

Figure 3. 8 Schematic representation of QCM-D measurement. (A) A diagram of quartz crystal is presented. (B) Oscillating crystal driven by the voltage is shown.

Before each measurement, the crystals were treated with oxygen plasma using a Plasma Cleaner (Harrick Plasma, Ithaca, N.Y., U.S.A.) at 29.6 W for 5 minutes. All measurements were recorded at the third overtone (15 MHz). A peristaltic pump

was used to introduce sample solution into the measurement chamber, with the flow rate fixed at 50 μL/min for all measurements.

3.4.2. Optical (light) Microscopy

Because of its micron-scale size, GUVs are capable of being directly monitored even by optical (light) microscopy (Eclipse Ti-U Microscope; Nikon, Japan). This feature enables one to monitor label-free (non-fluorescence labeled) GUV with its interactions against any possible foreign materials. While light microscopy images of GUV are able to produce distinguishable vesicle images, it has some limitations to clearly identify tracking membrane morphological changes. Below figure is the images of various sizes of GUVs captured by light microscopy.

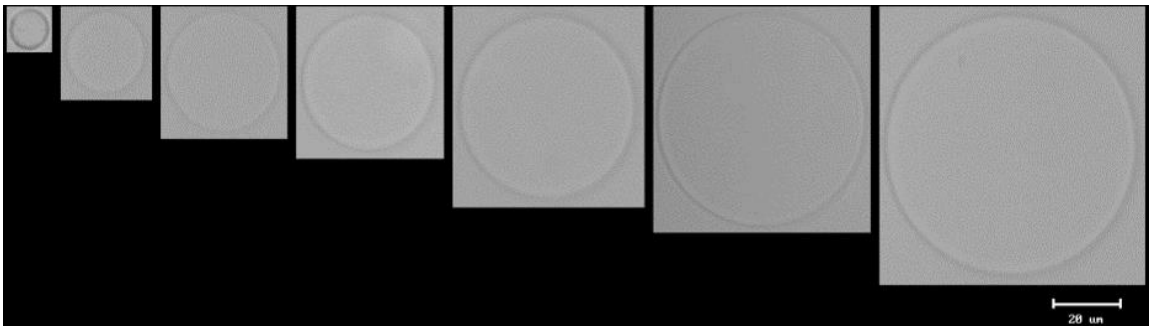

Figure 3. 9 Various diameters of GUVs imaged by light microscopy technique. Images were captured by 10x air objective lens. Note that the scale bar represents 20 μm.

3.4.3. Fluorescence Microscopy

Fluorescence Microscopy measurement technique[9] has become one of the essential techniques in the field of any bio and chemistry related scientific areas where real-time direct visualization of target sample is required. Hence, one can easily track any morphological changes by conducting real-time imaging of fluorophores tagged to molecules of interest. Both supported lipid bilayer and GUVs are well-suited to

be monitored by fluorescence microscopy. As the membranes are only nanometers thick and are confined in a planar geometry by solid supports, fluorescence imaging can be carried out without invoking the scanning in the axial direction. As for the GUV measurement, as abovementioned, the light microscopy images of GUV can still provide shape features of vesicles. To overcome the image resolution of the light microscopy and also to better capture sectioning images of such large volume objects, epifluorescence and spinning disk confocal microscopy (SDCM) techniques[10] were mainly employed throughout the main result chapters of the thesis. To further acquire more reliable sectioning images of GUVs, SDCM technique has been reported to be able to capture dynamics of GUVs or even living cells at high resolution and not sacrificing laser-source intensity preventing to have photobleaching issues during the measurement as shown in the following schematic figure briefly describing the structure of epifluorescence and SDCM microscope systems.

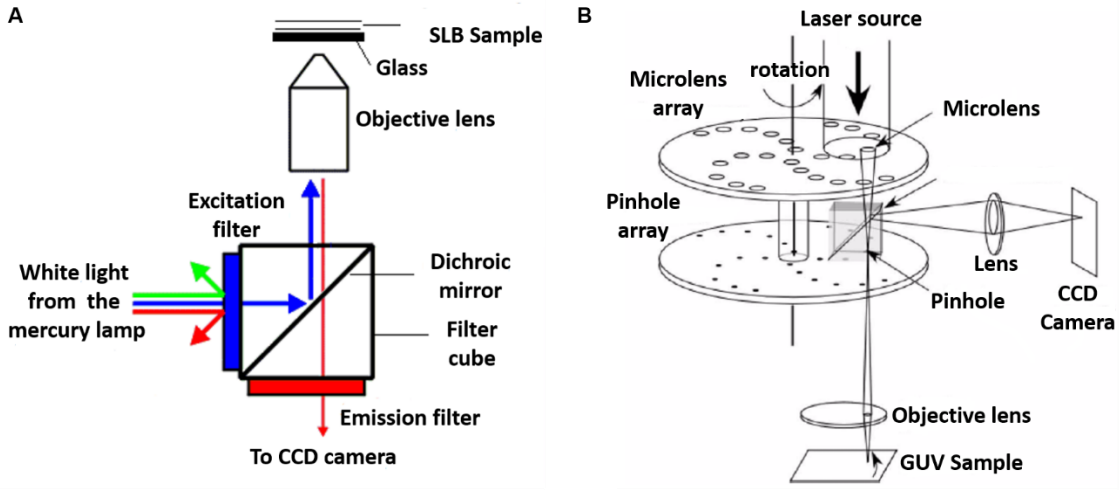

Figure 3. 10 Schematic diagram of comparing (A) epifluorescence and (B) spinning disc confocal microscopy.

SDCM measurements were carried out using an inverted Eclipse Ti-U microscope (Nikon) fitted with X-Light spinning-disk confocal unit (CrestOptics, Italy) and an Andor iXon+ EMCCD camera (Andor Technology, Northern Ireland). For

measurements, a 60× oil immersion objective (Numerical aperture of 1.49) was utilized. Rh-DPPE (Ex/Em; 560/583) was exposed with a 50 mW 561 laser line. At least 5 number of GUVs were imaged for each experiment. Acquired images were processed using NIS Element AIR (Nikon) and ImageJ software (National Institute of Health, U.S.A). Below figure is the representative micrographs showing both regular epifluorescence and SDCM images of DOPC GUVs.

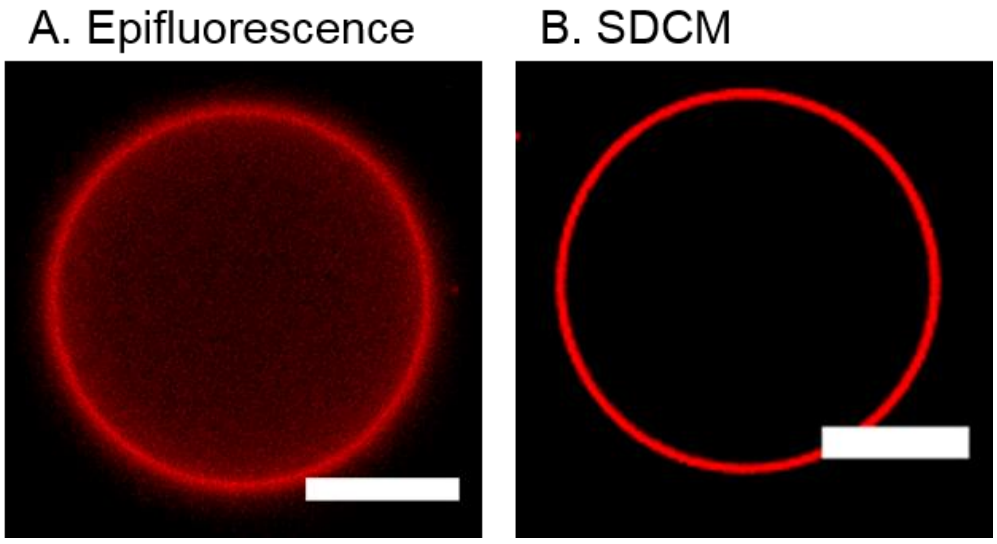

Figure 3. 11 Fluorescence micrographs of DOPC GUVs captured by (A) epifluorescence and (B) spinning disk confocal microscopy techniques. Both images were captured by using same 60x oil objective lens. Both scale bars indicate 10 μm.

3.4.4. Fluorescence Recovery After Photobleaching

In order to investigate lateral lipid diffusivity of the supported lipid bilayer to confirm the successful formation of bilayer on the substrate, fluorescence recovery after photobleaching (FRAP) measurement was conducted. Briefly, the SLB is illuminated by high intensity (typically, greater than 30-50 mW intensity) and a small circular sport on the bilayer is photobleached by the excitation light. As time progresses, the bleached fluorophores diffuse out of the bleached area and non-bleached fluorophores diffuse into the area as well. Hence, the overall fluorescence

intensity of the bleached spot can be recovered back to its original value up to ~ 95%. Before carrying out the measurement, 0.5% molar ratio of Rh-DPPE was mixed with the lipids to trace fluorescently labeled lipid molecules under epi-fluorescence microscopy. Subsequently, diluted vesicle solution was introduced and ruptured to form the SLBs on a clean and hydrophilic glass coverslip (Menzel-Glaser, Germany) placed in a custom-made flow cell chamber, a volume of 350µL, fitted onto the microscopy XY stage. The flow cell chamber mounted on the Eclipse TI-U microscope and a 60x magnification (NA 1.49) oil immersion objective were used for measurements resulting in a camera pixel size of 0.267 x 0.267µm. The measurements will be done at room temperature. A TRITC filter was used to filter out the excitation light and the emission light from the measurements with rhodamine fluorophores. Diode-pumped solid state lasers (Scherzo-532; Klastech GmbH, Germany) was employed to bleach the fluorophores at wavelength of 532nm to bleach the fluorophores. A fiber-coupled mercury lamp (Intensilight C-HGFIE; Nikon) was used to monitor the recovery of the fluorophores. Two pre-bleaching images will be obtained to correct for non-uniform illumination. Then, the center of imaging area will be bleached with the laser for 5 sec and following fluorescence recovery images will be collected for 2 minute at either 1 sec or 2 sec intervals. At least five different areas were bleached to improve statistics. The acquired images were analyzed using the Hankel Transform method which is based on circular averaging of each recovery image resulting a reduced spatial noise from the data analysis[11]. By comparing the Hankel Transform method with a traditional Axelrod method, the Hankel Transform method can compensate for temporal variation and drifts from illumination and bleaching during imaging[11-12]. Using the Hankel Transform method and stacked acquired image data, corresponding diffusion coefficient values from the normalized Hankel transform and fluorescence intensity recovery plots were obtained. Following schematic diagram briefly describes how the FRAP measurements are conducted.

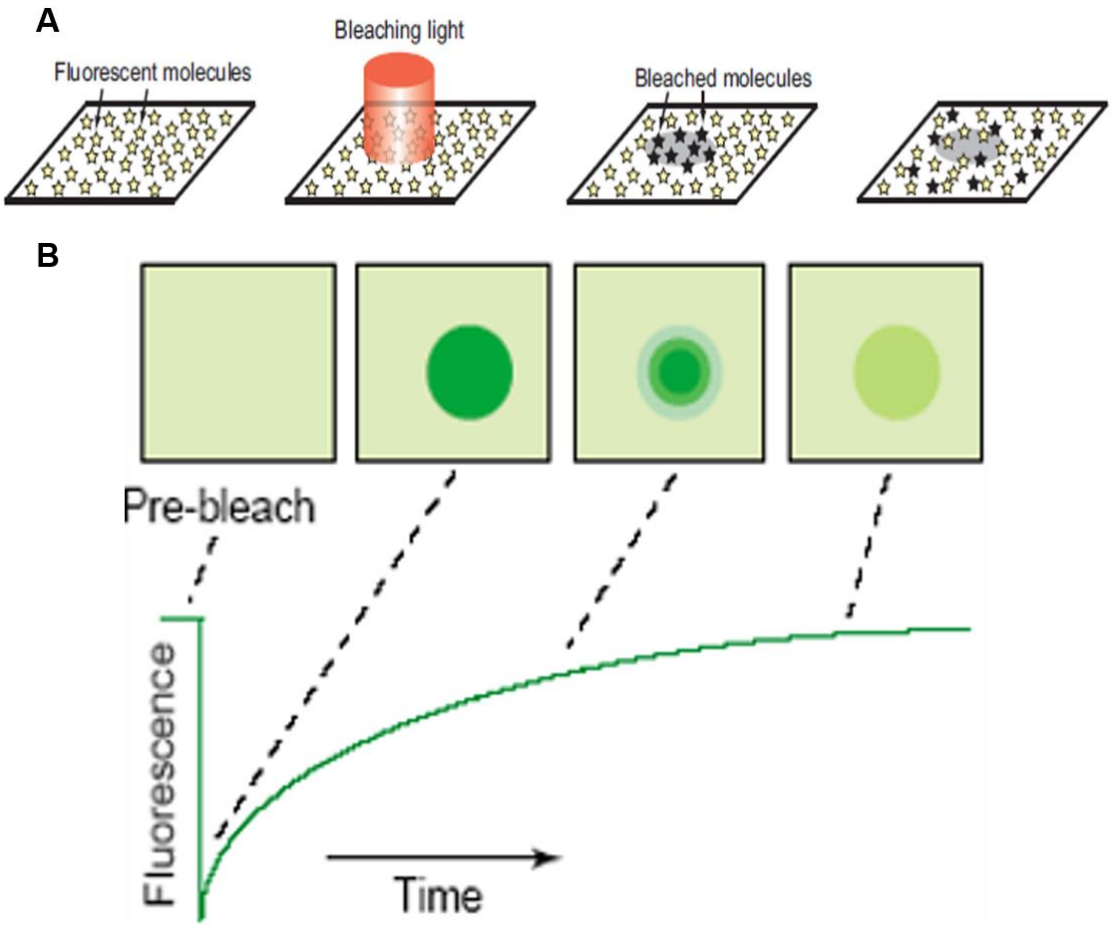

Figure 3. 12 A schematic representation of FRAP measurement conducted on supported lipid bilayers. (A) Brief experimental procedures of photobleaching are presented. (B) Simplified fluorescence intensity recovery plot is presented along with corresponding FRAP cartoon micrographs.

3.4.5. GUV Bending Modulus Analysis

Fluctuating vesicle membrane shape caused by membrane disruption due to any foreign interactions or environmental changes is measured and analyzed to calculate membrane rigidity. Contour of GUVs was determined from a two-dimensional cross section for specified time frame. The vesicle edge was measured and calculated using a developed MATLAB (The MathWorks, Natick, MA) code[13]. Briefly, a center of mass within the 2-dimensionally mapped vesicle image was estimated and

produced the selected time frame's images as sliced into angular wedges. From the newly generated slices, the bilayer edge was specified based on the maximum radial intensity gradient. Final value of bending modulus was calculated from the below equations using the edge profiles.

$$\xi(\gamma, t) = \frac{1}{2\pi R^2} \int_{\varphi=0}^{2\pi} [\rho(\varphi + \gamma, t) - \rho(t)][\rho(\varphi + t) - \rho(t)] d\varphi \quad \text{(Eq. 3.3)}$$

From the autocorrelation function respect to its angle is cosine decomposed, resulting in the mode amplitudes, χ_m. Then, the probability of distribution of amplitudes for a given mode gives exponential expression as following Eq 3.4,

$$\Gamma(\chi_m) \propto \exp\left[-L_m \frac{\chi_m}{2}\right] \quad \text{(Eq. 3.4)}$$

where $\Gamma_m(\chi_m)$ is the probability of acquiring an amplitude of χ_m and L_m is calculated from exponential fits to the estimated $\chi_m$values. Based on the expected theoretical from of the mode dependence of quasi-spherical vesicle fluctuations,

$$L_m\left(\frac{\kappa}{k_b T}, \bar{\sigma}\right) = \frac{\kappa}{k_b T} \frac{1}{\sum_{n \geq m}^{n_{max}} [Q_n^m(0)]^2 / \lambda(\bar{\sigma})} \quad \text{(Eq. 3.5)}$$

Where $L_m$values are fit by a least-square minimization. From the fit, κ becomes the final values of GUV bending modules, whereas $\bar{\sigma}$ becomes the reduced membrane tension.

3.4.6. Fluorescence Spectroscopy

In order to measure critical micelle concentration (CMC) values of all surfactants/fatty acids prepared in glucose buffer utilized in this thesis, fluorescence spectroscopy measurements were conducted. Cary Eclipse fluorescence spectrophotometer (Varian Inc., Australia) was employed to measure the fluorescence emission spectrum of the probe, 1-pyrenecarboxaldehyde, in 300 mM of glucose solution upon excitation at 365.5 nm in the presence of increasing concentrations of the test compound. The final concentration of the probe in the test

solution was set as 0.1 μM hydrated with the desired concentrations of tested samples. At least six times of emission spectrum were conducted and the values were averaged. Each averaged value was plotted and digressing point was determined as a CMC value.

References

1. Jackman, J. A.; Saravanan, R.; Zhang, Y.; Tabaei, S. R.; Cho, N. J., Correlation between membrane partitioning and functional activity in a single lipid vesicle assay establishes design guidelines for antiviral peptides. *Small* **2015,** *11* (20), 2372-2379.

2. Cho, N.-J.; Dvory-Sobol, H.; Xiong, A.; Cho, S.-J.; Frank, C. W.; Glenn, J. S., Mechanism of an Amphipathic α-Helical Peptide's Antiviral Activity Involves Size-Dependent Virus Particle Lysis. *ACS Chemical Biology* **2009,** *4* (12), 1061-1067.

3. Szoka Jr, F.; Papahadjopoulos, D., Comparative properties and methods of preparation of lipid vesicles (liposomes). *Annual review of biophysics and bioengineering* **1980,** *9* (1), 467-508.

4. Cho, N.-J.; Hwang, L. Y.; Solandt, J. J.; Frank, C. W., Comparison of extruded and sonicated vesicles for planar bilayer self-assembly. *Materials* **2013,** *6* (8), 3294-3308.

5. Angelova, M. I.; Soléau, S.; Méléard, P.; Faucon, F.; Bothorel, P., Preparation of giant vesicles by external AC electric fields. Kinetics and applications. In *Trends in Colloid and Interface Science VI*, Helm, C.; Lösche, M.; Möhwald, H., Eds. Steinkopff: Darmstadt, 1992; pp 127-131.

6. Shaklee, P. M.; Semrau, S.; Malkus, M.; Kubick, S.; Dogterom, M.; Schmidt, T., Protein incorporation in giant lipid vesicles under physiological conditions. *ChemBioChem* **2010,** *11* (2), 175-179.

7. Cho, N. J.; Frank, C. W.; Kasemo, B.; Höök, F., Quartz crystal microbalance with dissipation monitoring of supported lipid bilayers on various substrates. *Nat. Protoc.* **2010,** *5* (6), 1096-1106.

8. Sauerbrey, G., *Zeitschrift für physik* **1959,** *155* (2), 206-222.

9. Lichtman, J. W.; Conchello, J.-A., Fluorescence microscopy. *Nature methods* **2005,** *2* (12), 910-919.

10. Nakano, A., Spinning-disk Confocal Microscopy. A Cutting-Edge Tool for Imaging of Membrane Traffic. *Cell structure and function* **2002,** *27* (5), 349-355.

11. Jonsson, P.; Jonsson, M. P.; Tegenfeldt, J. O.; Hook, F., A Method Improving the Accuracy of Fluorescence Recovery after Photobleaching Analysis. *Biophys. J.* **2008,** *95* (11), 5334-5348.

12. Axelrod, D.; Koppel, D.; Schlessinger, J.; Elson, E.; Webb, W., Mobility measurement by analysis of fluorescence photobleaching recovery kinetics. *Biophys. J.* **1976,** *16* (9), 1055.

13. Loftus, A. F.; Noreng, S.; Hsieh, V. L.; Parthasarathy, R., Robust measurement of membrane bending moduli using light sheet fluorescence imaging of vesicle fluctuations. *Langmuir* **2013,** *29* (47), 14588-14594.

Chapter 4

Supported Lipid Bilayer Repair Mediated by Amphipathic, α-Helical Peptide*

The adsorption and fusion of small unilamellar lipid vesicles on silica-based substrates such as glass is a common method to fabricate supported lipid bilayers. Successful bilayer formation depends on a number of experimental conditions as well as on the quality of the vesicle preparation. Inevitably, a small fraction of unruptured vesicles always remains in a supported bilayer, and this kind of defect can have devastating influences on the morphological and electrical properties of the supported bilayer when used as a biosensing platform. Here, we report a simple method to improve the completeness of supported bilayers by adding a vesicle-rupturing peptide as a final step in the fabrication process. Peptide treatment reduces the fraction of unruptured vesicles to less than 1%, as determined by epifluorescence microscopy and quartz crystal microbalance-dissipation (QCM-D) experiments. This protocol step can be easily incorporated into existing procedures for preparing high-quality supported lipid bilayers.

*This chapter has been published as "**Kim MC**, Gunnarsson A., Tabaei SR, Höök, F. and Cho NJ. Supported Lipid Bilayer Repair Mediated by AH Peptide. Physical Chemistry Chemical Physics 2016, 18, 3040-3047".

4.1. Introduction

Formation of planar lipid bilayers on solid supports using phospholipid self-assembly is broadly utilized in scientific research as a versatile means to generate biomimetic model platforms enabling detailed studies of highly complex biological cell membranes[1-2]. Progress made since the first discovery of the successful formation of a model membrane mimicking cell membranes[1] has opened up a large variety of applications ranging from understanding fundamental phenomena of cellular membranes to highly advanced biomedical assays, including cell culture platforms[3, 4, 5, 6], biosensor development[3-4], drug screening[4-5] and medical diagnostics[6].

A large number of model membrane platforms has been explored, including the polymer-cushioned lipid bilayer[5, 7], tethered lipid bilayer[8-9], black lipid bilayer[10-11]and planar lipid bilayer[12-15]. Among the options, the planar supported lipid bilayer (SLB) has gained high popularity due to its high stability and the relatively simple procedures by which it can be formed[12, 15]. SLBs are typically produced by either Langmuir-Blodgett (LB) deposition[16] , solvent-assisted lipid bilayer (SALB) formation method[17-22] or surface-mediated vesicle fusion[23]. While LB deposition requires advanced equipment and several steps to sequentially transfer lipid monolayers to the solid substrate, the vesicle fusion method simply utilizes vesicle adsorption, followed by spontaneous rupture when a critical vesicle coverage has been reached on certain hydrophilic substrates including mica, glass or other silica-based surfaces[24]. For the vesicle fusion method, the pathways to cause vesicle rupture-forming lipid bilayers on solid supports are complex, and representative parameters responsible for vesicle fusion and rupture are numerous and include vesicle size[22], lipid composition[25], osmotic pressure[26], ionic strength[27], temperature[28], solution pH[29] and the presence of divalent cations[30].

Based on the aforementioned parameters, the interactions between lipid vesicles and solid supports can be tuned in order to promote or inhibit vesicle rupture leading to SLB formation. Nevertheless, the quality of the SLB with respect to defect density,

lateral mobility and the remaining number of non-ruptured vesicles may vary not only from situation to situation but also when attempts are made to perfectly reproduce identical experimental conditions. The imperfections may create significant fractions of inhomogeneity within the bilayer, which may in turn produce short circuits interrupting the measurement of electrical properties of membrane-bound channels[31] and also create artifacts when conducting fluorescence-based bilayer related assays.

Herein, we present a simple method to improve the completeness of supported lipid bilayers through a repair step that is aided by the capacity of an amphipathic α-helical (AH) peptide to induce vesicle rupture[32-34]. In a series of publications[20, 33, 34, 35, 36, 37, 38] from our groups and others, the capacity of this AH peptide to promote SLB formation has been explored, in particular on substrates[32-33, 35-36] and lipid compositions[15, 34, 37-38] that are not compatible with vesicle adsorption-induced SLB formation[15, 34, 37-38]. For example, Hardy *et al.* succeeded in employing the AH peptide to rupture HIV lipid envelope-mimicking vesicles into SLBs containing high fractions of cholesterol[39], recently extended by exploring concentration-dependent behaviors of SLB-peptide interactions using atomic force microscopy[40]. It has also been shown that using a tethered unilamellar vesicle assay with single-vesicle resolution, 100 nM AH peptide caused single zwitterionic lipid vesicles to rupture at rates that were inversely related to the vesicle diameter[41-43] and similar vesicle-rupture behavior was also observed with another related peptide analogue[38]. Inspired by these reports, we have in this work explored the possibility of using the AH peptide to repair inevitably occurring imperfections in SLBs generated using the vesicle fusion method. The AH peptide-controlled SLB repair process was investigated using the quartz crystal microbalance with dissipation (QCM-D) monitoring and epifluorescence microscopy techniques. Particular emphasis was put on exploring the possibility to generate high-quality and complete supported lipid bilayers utilizing lipid vesicles with increasing geometrical dimensions. Collectively, this new repair method is anticipated to provide an attractive tool

towards creating a defect-free supported lipid bilayer as a broad platform for various bioanalytical applications.

4.2. Experimental Methods

4.2.1. Lipid vesicle preparation

Various populations of lipid vesicles composed of 1-palmitoyl-2-oleoyl-*sn*-glycero-3-phosphocholine (POPC) lipid (Avanti Polar Lipids, Alabaster, AL) were prepared by the extrusion method[44]. Vesicles were extruded by using a Mini Extruder (Avanti Polar Lipids) through track-etched polycarbonate membranes (Whatman Schleicher & Schuell, Dassel, Germany) with pores ranging from 50 to 400 nm diameter. POPC lipids dissolved in chloroform were dried under a gentle stream of nitrogen gas and kept in vacuum to remove any remaining chloroform residue. To create various sizes of unilamellar vesicles, the vesicles were passed through the different-size pore membranes between 7 to 27 times by using the Mini Extruder. Each vesicle suspension was diluted to 0.2 $mg \cdot mL^{-1}$ before experiment. An aqueous buffer solution of 150 mM NaCl and 10 mM Tris in 18.2 MΩ·cm Milli-Q-treated water (Millipore, MA, USA) at pH 7.5 was used in all measurements.

4.2.2. Peptide reagent

The amphipathic, α-helical (AH) peptide was synthesized by Anaspec Corporation (San Jose, CA). The sequence of AH peptide is H-Ser-Gly-Ser-Trp-Leu-Arg-Asp-Val-Trp-Asp-Trp-Ile-Cys-Thr-Val-Leu-Thr-Asp-Phe-Lys-Thr-Trp-Leu-Gln-Ser-Lys-Leu-Asp-Tyr-Lys-Asp-NH_2. The peptide was prepared and diluted in Tris buffer before the measurements.

4.2.3. Dynamic light scattering

Dynamic light scattering (DLS) measurements were conducted on a 90Plus Particle Size Analyzer with a 658.0 nm monochromatic laser (Brookhaven Instruments Corporation, NY, USA) to measure size distributions of extruded vesicles. Every measurement was taken at a scattering angle of 90° at 25 °C. The light scattering data were collected by digital autocorrelator software (Brookhaven Instruments Corporation). In order to check for multi-modal distributions and to calculate the intensity-weighted Gaussian profile of various size distributions including average effective diameter and polydispersity, all autocorrelation functions acquired were analyzed by CONTIN and Non-Negatively Constrained Least Squares (NNLS) algorithms.

4.2.4. Quartz crystal microbalance-dissipation monitoring

Adsorption kinetics and properties of the adsorbed layer were monitored using the quartz crystal microbalance-dissipation (QCM-D) technique with a Q-Sense E4 instrument (Q-Sense AB, Gothenburg, Sweden). In QCM-D experiments, the resonance frequency and energy dissipation of the quartz crystal can be simultaneously obtained[15]. Silicon oxide-coated QCM crystal sensor chips (AT-cut quartz crystals) (Q-Sense) were used for each measurement. Before experiment, the crystals were treated with oxygen plasma using a Plasma Cleaner (Harrick Plasma, Ithaca, NY) at 80 W for 5 min. Experimental data were measured at various overtones (n = 3, 5, 7, 9 and 11), and corresponding changes in resonance frequency and energy dissipation were monitored. The obtained experimental data from the third to seventh overtones were fitted to the Sauerbrey model in order to calculate the effective thickness of the adsorbed layer[36].

4.2.5. Epifluorescence microscopy measurements

Epifluorescence imaging of supported lipid bilayers formed on a glass substrate was done with an inverted optical microscope (Eclipse TI-U microscope; Nikon, Japan). Imaging was done by using a 60x magnification (NA=1.49) oil immersion objective (Nikon) for measurements resulting in a camera pixel size of 0.267 x 0.267μm. iXon 512x512 pixel EMCCD camera (Andor Technology, Northern Ireland) was used to capture the fluorescence images, and a fiber-coupled mercury lamp (Intensilight C-HGFIE; Nikon) was used to excite the fluorophores. A TRITC filter was used to filter out the excitation light and the emission light from the measurements with Rh-PE fluorophores.

4.2.6. Fluorescence recovery after photobleaching

To conduct fluorescence recovery after photobleaching (FRAP) measurements, a circular spot of 20 μm diameter was photobleached for 5 sec by a 532 nm, 100mW laser (Klastech, Germany). Fluorescence micrographs were imaged for 90 sec at one sec interval, and the corresponding lateral diffusion coefficients were obtained based on the Hankel transform method[45].

4.3. Principle Outcomes & Discussion

The mechanism of vesicle fusion includes a complex sequence of steps involving vesicle adsorption, deformation, fusion, and rupture leading to reassembly that may eventually result in SLB formation (Figure 4. 1A and Figure 4. 2).

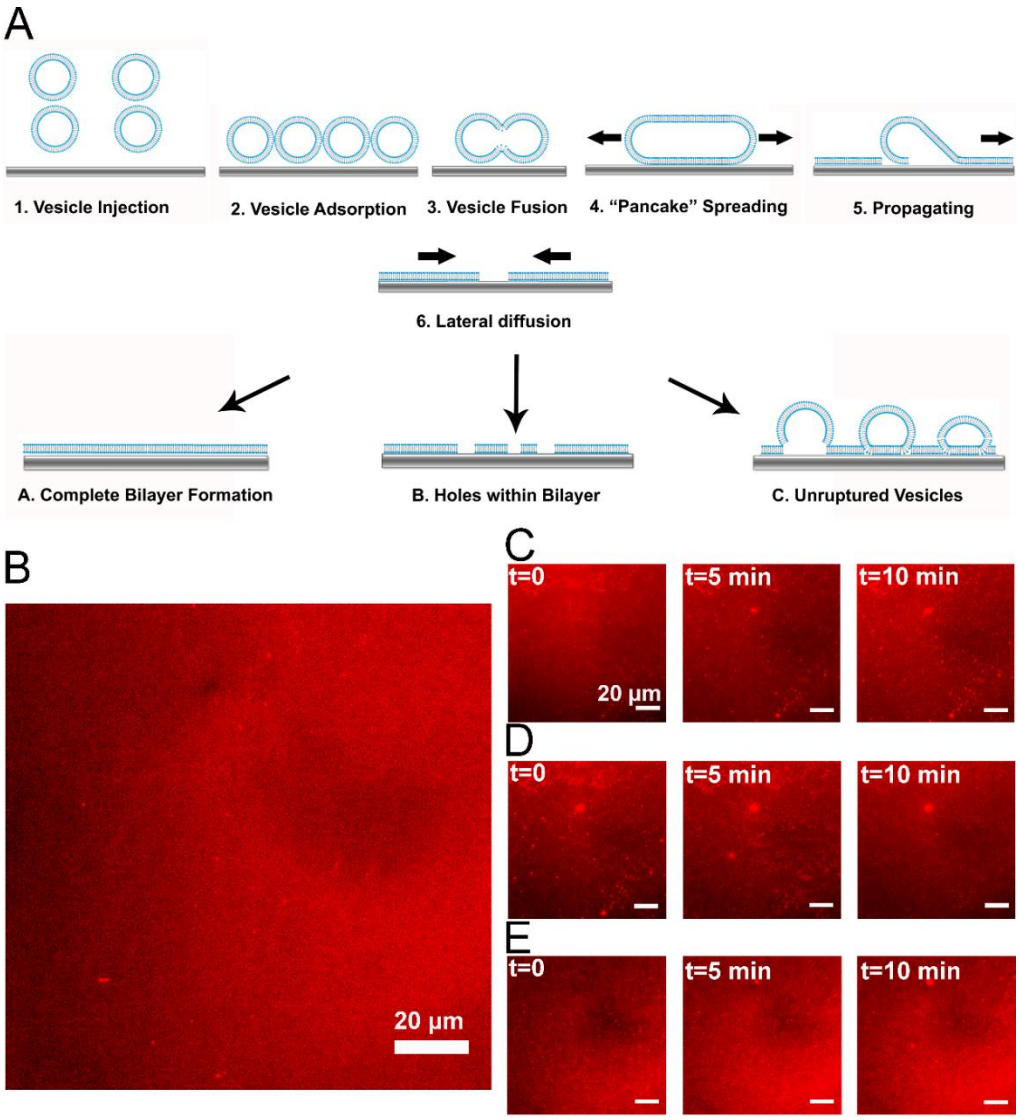

Figure 4. 1 Formation of supported lipid bilayer on glass substrate and its experimental defective cases. Schematics of (A) an overall process of supported lipid bilayer formation via vesicle fusion method on the glass substrate and its possible results after the critical vesicle rupture and following buffer washing. Supported lipid bilayer was formed on a glass substrate via vesicle fusion method using 30 nm. sized membrane filtered lipid vesicles. Herein, good and defective cases of planar lipid bilayer fluorescence images are presented, (B) complete lipid bilayer and (C-E) unruptured vesicles trapped on bilayers. After the rupture of the adsorbed vesicles, the lipid bilayer was washed with three different solvents, (C) initial Tris buffer (10 mM Tris, 150 mM NaCl and pH 7.5) (D) Milli-Q water and (E) Tris buffer (10mM Tris, 1 M NaCl and pH 7.5). Note that fluorescence image traces of each washing process were collected for 15 minutes. Each scale bar represents 20 μm.

Figure 4. 1B presents a typical fluorescence micrograph of a good-quality SLB (Figure S1C). However, even under optimal fabrication conditions, it is our experience that there always remain a number of unruptured or entrapped vesicles in the SLB, which can be easily visualized using epi- or total internal reflection-fluorescence microscopy measurements[46], as illustrated in Figures 4. 1(C)-(E). Upon SLB formation on silica using vesicles with a mean diameter of ca. 91 nm composed of POPC lipid, a significant number (1,000 per 136×136 μm^2) of unruptured vesicles remained bound also after extensive rinsing, either in Tris buffer or in deionized water, the latter of which induces a large osmotic pressure difference that could tentatively aid vesicle removal and SLB repair[26] (Figure 4. 1C, D). The limited effect obtained by rinsing in deionized water highlights that incomplete rupture or imperfect formation of SLB is common not only when there are large unruptured vesicles[47], but also when SLBs are formed using small vesicles (diameter less than 100 nm, See Figure 4. 3 for vesicle size distribution) owing to steric effect in saturated adlayers. Hence, a post-assembly repair method that could aid the formation of defect-free SLBs would be highly desirable.

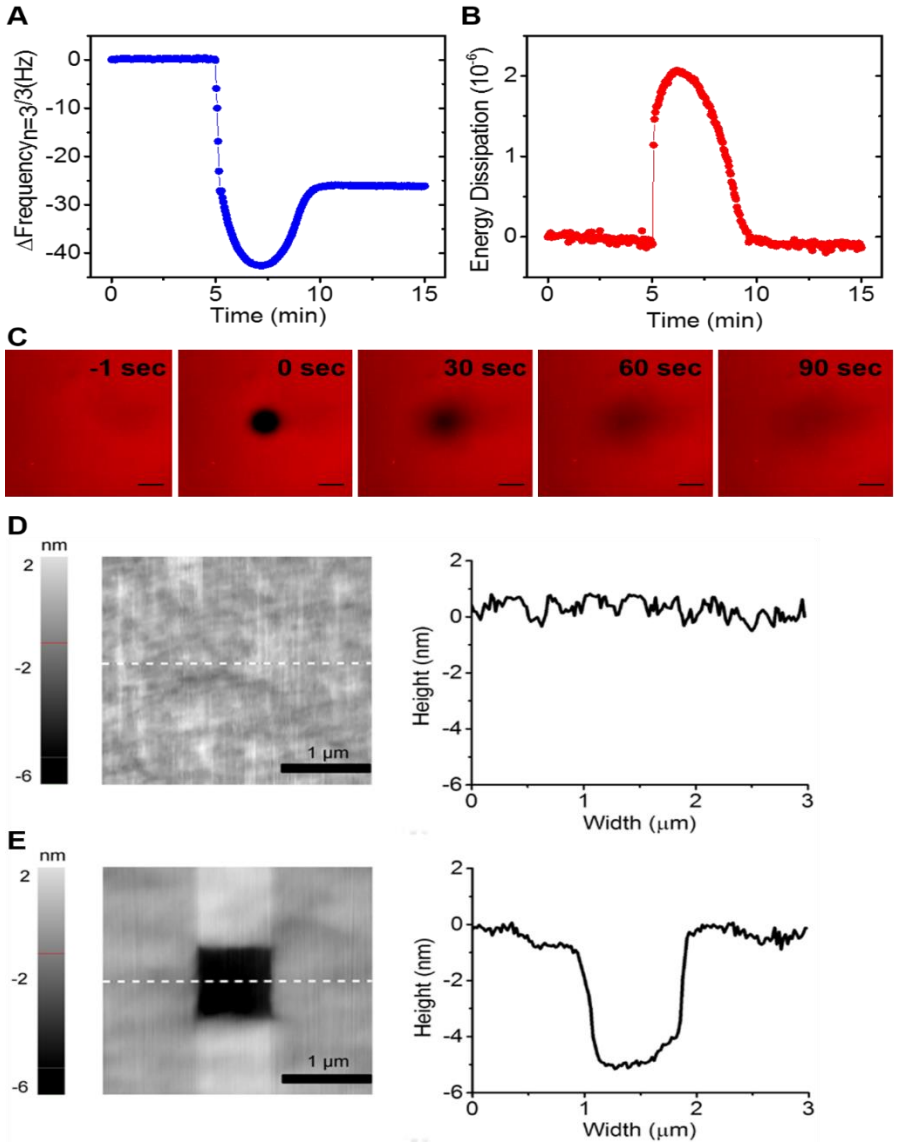

Figure 4. 2 Various characterizations on formation of complete supported lipid bilayer. (A-B) QCM-D monitoring of SLB formation on a silicon oxide substrate using 30nm filtered POPC vesicle fusion method. Changes in resonance frequency and energy dissipation were recorded at ~26 Hz and ~0, respectively. (C) Fluorescence recovery after photobleaching was conducted on the rhodamine-labeled (0.5 mol %) lipid bilayer. Time-lapse images before and after the photo bleaching were taken in 30 sec intervals. (D) Atomic force microscopy (AFM) image of supported lipid bilayer. AFM height image was taken on SLB formed on QCM-D silicon oxide substrate. (E) AFM height image after conducting a square test on the SLB. The test was conducted to measure the thickness of SLB by

scratching the bilayer SLB with an AFM cantilever tip which the imaging protocol described in Wallin et al[48].

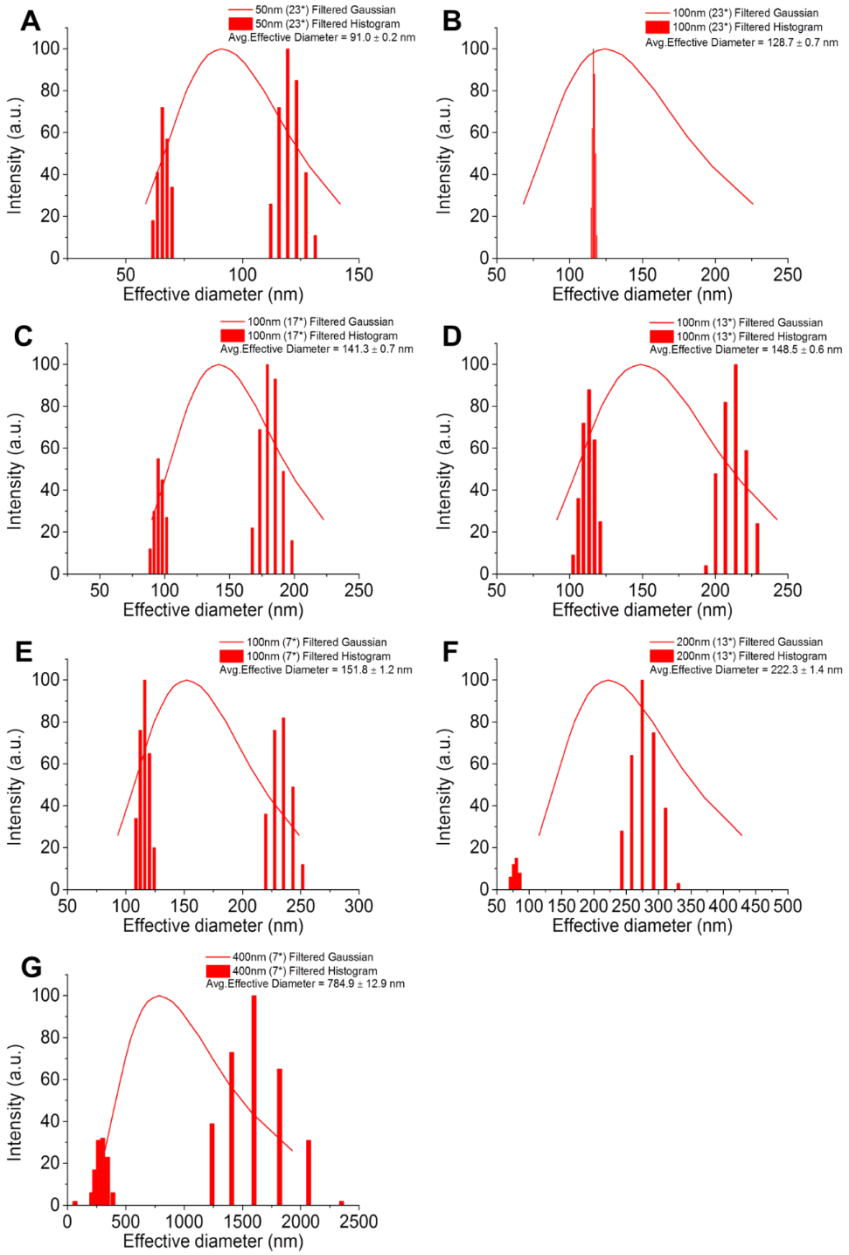

Figure 4. 3 Intensity-weighted size distribution of extruded vesicles as a function of extrusion pore diameter. Dynamic light scattering measurements were conducted on the extruded POPC vesicles. (A-G) Intensity-weighted Gaussian distributions and histogram are shown as functions of the extrusion pore diameter (50 to 400 nm diameter). While the histogram distribution reflects the relative amount of light that scattered by vesicles in

different size ranges, the Gaussian distribution assumes that the vesicle size distribution is centered on a mean particle size. The numbers with asterisk indicate how many times vesicle solutions were passed through the extrusion pore membranes.

4.2.7. Repair of unruptured trapped vesicles within SLBs

Based on the aforementioned studies[15, 33-35, 37-38, 41], it may be possible to rupture the bound vesicles trapped on the initially formed lipid bilayer by AH peptide. To date, AH peptide has been shown to be highly effective towards rupturing vesicles composed of any fluid-phase lipid compositions. In fact, Zan et al[34] reported that formation both positively and negatively charged SLB (tested up to 30 mol % of POEPC or POPS lipids) on titanium oxide substrate after the addition of AH peptide. Spontaneous SLB formation using highly negatively charged lipid vesicles (20 mol % or higher) was not possible on both silicon oxide and titanium oxide substrates without using AH peptide. Hardy et al reported that a successful SLB formation is containing large amount of cholesterol (45 mol %) using AH peptide[39]. Specifically, vesicles composed of POPC : POPE : POPS : sphingomyelin : cholesterol (9.35: 19.25: 8.25: 18.15: 45.00) mimicking the native lipid composition of the human immunodeficiency virus-1 (HIV-1) were used to form an intact vesicle layer adsorbed on silicon oxide substrate, and then AH peptide was introduced to rupture the adsorbed vesicle layer transforming them to complete lipid bilayer. Both reported studies support that AH peptide can promote bilayer formation via rupture process on substrates that are intractable to conventional (spontaneous) vesicle fusion methods. Hence, AH peptide can be used to rupture lipid vesicles across a wide range of membrane compositions, including highly charged phospholipids, large fractions of cholesterol, and sphingomyelin. We have previously proposed a mechanism for AH mediated transformation of intact vesicles to the bilayer by simultaneous QCM-D and optical reflectometry measurements[33]. Using the combined technique, we could monitor the time-dependent variation in adsorbed molecular mass (optical mass), adsorbed molecular mass and solvent mass (acoustic

mass), effective thickness, and effective reflective index of lipid adlayer during the course of AH interaction with surface-adsorbed lipid vesicles. Briefly, the process of AH-induced vesicle to bilayer transformation comprises of three steps: 1) AH peptide binding to vesicles, 2) swelling of vesicles 3) desorption of AH peptide and lipids resulting in formation of an adlayer with a thickness of ~5.1 nm and an effective refractive index of ~1.45, which are in very good agreement with expected values for a lipid bilayer. In order to explore this possibility, we utilized the QCM-D technique for tracking the kinetic changes upon addition of AH peptide and subsequent interaction with trapped unruptured vesicles. To obtain a sufficient number of unruptured vesicles trapped on and within the bilayer, we intentionally fabricated large vesicles (~220 nm) for substrate deposition as shown in Figure 4. 4A and B.

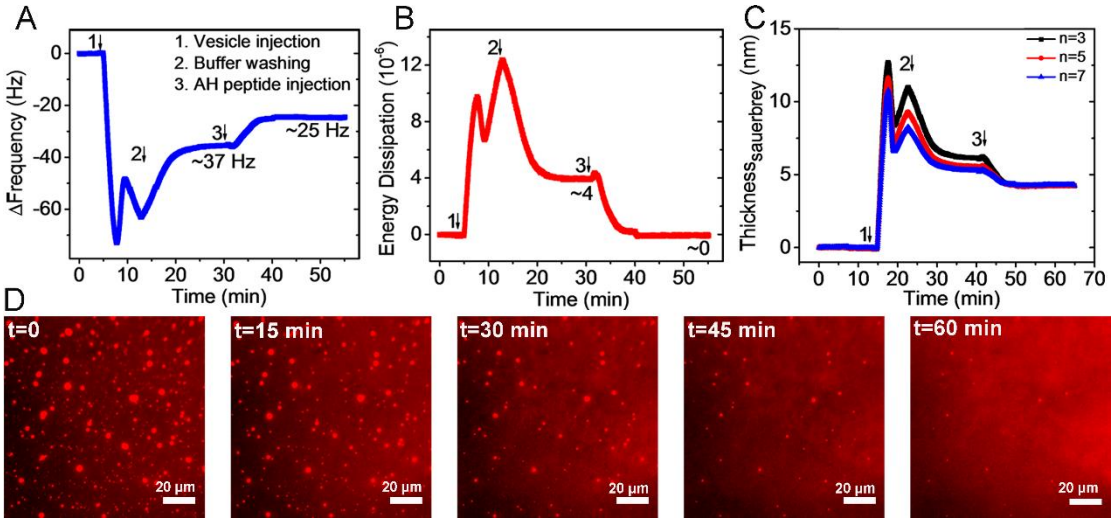

Figure 4. 4 SLB formation and its repairing mediated by AH peptide. After the vesicle (diameter ~ 222.1 nm) adsorption, initial rupture and AH peptide injection, changes in (A) resonant frequency and (B) energy dissipation were monitored. (C) Sauerbrey thickness of the adlayer. n = 3 (black line), n = 5 (red line), and n = 7 (blue line) overtones. (D) Time-lapse fluorescence micrographs of AH peptide-mediated SLB repair formed by 188-nm diameter lipid vesicles. Scale bars are 20 μm.

Upon injection of large-size vesicles onto the silicon oxide substrate, we typically

observed two-step kinetics[25] indicative of reaching a critical surface coverage of adsorbed vesicles before the fusion and rupture processes were initiated. However, during the latter process, vesicles were continuously adsorbed onto the substrate which is evidenced by the frequency decrease and dissipation increase after the first peak. Upon subsequent injections of Tris buffer, the frequency shift increased from -65.3 Hz to -37 Hz and the energy dissipation shift decreased from 12.2 to 4.0×10^{-6} (Figure 4. 4A-B), demonstrating suppressed vesicle adsorption and that a significant fraction of adsorbed unruptured vesicles were rinsed off. Nevertheless, the final changes in Δf and ΔD still deviated significantly from those corresponding to a complete SLB under (Δf ~ 26 Hz and ΔD ~ 0 x 10^{-6})[15], which indicates that a significant fraction of unruptured vesicles remained entrapped on the bilayer. To independently verify this suspicion, we employed epifluorescence microscopy to visualize unruptured vesicles, which were clearly visible as bright dots surrounded by a uniform lipid bilayer (Figure 4. 1C-E). Taking the contribution to the frequency shift originating from coupled water into account[49], the vesicle coverage estimated by the two methods are in good agreement with each other.

In order to promote complete SLB formation or repair the defects, 8 μM AH peptide were added to the bilayer, and time-sequential fluorescence micrographs were captured as shown in Figure 4. 4D. In addition, as a result of the peptide injection (see arrow 3 in Figure 4. 4A-B), the saturated QCM-D response upon peptide injection corresponded to the responses expected for a complete SLB,[24] i.e. Δf ~ -26 Hz and ΔD ~0×10^{-6} (Figure 4.3A-B). In order to further characterize the properties of the resulting adlayer, we applied the Sauerbrey model[36] to compute the effective thickness of the adlayer. For the calculations, 1,000 $kg\cdot m^{-3}$ was assumed as the density of the adlayer[36]. The Sauerbrey thickness for the different overtones reached saturation at ~12.7, ~10.9, and ~6.2 nm, respectively (Figure 4. 4C). As a result of AH peptide-mediated repair, the end-resulting thickness of the SLB obtained from the Sauerbrey was resulted at ~4.2 nm indicating that a complete SLB is formed with the aid of AH peptide.

Further to confirm the successful repair, the process of AH peptide-mediated rupturing of the remaining vesicles was visualized using a small fraction (0.5 mol %) of Rhodamine-labeled lipid vesicles imaged using epifluorescence microscopy, as shown in time-sequential micrographs (Figure 4. 4C). The AH peptide was injected after the vesicle fusion of large size vesicles (ca. ~188 nm diameter) and a subsequent buffer washing step. The presented micrographs show time-lapsed images after AH-peptide injection. After peptide injection, a vast majority of trapped vesicles were ruptured, signaling efficient repair of the SLB. The epifluorescence images were captured for a total of ~ 50 min after the injection and each frame of the sequential micrographs is shown at an interval of ~ 5.6 min. Note that there is a large deviation in time scales between that of QCM-D kinetic profiles and epifluorescence imaging, which is attributed to the different measurement chamber geometries and corresponding flow conditions and possibly also the different substrates (glass versus sputtered SiO_2).

To confirm the retainment of lateral diffusivity after AH-peptide addition, FRAP measurements were conducted before and after the repair as shown in Figure 4.4. It was confirmed that lipid mobility was still retained with a moderate drop of the diffusion coefficient from ~2.3 $\mu m^2 \cdot s^{-1}$ to ~0.9 $\mu m^2 \cdot s^{-1}$, but still displaying a mobile fraction of 89 % as shown in Figure 4. 5B. The decrease in lateral diffusivity of the SLB is likely due to a small fraction of bound AH peptide[35].

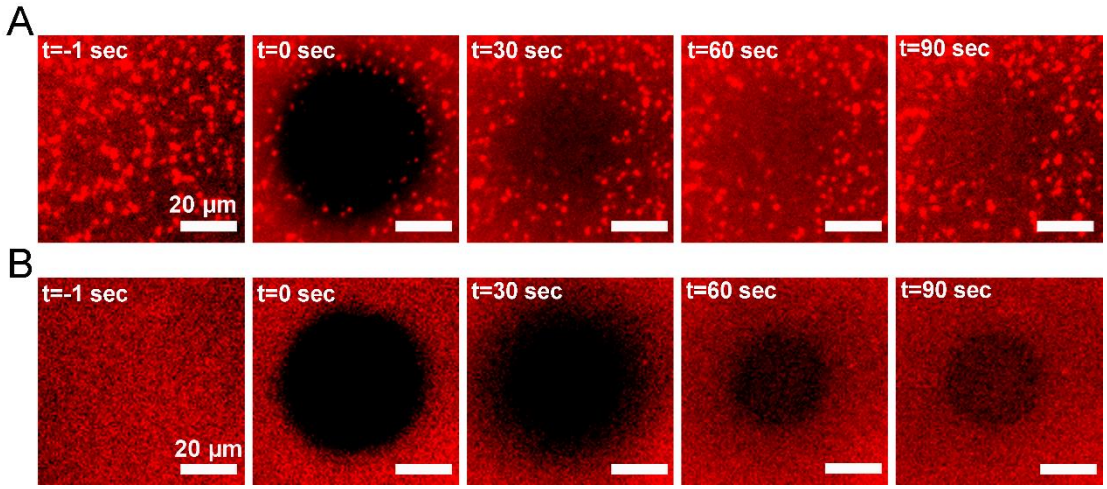

Figure 4. 5 FRAP micrographs of SLB showing pre- and post-repair by AH peptide. Each post bleaching micrograph is shown at 30 sec interval. Scale bar represents 10 μm.

As a final verification of the repair process, we investigated if an AH peptide-treated zwitterionic SLB remained resistant to nonspecific adsorption of bovine serum albumin (BSA)[50]. Since BSA protein binding was not detectable using the QCM-D technique, the orders of magnitude higher sensitivity offered by epifluorescence microscopy was used to probe the binding of fluorescently labeled BSA upon addition the SLB either without or with prior AH peptide treatment and the amount bound was quantified by the fluorescence intensity per unit area (Figure 4. 6A).

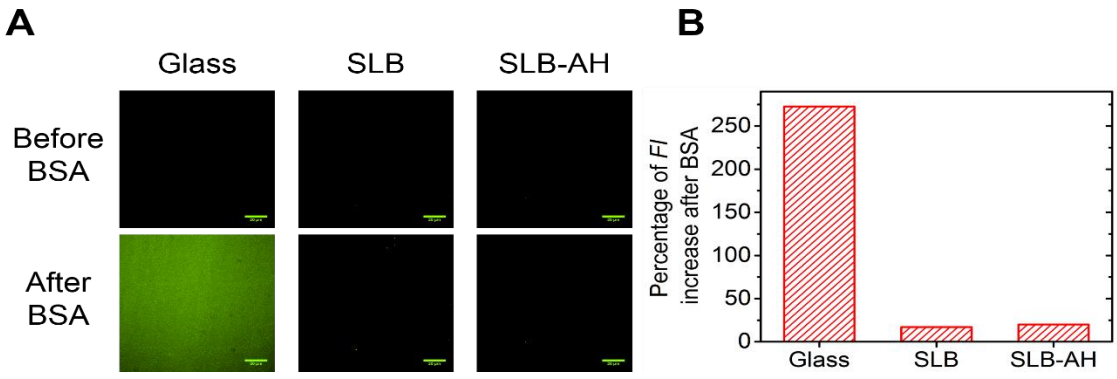

Figure 4. 6 Evaluation of nonspecific adsorption of BSA protein to bilayer before and after SLB repair. Fluorescence micrographs of (A) bare glass, (B) POPC bilayer and (C) POPC bilayer treated with AH peptide, before (top panel) and after (bottom panel)

incubation with fluorescein-labeled BSA. Fluorescein-labeled BSA (0.05 mg/ml) was injected and incubated for ~ 15 min. Then, it was followed by Tris buffer washing to remove any unbound BSA. Each set of images was normalized by subtracting from background fluorescence intensity values. Each scale bar indicates 20 μm. (B) Percentage of average fluorescence intensity increments after the BSA treatment.

In both cases, protein adsorption was minimal and is consistent with AH peptide-mediated vesicle rupture leading to localized SLB formation, which in turn improves the completeness of the SLB platform as a whole. As a control, BSA adsorption onto the bare glass substrate was also tested and, as expected, there was a significantly larger amount of adsorbed protein. There was a greater than 30-fold reduction in adsorbed proteins to the SLBs versus the glass substrate, verifying that AH peptide treatment preserves the anti-biofouling properties of zwitterionic SLBs (Figure 4. 6B). The collective set of measurement data indicates that AH peptide-mediated SLB repair acts via converting adsorbed, unruptured vesicles into SLB fragments that fill in the defect sites (i.e., the sites of previously unruptured vesicles), leading to a complete and homogenous SLB platform.

4.2.8. Vesicle size dependent SLB formation and repair

The repair ability of AH peptide was further tested for supported lipid bilayers formed using a broad range of lipid vesicles sizes ranging from ~90 to ~800 nm. Smaller vesicles with a diameter less than 100 nm were previously demonstrated to rupture and form an essentially complete bilayer whereas larger vesicles tend to form mixed layers of SLB fragments with a high number of entrapped vesicles[24]. Here, we focus our attention on addition of AH peptide after vesicle adsorption and monitored the corresponding changes in the kinetics of vesicle rupture upon the addition of AH peptide for different vesicle sizes. In order to explore more detailed

effects of differently sized vesicles on AH peptide mediated repair, adsorption kinetic profiles from QCM-D measurements were set to zero after the initial vesicle adsorption and fusion step and subsequent rinsing in buffer (Figure 4. 7).

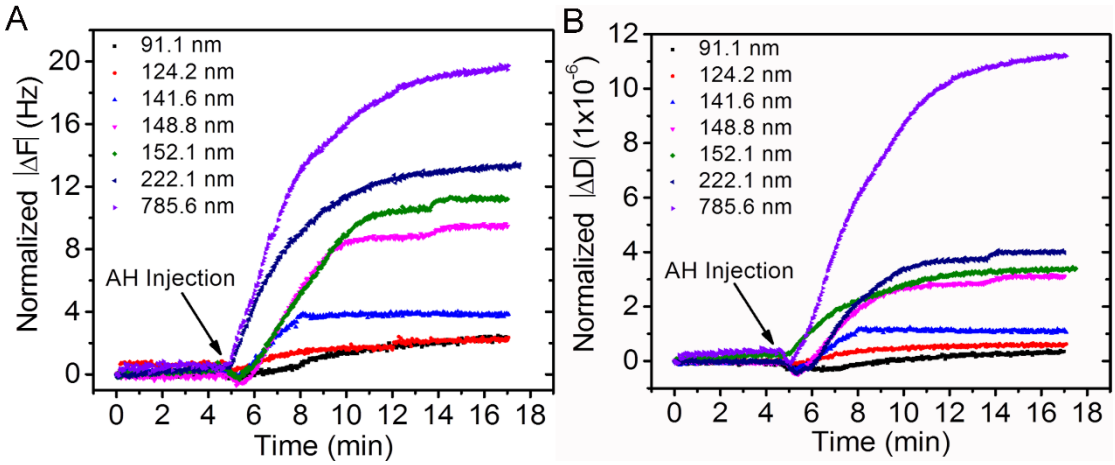

Figure 4. 7 Influence of vesicle size on AH peptide-mediated SLB repair. Kinetic profiles of repairing on various sizes of vesicles were monitored by QCM-D. After the rupture of each different size of vesicles, (A) changes in resonant frequency and (B) energy dissipation at third overtone were normalized at t = 0 min. Arrows indicate injection of AH peptide.

It was shown that the kinetics of AH peptide mediated repairing occurs in a vesicle size-dependent manner, displaying a trend in terms of Δf and ΔD increasing from ~2.4 to ~20 Hz and ~0.3×10^{-6} to ~11×10^{-6}, respectively, for vesicles increasing in size from ca. 91.1 nm to 785.6 nm (Figure 4. 7 and Table 4. 1).

Table 4. 1 Summary table for supported lipid bilayer repair mediated by AH peptide. Initial/final changes in resonance frequency and energy dissipation at third overtone before and after the repair are reported as a function of extrusion filter size. To note that each subscript value 1 indicates before the repair while the value 2 corresponds to the final kinetic values after the repair. The numbers with asterisk indicate how many times vesicle containing solutions were passed through the extrusion membrane filters.

Extrusion Filter Size (nm)	DLS Measurement Size (nm)	Polydispersity	ΔF_1 (Hz)	ΔF_2 (Hz)	ΔD_1 (1×10^{-6})	ΔD_2 (1×10^{-6})
50 (23*)	91.0 ± 0.2	0.079	28.78	26.37	0.5122	0.1576
100 (23*)	128.7 ± 0.7	0.058	28.82	26.34	0.5836	0.0137
100 (17*)	141.3 ± 0.7	0.078	29.75	26.13	1.0941	0.0126
100 (13*)	148.5 ± 0.6	0.092	37.01	27.63	3.2182	0.1286
100 (7*)	151.8 ± 1.2	0.093	38.39	27.00	3.5131	0.2933
200 (13*)	221.3 ± 1.4	0.173	37.16	25.00	4.0272	0.0127
400 (7*)	784.9 ± 12.9	0.347	46.34	26.25	11.4280	0.0469

The trend of increasing frequency and dissipation shifts with larger vesicle sizes is attributed to both the number of unruptured vesicles which tends to increase with vesicle size as well as the size of individual vesicles which leads to a greater response per vesicle upon AH peptide-mediated rupture. Indeed, the measurement signatures are interpreted as a direct consequence of efficient AH peptide-induced rupture of vesicles trapped in the initially formed SLB. Thus, it was demonstrated that the AH peptide can act as a broadly applicable repair agent of trapped vesicles even in unfavorable conditions for SLB formation.

4.2.9. SLB repair pathway

To gain further insight into the repair process, the vesicle size-dependent repair mediated by AH peptide was imaged (Figure 4. 8A-C), and the corresponding

numbers of unruptured vesicles before and after repair were estimated based on a fluorescence threshold (Figure 4. 8D).

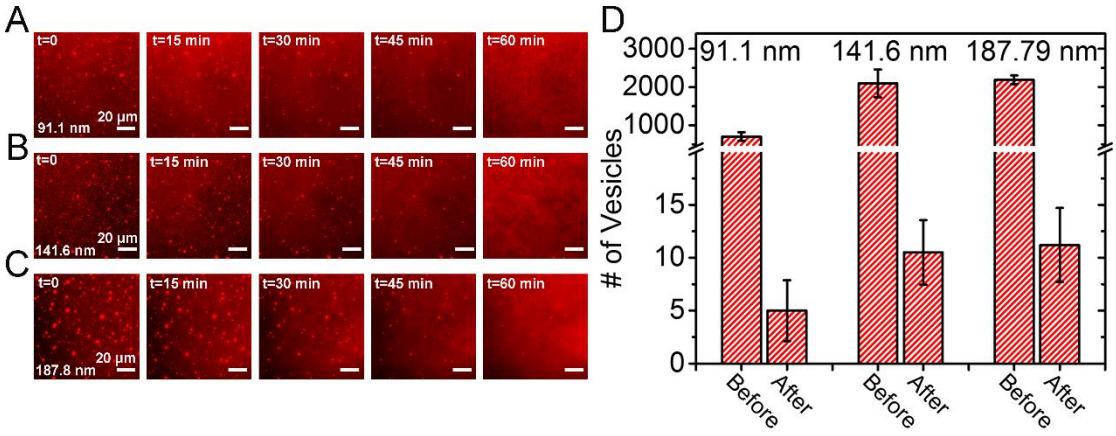

Figure 4. 8 Time-lapse fluorescence micrographs of AH peptide-mediated SLB repair. (A-C) Fluorescence micrographs of bilayer repair process as a function of vesicle size. Scale bars indicate 20 μm. (D) Number of unruptured vesicles before and after AH peptide treatment.

Three different SLBs formed using various sizes of vesicles showed distinctive characteristics. For the case of ~ 90 nm (Figure 4. 8A), a much lower number of unruptured vesicles was observed compared to the other bilayers formed using larger sizes of vesicles. This is consistent with previously reported findings that smaller vesicles easily rupture to form a relatively complete bilayer, while larger vesicles tend to form a mixed layer of SLB and intact vesicles[47]. Regardless of the size of vesicles used to form the bilayer, all three cases investigated (91.1, 141.6 and 187.79 nm) resulted in less than ~10 unruptured or trapped vesicles per field of view (136×136 μm^2) on the bilayer after treatment with AH peptide. From the fluorescence micrographs, features signaling a structural transformation of the intact vesicles upon binding with AH peptide was observed. This experimental finding supports the previously reported mechanism[32] that vesicle rupture mediated by AH peptide is caused by expansion/swelling of intact vesicles, which was here observed to include creation of microvilli or finger-like structures on the outer leaflet of the vesicles. The kinetic profiles from QCM-D measurements (cf. Figure 4. 4A and 4.

5A) are consistent with a structural transformation, although structural details cannot be revealed from ensemble averaging data alone.

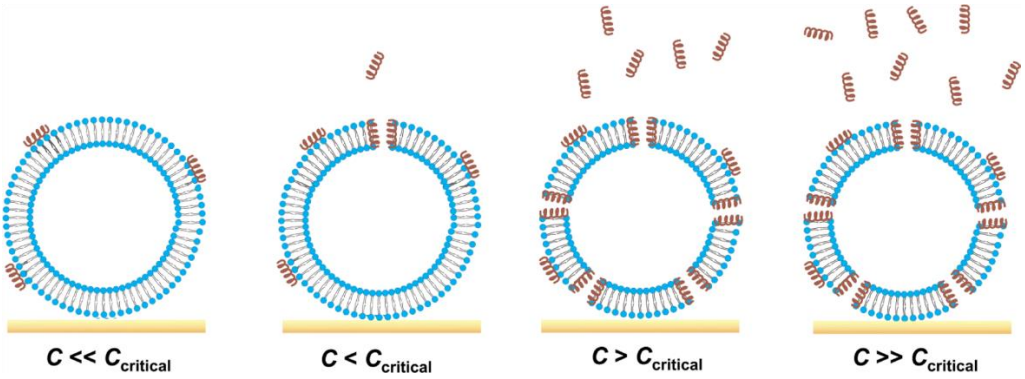

Figure 4. 9 Physical model of membrane lysis at the critical pore concentration. At very low peptide concentrations (c), there is a proportional increase in the amount of bound peptide. Above a certain peptide concentration, the bound peptides assemble into pores in the lipid membrane. The number of pores in the membrane increases with increasing peptide bulk concentration. Above a critical peptide concentration ($C_{critical}$), the number of pores in the membrane reaches a sufficiently high density in order to induce membrane lysis. Vesicle rupture occurs only at or above $C_{critical}$. The schematic representation is adapted from Jackman et al[43].

To complement more of mechanistic discussion on small lipid vesicle lysis via AH peptide interaction, following two major points have been reported from the literature. First, AH peptide prefers to form pores in highly curved membranes (i.e. small unilamellar vesicles) reported by Tabaei et al[41]. The single vesicle tethered experiments revealed that rapid and narrow release profile of the vesicle-encapsulated dye, which is attributed to pore formation, precedes the release of lipids that is induced by membrane destabilization upon vesicle rupturing. This suggests an appropriate reasoning to the previously observed structural transformation of vesicles, suggesting that the overall vesicle rupture process is mainly related to the pore formation step occurring before membrane destabilization and eventual lipid release. The initial pore formation likely induces membrane destabilization by damaging membrane integrity upon reaching a critical concentration of pores. It helps to explain the vesicle size-dependent rupture

efficiency observed for supported lipid bilayer repair as shown in Figure 4. 7. Secondly, having mentioned the critical concentration of pore as also presented in the above figure (Figure 4. 9) showing AH peptide-SUV interaction schematic diagram, the vesicle rupture happens once a critical number of pores is formed. As AH peptide interacts upon the vesicle, it exerts strains on the membrane which eventually leads to rupture via the pore formation process. Regarding pore formation rate, the virucidal AH peptide's pore formation rate increases with decreasing vesicle size. This finding well agrees with the observation made in Figure 4. 7 where large diameters of vesicles took a longer time to facilitate ruptures of the unruptured vesicles trapped on bilayer.

To note that besides employing foreign materials including AH peptide and other antiviral & antimicrobial peptides to promote rupture of the lipid vesicles (liposome), there are several other strategies to aid vesicle rupture based on controlling experimental parameters. pH-driven SLB formation was reported by Cho et al[29] that spontaneous vesicle rupture to form self-assembled bilayer on titanium oxide surface is achieved under the highly acidic environment (pH 3.5). Specifically, the titanium oxide surface's positive surface charge plays a huge role in promoting spontaneous SLB formation through attractive interactions between positively charged oxide groups and the slightly negatively charged lipid vesicles. Taken together, pH modulations can adjust electrostatic interactions between vesicles and titanium oxide shift from repulsive at higher pH to attractive at lower pH promoting the SLB formation. Hence, pH-modulation of buffer condition can facilitate the self-assembly of a lipid bilayer on unfavorable substrate including titanium oxide. Inducing a positive osmotic pressure across the vesicle's bilayer has been reported to aid vesicle rupture[26]. It was reported that positive osmotic pressure promotes the rupture of adsorbed vesicles on silicon oxide substrate, while negative osmotic pressure facilitates to stabilize the adsorbed vesicles. This finding indicates that the modulating ionic strength of buffer used inside and outside of vesicles is one of the important factors controlling the adsorption kinetics of adsorbed vesicles forming the supported lipid bilayer on the substrate. Another strategy for rupturing adsorbed

lipid vesicles is to utilize divalent cations including Mg^{2+}, Ca^{2+}, and Sr^{2+} for mediating complete rupture of adsorbed vesicles on the substrates[51]. It was observed that the divalent cations promote increased deformation of adsorbed zwitterionic lipid vesicles (i.e., phosphatidylcholine lipids) on both titanium oxide and silicon oxide surfaces.

4.4. Conclusion

Collectively, the experimental findings and analytical results presented here demonstrate a post-assembly repair process mediated by AH peptide allowing the generation of a complete and homogenous supported lipid bilayer with somewhat reduced but still retained lateral fluidity. This is the first report in which AH peptide is reported to repair defects on supported lipid bilayers formed via vesicle fusion, demonstrating complete SLBs with a negligible amount of unruptured vesicles. This method can be applied to form supported lipid bilayers using large size vesicles which typically cause steric hindrance that disrupts complete rupture of absorbed vesicles. Although further electrical measurements are needed in order to evaluate the insulating properties of AH-treated bilayers, this new SLB repair approach can improve the feasibility of supported lipid bilayers as a biosensor platform, particularly in cases where high-quality SLBs are needed. It might also be an interesting means to form planar supported lipid bilayers from native cell membranes, which attracts increased attendance in membrane-protein chromatography applications.

References

1. Sackmann, E., Supported membranes: Scientific and practical applications. *Science* **1996,** *271* (5245), 43-48.

2. Chan, Y. H.; Boxer, S. G., Model membrane systems and their applications. *Current Opinion in Chemical Biology* **2007,** *11* (6), 581-7.

3. Jung, H.; Robison, A. D.; Cremer, P. S., Detecting Protein− Ligand Binding on Supported Bilayers by Local pH Modulation. *Journal of the American Chemical Society* **2009,** *131* (3), 1006-1014.

4. Jeong, J. H.; Choi, J.-H.; Kim, M. C.; Park, J. H.; Herrin, J. S.; Kim, S. H.; Lee, H.; Cho, N.-J., Elucidating how bamboo salt interacts with supported lipid membranes: influence of alkalinity on membrane fluidity. *European Biophysics Journal* **2015**, 1-9.

5. Wagner, M. L.; Tamm, L. K., Reconstituted syntaxin1a/SNAP25 interacts with negatively charged lipids as measured by lateral diffusion in planar supported bilayers. *Biophysical Journal* **2001,** *81* (1), 266-275.

6. Yorulmaz, S.; Tabaei, S. R.; Kim, M.; Seo, J.; Hunziker, W.; Szebeni, J.; Cho, N.-J., Membrane attack complex formation on a supported lipid bilayer: initial steps towards a CARPA predictor nanodevice. *European Journal of Nanomedicine* **2015,** *7* (3), 245-255.

7. Munro, J. C.; Frank, C. W., In situ formation and characterization of poly (ethylene glycol)-supported lipid bilayers on gold surfaces. *Langmuir* **2004,** *20* (24), 10567-10575.

8. Purrucker, O.; Förtig, A.; Jordan, R.; Tanaka, M., Supported Membranes with Well-Defined Polymer Tethers—Incorporation of Cell Receptors. *ChemPhysChem* **2004,** *5* (3), 327-335.

9. Jackman, J. A.; Knoll, W.; Cho, N.-J., Biotechnology applications of tethered lipid bilayer membranes. *Materials* **2012,** *5* (12), 2637-2657.

10. Römer, W.; Steinem, C., Impedance analysis and single-channel recordings on nano-black lipid membranes based on porous alumina. *Biophysical Journal* **2004,** *86* (2), 955-965.

11. Weiskopf, D.; Schmitt, E. K.; Klühr, M. H.; Dertinger, S. K.; Steinem, C., Micro-BLMs on highly ordered porous silicon substrates: Rupture process and lateral mobility. *Langmuir* **2007,** *23* (18), 9134-9139.

12. Cremer, P. S.; Boxer, S. G., Formation and spreading of lipid bilayers on planar glass supports. *Journal of Physical Chemistry B* **1999,** *103* (13), 2554-2559.

13. Reviakine, I.; Brisson, A., Formation of supported phospholipid bilayers from unilamellar vesicles investigated by atomic force microscopy. *Langmuir* **2000,** *16* (4), 1806-1815.

14. Anderson, T. H.; Min, Y.; Weirich, K. L.; Zeng, H.; Fygenson, D.; Israelachvili, J. N., Formation of supported bilayers on silica substrates. *Langmuir* **2009,** *25* (12), 6997-7005.

15. Cho, N. J.; Frank, C. W.; Kasemo, B.; Höök, F., Quartz crystal microbalance with dissipation monitoring of supported lipid bilayers on various substrates. *Nature Protocols* **2010,** *5* (6), 1096-1106.

16. Vila, N.; Puggelli, M.; Gabrielli, G., Langmuir-Blodgett monolayers and multilayers of gramicidin A and lipids as membrane-mimetic models. *Colloids and Surfaces A: Physicochemical and Engineering Aspects* **1996,** *119* (2), 95-104.

17. Tabaei, S. R.; Choi, J.-H.; Haw Zan, G.; Zhdanov, V. P.; Cho, N.-J., Solvent-Assisted Lipid Bilayer Formation on Silicon Dioxide and Gold. *Langmuir* **2014,** *30* (34), 10363-10373.

18. Tabaei, S. R.; Jackman, J. A.; Kim, S.-O.; Liedberg, B.; Knoll, W.; Parikh, A. N.; Cho, N.-J., Formation of Cholesterol-Rich Supported Membranes Using Solvent-Assisted Lipid Self-Assembly. *Langmuir* **2014,** *30* (44), 13345-13352.

19. Tabaei, S. R.; Vafaei, S.; Cho, N.-J., Fabrication of Charged Membranes by the Solvent-Assisted Lipid Bilayer (SALB) Formation Method on SiO2 and Al2O3. *Physical Chemistry Chemical Physics* **2015**.

20. Jackman, J. A.; Tabaei, S. R.; Zhao, Z.; Yorulmaz, S.; Cho, N.-J., Self-Assembly Formation of Lipid Bilayer Coatings on Bare Aluminum Oxide: Overcoming the Force of Interfacial Water. *ACS Applied Materials & Interfaces* **2015,** *7* (1), 959-968.

21. Tabaei, S. R.; Jackman, J. A.; Kim, S.-O.; Zhdanov, V. P.; Cho, N.-J., Solvent-Assisted Lipid Self-Assembly at Hydrophilic Surfaces: Factors Influencing the Formation of Supported Membranes. *Langmuir* **2015,** *31* (10), 3125-3134.

22. Tabaei, S. R.; Jackman, J. A.; Liedberg, B.; Parikh, A. N.; Cho, N.-J., Observation of Stripe Superstructure in the β-Two-Phase Coexistence Region of Cholesterol–Phospholipid Mixtures in Supported Membranes. *Journal of the American Chemical Society* **2014,** *136* (49), 16962-16965.

23. Tamm, L. K.; McConnell, H. M., Supported phospholipid bilayers. *Biophysical Journal* **1985,** *47* (1), 105-113.

24. Keller, C.; Kasemo, B., Surface specific kinetics of lipid vesicle adsorption measured with a quartz crystal microbalance. *Biophysical Journal* **1998,** *75* (3), 1397-1402.

25. Jackman, J. A.; Cho, N.-J.; Duran, R. S.; Frank, C. W., Interfacial binding dynamics of bee venom phospholipase A_2 investigated by dynamic light scattering and quartz crystal microbalance. *Langmuir* **2009,** *26* (6), 4103-4112.

26. Jackman, J. A.; Choi, J.-H.; Zhdanov, V. P.; Cho, N.-J., Influence of osmotic pressure on adhesion of lipid vesicles to solid supports. *Langmuir* **2013,** *29* (36), 11375-11384.

27. Boudard, S.; Seantier, B.; Breffa, C.; Decher, G.; Felix, O., Controlling the pathway of formation of supported lipid bilayers of DMPC by varying the sodium chloride concentration. *Thin Solid Films* **2006,** *495* (1), 246-251.

28. Reimhult, E.; Höök, F.; Kasemo, B., Temperature dependence of formation of a supported phospholipid bilayer from vesicles on SiO 2. *Physical Review E: Statistical, Nonlinear, and Soft Matter Physics* **2002,** *66* (5), 051905.

29. Cho, N.-J.; Jackman, J. A.; Liu, M.; Frank, C. W., pH-Driven assembly of various supported lipid platforms: A comparative study on silicon oxide and titanium oxide. *Langmuir* **2011,** *27* (7), 3739-3748.

30. Seantier, B.; Kasemo, B., Influence of mono-and divalent ions on the formation of supported phospholipid bilayers via vesicle adsorption. *Langmuir* **2009,** *25* (10), 5767-5772.

31. Terrettaz, S.; Mayer, M.; Vogel, H., Highly electrically insulating tethered lipid bilayers for probing the function of ion channel proteins. *Langmuir* **2003,** *19* (14), 5567-5569.

32. Cho, N.-J.; Cho, S.-J.; Cheong, K. H.; Glenn, J. S.; Frank, C. W., Employing an amphipathic viral peptide to create a lipid bilayer on Au and TiO2. *Journal of the American Chemical Society* **2007,** *129* (33), 10050-10051.

33. Cho, N.-J.; Wang, G.; Edvardsson, M.; Glenn, J. S.; Hook, F.; Frank, C. W., Alpha-helical peptide-induced vesicle rupture revealing new insight into the vesicle fusion process as monitored in situ by quartz crystal microbalance-dissipation and reflectometry. *Analytical chemistry* **2009,** *81* (12), 4752-4761.

34. Zan, G. H.; Jackman, J. A.; Cho, N.-J., AH peptide-mediated formation of charged planar lipid bilayers. *Journal of Physical Chemistry B* **2014,** *118* (13), 3616-3621.

35. Cho, N.-J.; Cho, S.-J.; Hardesty, J. O.; Glenn, J. S.; Frank, C. W., Creation of lipid partitions by deposition of amphipathic viral peptides. *Langmuir* **2007,** *23* (21), 10855-10863.

36. Cho, N.-J.; Kanazawa, K. K.; Glenn, J. S.; Frank, C. W., Employing two different quartz crystal microbalance models to study changes in viscoelastic behavior upon transformation of lipid vesicles to a bilayer on a gold surface. *Analytical chemistry* **2007,** *79* (18), 7027-7035.

37. Jackman, J. A.; Zan, G. H.; Zhdanov, V. P.; Cho, N.-J., Rupture of lipid vesicles by a broad-spectrum antiviral peptide: influence of vesicle size. *Journal of Physical Chemistry B* **2013,** *117* (50), 16117-16128.

38. Zan, G. H.; Cho, N.-J., Rupture of zwitterionic lipid vesicles by an amphipathic, α-helical peptide: Indirect effects of sensor surface and implications for experimental analysis. *Colloids and Surfaces B: Biointerfaces* **2014,** *121*, 340-346.

39. Hardy, G. J.; Nayak, R.; Alam, S. M.; Shapter, J. G.; Heinrich, F.; Zauscher, S., Biomimetic supported lipid bilayers with high cholesterol content formed by α-helical peptide-induced vesicle fusion. *Journal of Materials Chemistry* **2012,** *22* (37), 19506-19513.

40. Wang, J.; Liu, K.-W.; Biswal, S. L., Characterizing α-Helical Peptide Aggregation on Supported Lipid Membranes Using Microcantilevers. *Analytical chemistry* **2014,** *86* (20), 10084-10090.

41. Tabaei, S. R.; Rabe, M.; Zhdanov, V. P.; Cho, N.-J.; Höök, F., Single vesicle analysis reveals nanoscale membrane curvature selective pore formation in lipid membranes by an antiviral α-helical peptide. *Nano Letters* **2012,** *12* (11), 5719-5725.

42. Cho, N.-J.; Dvory-Sobol, H.; Xiong, A.; Cho, S.-J.; Frank, C. W.; Glenn, J. S., Mechanism of an Amphipathic α-Helical Peptide's Antiviral Activity Involves Size-Dependent Virus Particle Lysis. *ACS Chemical Biology* **2009,** *4* (12), 1061-1067.

43. Jackman, J. A.; Saravanan, R.; Zhang, Y.; Tabaei, S. R.; Cho, N. J., Correlation between membrane partitioning and functional activity in a single lipid vesicle assay establishes design guidelines for antiviral peptides. *Small* **2015,** *11* (20), 2372-2379.

44. MacDonald, R. C.; MacDonald, R. I.; Menco, B. P. M.; Takeshita, K.; Subbarao, N. K.; Hu, L.-r., Small-volume extrusion apparatus for preparation of large, unilamellar vesicles. *Biochimica et Biophysica Acta (BBA)-Biomembranes* **1991,** *1061* (2), 297-303.

45. Jönsson, P.; Jonsson, M. P.; Tegenfeldt, J. O.; Höök, F., A method improving the accuracy of fluorescence recovery after photobleaching analysis. *Biophysical Journal* **2008,** *95* (11), 5334-5348.

46. Richter, R. P.; Bérat, R.; Brisson, A. R., Formation of solid-supported lipid bilayers: An integrated view. *Langmuir* **2006,** *22* (8), 3497-3505.

47. Reimhult, E.; Höök, F.; Kasemo, B., Intact vesicle adsorption and supported biomembrane formation from vesicles in solution: influence of surface chemistry, vesicle size, temperature, and osmotic pressure. *Langmuir* **2003,** *19* (5), 1681-1691.

48. Wallin, M.; Choi, J.-H.; Kim, S. O.; Cho, N.-J.; Andersson, M., Peptide-induced formation of a tethered lipid bilayer membrane on mesoporous silica. *European Biophysics Journal* **2015,** *44* (1-2), 27-36.

49. Bingen, P.; Wang, G.; Steinmetz, N. F.; Rodahl, M.; Richter, R. P., Solvation effects in the quartz crystal microbalance with dissipation monitoring response to biomolecular adsorption. A phenomenological approach. *Analytical chemistry* **2008,** *80* (23), 8880-8890.

50. Glasmästar, K.; Larsson, C.; Höök, F.; Kasemo, B., Protein adsorption on supported phospholipid bilayers. *Journal of Colloid and Interface Science* **2002,** *246* (1), 40-47.

51. Dacic, M.; Jackman, J. A.; Yorulmaz, S.; Zhdanov, V. P.; Kasemo, B.; Cho, N.-J., Influence of Divalent Cations on Deformation and Rupture of Adsorbed Lipid Vesicles. *Langmuir* **2016,** *32* (25), 6486-6495.

Chapter 5

Influence of GUV Membrane Composition on the Morphological Responses Induced by an Amphipathic, α-Helical Peptide

There have been numerous approaches employing giant unilamellar vesicles (GUV) composed of purely synthetic lipids as a cell membrane-mimetic platform to study dynamic membrane morphological responses upon interaction with various membrane-active agents. Herein, I describe the preparation of GUVs incorporating fractions of human liver microsome (HLM) extracts as a biomimetic platform to study the interactions between biologically relevant membrane components in GUVs and membrane-active agents. In these experiments, I studied the interaction between GUVs and an amphipathic, α-helical (AH) peptide derived from nonstructural protein (NS5A) of the hepatitis C virus. Based on the experimental results obtained at different HLM fractions and peptide concentrations, it was determined that HLM-GUVs were more resistant to peptide-induced disruption compared to single component DOPC-GUVs. Various membrane biophysical responses of GUVs were examined by employing spinning disc confocal microscopy measurements, conductance measurement studies using tethered supported lipid bilayer (tSLB) assembly and kinetics of peptide binding onto non-labeled vesicles. The experiment also demonstrates the application of tSLB system for bilayer assembly and conductance studies in complex lipid mixtures for the first time.

5.1. Introduction

AH peptide is sensitive to membrane curvature and ruptures only small vesicles[1-2]. Addition of AH peptide after the formation of supported lipid bilayer on the glass or silicon oxide substrates via vesicle fusion method[3], un-ruptured vesicles ruptured leading to form a complete defect-less lipid bilayer[4]. This response of the bilayer and AH peptide could potentially be developed into a reliable biosensor platform for drug-membrane interaction applications[5]. In order to develop such a platform, a thorough understanding of the AH peptide membrane interaction involving morphological information and biophysical characterization of the bilayer is essential. In this regard, GUVs are a promising model system that has been widely explored for membrane-active compounds[6-7].

GUVs have been widely used to study antimicrobial peptides, including AH peptide[2], melittin[8], maginin[9], aurein[10], mastoparan[11], pailiocin[12], arenacin-1[13], psacotheasin[14] and alamethicin[15]. The key information obtained from these experiments includes pore formations induced by melittin[8], mastoparan[11], pailiocin[12] and alamethicin[15]. In addition, various membrane morphological responses were also observed including vesicle shape transformations into prolate and connected spheres via a narrow neck induced by magainin[9], and membrane softening induced by membrane thinning effect from peptide binding[16-17]. Even membrane destabilization leading to vesicle rupture induced by citropin[10]. Recently, Hanson et al. showed that AH peptide induces membrane softening of zwitterionic lipid GUVs[2]. However, how this extends to more complex biologically relevant model membranes still remains to be understood.

One previous study utilizing the supported lipid bilayer platform showed that the peptide interacts differentially with synthetic membranes in comparison to microsome-based membranes, suggesting the importance of proteinaceous components in the peptide-lipid interaction and membrane perturbation[18]. Small unilamellar vesicles are another class of bilayer platform systems that have been used extensively for understanding membrane-biomolecule interaction[19-21]; drug

encapsulation and delivery as well as pre-cursors for planar bilayer formation for AFM and QCM-D based studies[22-23]. Despite their wide scale applications, some shortcomings such as extraction of cumulative behavior as opposed to single membrane interactions, complications due to highly curved membrane structure use of SUVs are limited[24-26]. So far, the development of microsome - based membranes in the GUV format has been mainly limited to membrane protein synthesis and incorporation[27-28]. The potential of applying the GUVs to study membrane-active agents, including amphipathic peptides, and corresponding biophysical interactions remains unexplored.

In this chapter, in order to explore membrane interactions of AH peptide against more complex biologically relevant membrane compositions, we incorporated liver microsome derived from human liver into the bilayer of a giant unilamellar vesicle. From the measurements, we find that interactions with of human liver microsome (HLM) incorporated into pure DOPC GUVs are significantly different from their pure DOPC membrane counterparts. By employing spinning disc confocal microscopy measurement technique, changes of vesicle membrane morphologies were tracked enabling direct comparisons between GUVs incorporated with and without human liver microsome. Comparison of two different concentrations of HLM in DOPC revealed that addition of AH peptide has a stabilizing effect on the bilayer containing HLM fractions. Further stabilizing effects were analyzed by the electrophysiological measurements on tethered supported lipid bilayer (tSLB) technique and binding kinetic assessments of fluorescence labeled AH peptide on non-labeled GUVs. Taken all together, the presented study demonstrates that the interactions of AH peptide with biologically relevant cell-sized model platform significantly differs from simple GUV model platforms composed of only synthetic lipids.

5.2. Materials & Experimental Methods

5.2.1. Materials

1,2-Dioleoyl-sn-glycero-3-phosphocholine (DOPC) and 1,2-dioleoyl-*sn*-glycero-3-phosphoethanolamine-N-(lissamine rhodamine B sulfonyl) (Ammonium salt) (Rh-PE fluorophore) were purchased from Avanti Polar Lipids, Inc. (Alabaster, AL). Human liver microsome pooled from male human liver was purchased from Sigma-Aldrich (St Louis, MO, USA). Glucose and sucrose were obtained from Sigma-Aldrich. All solutions were prepared with Milli-Q-treated water (>18 MΩ·cm) (Millipore, Billerica, MA).

5.2.2. Giant unilamellar vesicle preparation

Giant unilamellar vesicles (GUVs) were prepared using the electroformation method[29-30]. Stock solutions of lipid mixtures (mol:mol) were prepared at 1 mg/ml in chloroform (all lipids were purchased from Avanti Polar Lipids). 20 µL of the stock solution were spread onto the ITO-coated glass slides within an area delimited by an O-ring and allowed to dry in vacuum for at least 1 hr. Electroformation was performed with a 300 mM sucrose solution by using a commercial Vesicle Prep Pro (Nanion, Munich, Germany). GUVs were electroformed by applying an AC current at 5 Hz, 3 V and at 45°C for 120 min. Then the GUVs were diluted in a 300 mM glucose solution for microscopy imaging. Only fresh batch of GUV samples were utilized for each experiment.

5.2.3. Human liver microsome-GUV preparation

Human liver microsome incorporated giant unilamellar vesicles (HLM-GUV) were prepared using synthetic lipids (DOPC and fluorescence labeled Rh-PE) and commercially available human liver extract microsome. HLM-GUV formation was conducted based on electroformation method of incorporating membrane proteins by Fenz et al[28]. Briefly, 20 µL of DOPC (20 µg) dissolved in chloroform was

deposited onto ITO coated glass slides and completely dried in vacuum for at least 1 hr. Then, for the actual GUV electroformation involving HLM incorporation was conducted by first depositing 2 µL of HLM (stock concentration was 0.5 mg/ml diluted in 300 mM of sucrose for 5% HLM-GUV) sample onto the area of dried lipid film. Lastly, 300 mM sucrose solution was utilized as a re-hydrating buffer solution for 2 hr of electroformation. During the electroformaiton, regular AC current at 5 Hz and 3 V was applied. HLM-GUV sample was collected and used immediately for the fluorescence microscopy measurements.

5.2.4. Spinning disc confocal microscopy measurements

Spinning disk confocal microscopy measurements were employed using an inverted Eclipse Ti-U microscope (Nikon) combined with X-Light spinning-disk confocal unit (CrestOptics, Italy) and an Andor iXon+ EMCCD camera (Andor Technology, Northern Ireland). For measurements, 60× oil immersion objective lens (NA 1.49) was employed, and Rh-DOPE (Excitation/Emission: 560/583) was exposed with a 50 mW 561 laser line. At least 5 vesicle samples were imaged for each experimental trial.

5.2.5. AH peptide preparation

The amphipathic, α-helical (AH) peptide was synthesized by Anaspec Corporation (San Jose, CA). The amino acid sequence of AH peptide is H-Ser-Gly-Ser-Trp-Leu-Arg-Asp-Val-Trp-Asp-Trp-Ile-Cys-Thr-Val-Leu-Thr-Asp-Phe-Lys-Thr-Trp-Leu-Gln-Ser-Lys-Leu-Asp-Tyr-Lys-Asp-NH_2. The peptide was prepared and diluted in 300 mM of glucose solution before the measurements.

5.2.6. Tethered Supported Lipid Bilayer

The changes in the membrane permeability from the result of addition of AH peptide were confirmed by measuring the conductance of bilayer using tethered Supported Lipid Bilayers obtained from SD_X Tethered Membranes device (Australia).

5.3. Principal Outcomes

5.3.1. Concentration-dependent effects of AH peptide against HLM-absent Vesicles

To explore the effects of AH peptide on single lipid composition of GUV, DOPC-GUVs doped with 1 mol% of Rhodamine labeled lipid (Rh-PE) were employed for monitoring AH peptide-membrane interactions against various concentrations of AH peptide. Similar studies were conducted by Hanson et al[2] specifically using AH peptide on zwitterionic POPC GUVs, however the effect of various concentrations of AH peptide were not thoroughly explored. Here, we tested four different concentrations of AH peptide to investigate the effect of the amount of AH peptide on vesicles (10-30 μm diameters).

First, 0.5 μM of AH peptide was administered into a well containing DOPC-GUV sample solution. Following figure (Figure 5. 1) presents time-lapse micrographs of selected vesicle undergoing morphological changes after the injection of 0.5μM peptide.

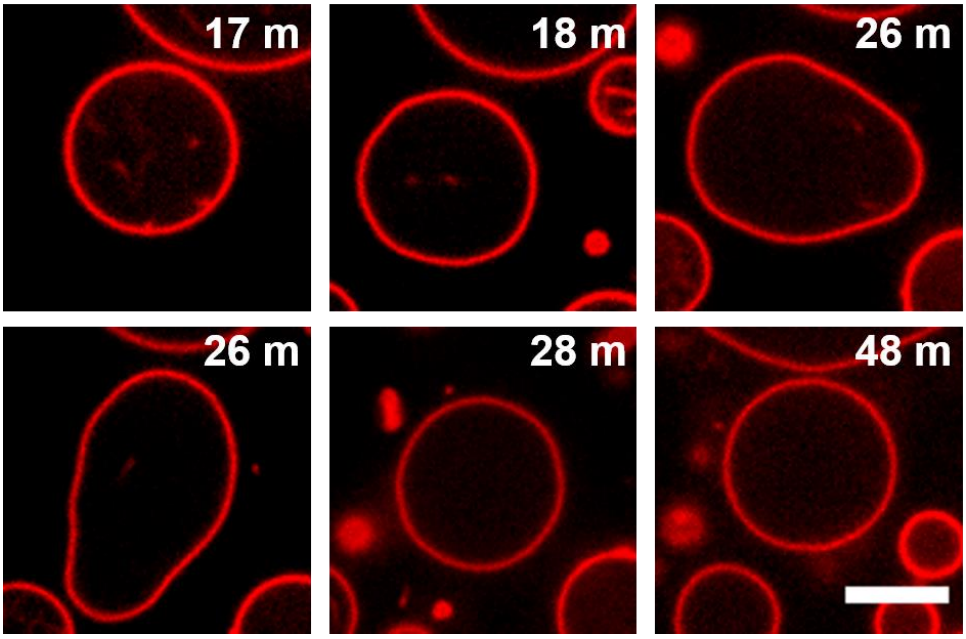

Figure 5. 1 Morphological changes induced by the addition of 0.5 µM AH peptide. Spinning disc confocal microscopy images of GUVs consisting of DOPC doped with Rho-DPPE upon incubation with 0.5 µM AH peptide in 300 mM glucose. Each labeled time corresponds to the peptide injection time. Scale bar represents 10 µm.

As presented in the recorded micrographs (Figure 5. 1), injection of AH peptide initially caused some membrane deformation (Fig 5.1, at 18, 26 min) where the spherical membrane became flaccid. However, the vesicle retained its spherical geometry after about half an hour and remained spherical for several minutes more than an hour (data not shown).

When the amount of AH peptide is increased to 1µM, the bilayer did not show any visible deformations. However, after half an hour of peptide injection, the vesicles collapsed (Fig 5.2). Upon further increase in AH peptide concentration to 2.5 µM, the vesicle collapsed in less than half an hour (in about 20 minutes) as shown in Fig 5. 3. Finally an increase to 5 µM of AH peptide, the vesicles started bursting at 13 minutes. These observations show that addition of AH peptide to pure DOPC membrane cause membrane instability in a concentration dependent manner.

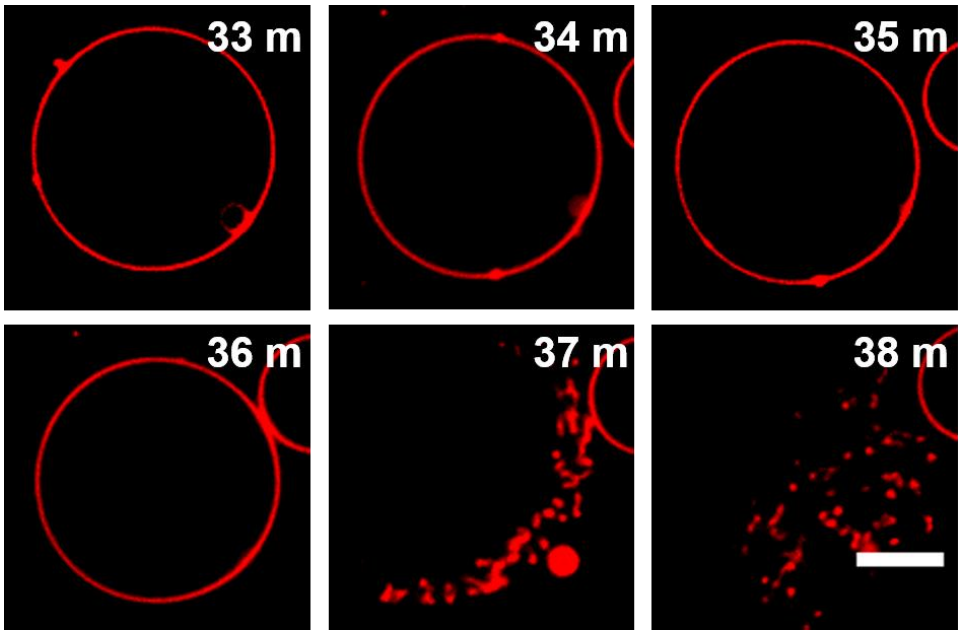

Figure 5. 2 DOPC-GUV collapse induced by the interaction with 1 µM AH peptide. Fluorescence micrographs were captured by SDCM measurements. Each indicated time scale corresponds to the peptide injection time. Scale bar is 10 µm.

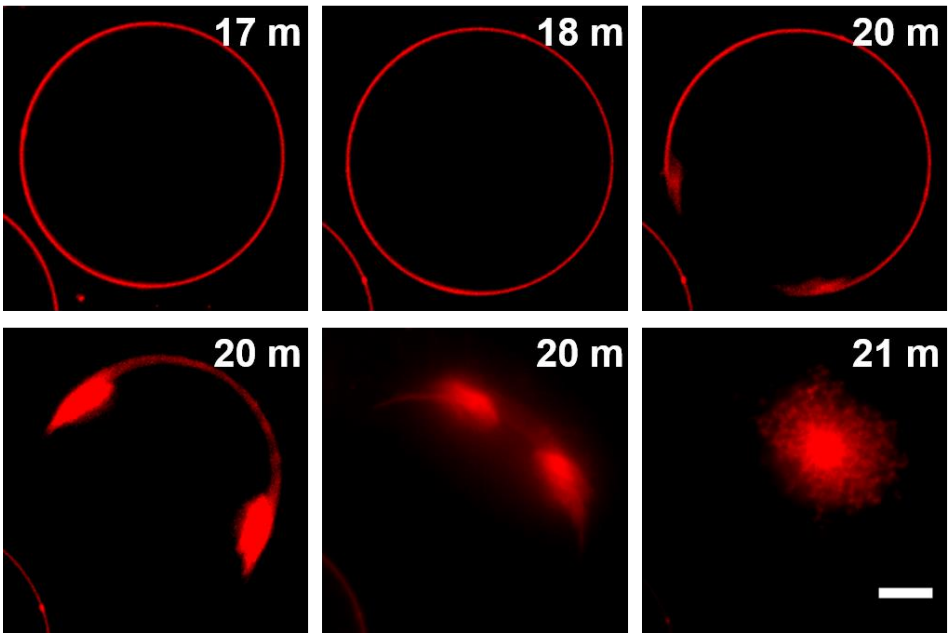

Figure 5. 3 GUV collapse induced by 2.5 µM AH peptide interaction. Fluorescence micrographs were captured by SDCM measurements. Note that each indicated time scale corresponds to the AH peptide injection time. Scale bar represents 10 µm.

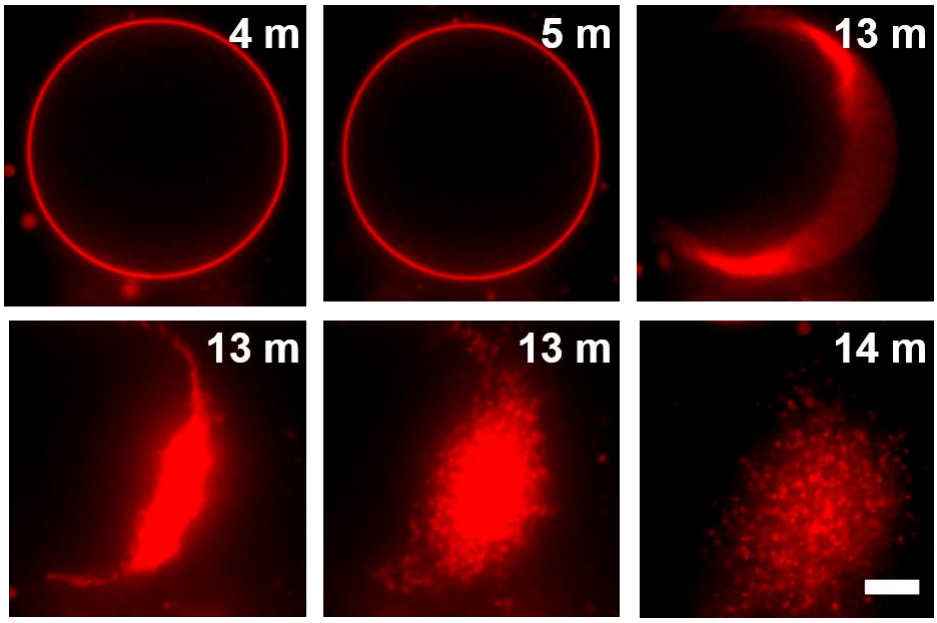

Figure 5. 4 GUV collapse induced by 5 µM AH peptide interaction. Fluorescence micrographs were recorded by SDCM measurements. Note that each indicated time scale corresponds to the peptide injection time. Scale bar indicates 10 µm.

Next effect of AH peptide on GUVs made from a mixture of DOPC and Human Liver Microsome membranes were investigated as described in the next section (Section 5.3.2)

5.3.2. HLM concentration effect of against AH peptide (1% and 5% HLM)

In order to explore effects of AH peptide on HLM membranes, human liver microsome (HLM) containing GUVs were prepared. The formation of GUVs using electroformation was challenging even at concentrations as low as 5%. As a result, GUVs with compositions, one containing 1% HLM in DOPC and the second containing 5% HLM in DOPC were investigated. First set of HLM-GUV was 1 mol % and the other amount was 5 mol %.

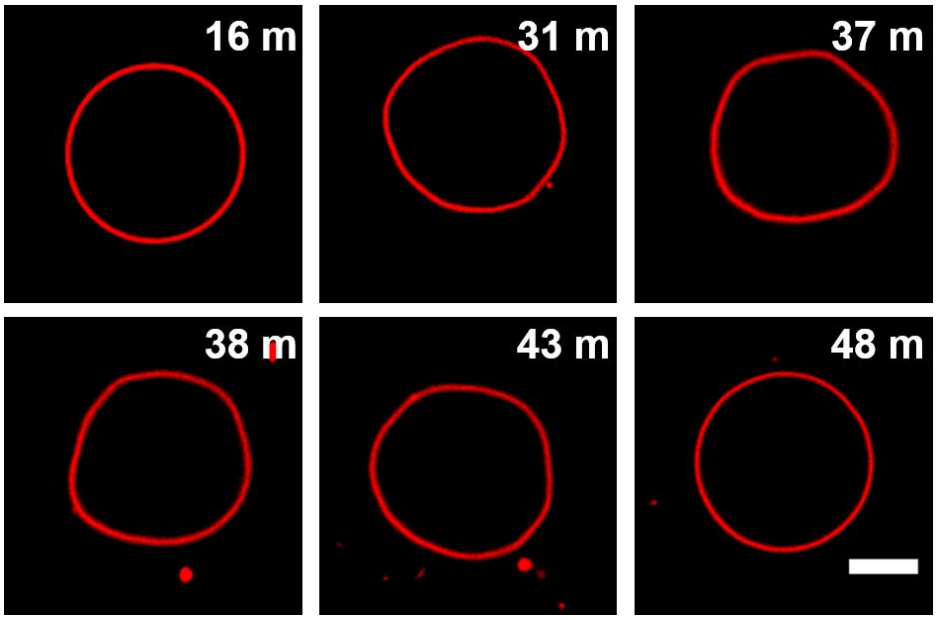

Figure 5. 5 Membrane fluctuation of 1% HLM-GUV induced by the introduction of 0.5 µM AH peptide. Spinning disc confocal microscopy images of GUVs consisting of 1 mol % of HLM, 98 mol % of DOPC doped with 1 mol % of Rho-B DPPE upon interaction with 0.5 µM AH peptide in 300 mM glucose. Each labeled time corresponds to the peptide injection time. Scale bar indicates 10 µm.

Interaction between 0.5 µM of AH peptide and 1% HLM-GUV (presented in Figure 5. 5) resulted in membrane fluctuation behavior which was also similar to the observed behavior of DOPC-GUV interacting with 0.5 µM of AH peptide. As it was observed in DOPC-GUV case, the fluctuating membrane came back to its normal tense spherical shape state after going through approximately 10 minutes, 1% HLM containing GUVs showed a similar trend. The HLM-GUVs however did not deform as much as the pure DOPC vesicles upon addition of AH peptide.

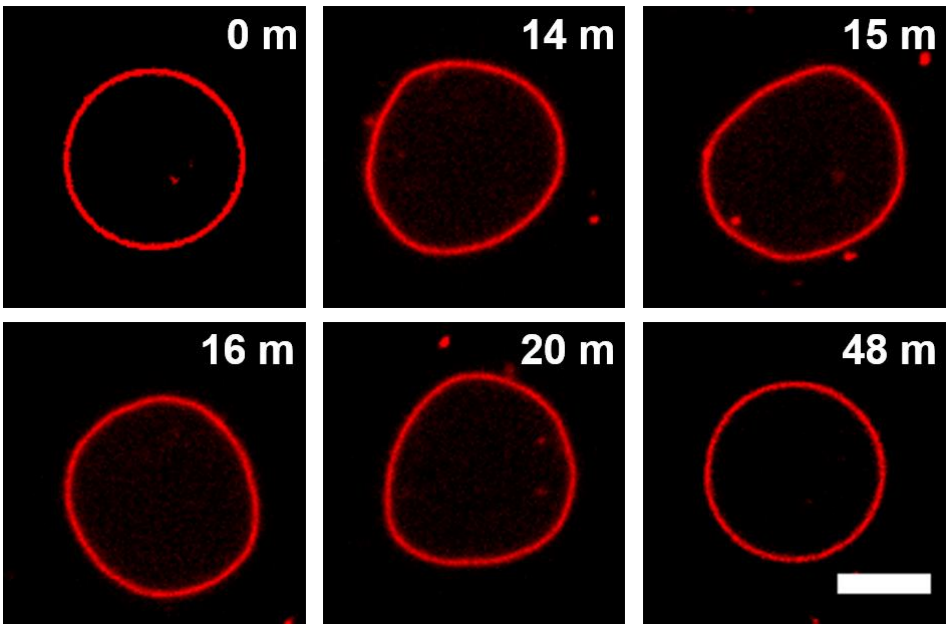

Figure 5. 6 Morphological changes of 1% HLM-GUV induced by the interaction with 1 µM AH peptide. Fluorescence micrographs were captured by SDCM measurements. Each indicated time scale corresponds to the peptide injection time. Scale bar represents 10 µm.

When the amount of AH peptide was increased to 1 µM, HLM containing GUVs did not rupture for more than an hour unlike the pure DOPC vesicles where the vesicles ruptured in about 37 minutes as shown in Figure 5. 2. The addition of HLM to DOPC stabilized membrane against AH peptide addition for this composition. Upon further increase in AH peptide concentration to 2.5 and 5 µM the vesicles rupture time was not significantly different from that of pure DOPC vesicles. For 2.5 µM, the vesicles ruptured at 14 minutes after the induction of AH whereas for 5 µM the rupture time was around 16 min.

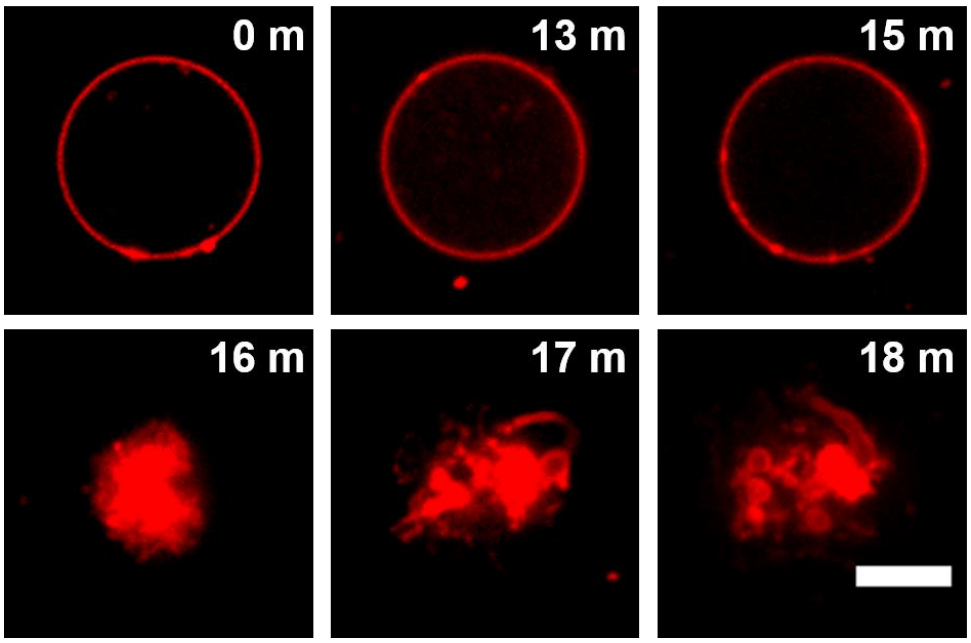

Figure 5. 7 1% HLM-GUV collapse induced by 2.5 µM AH peptide interaction. Fluorescence micrographs were captured by SDCM measurements. Note that each indicated time scale corresponds to the AH peptide injection time. Scale bar is 10 µm.

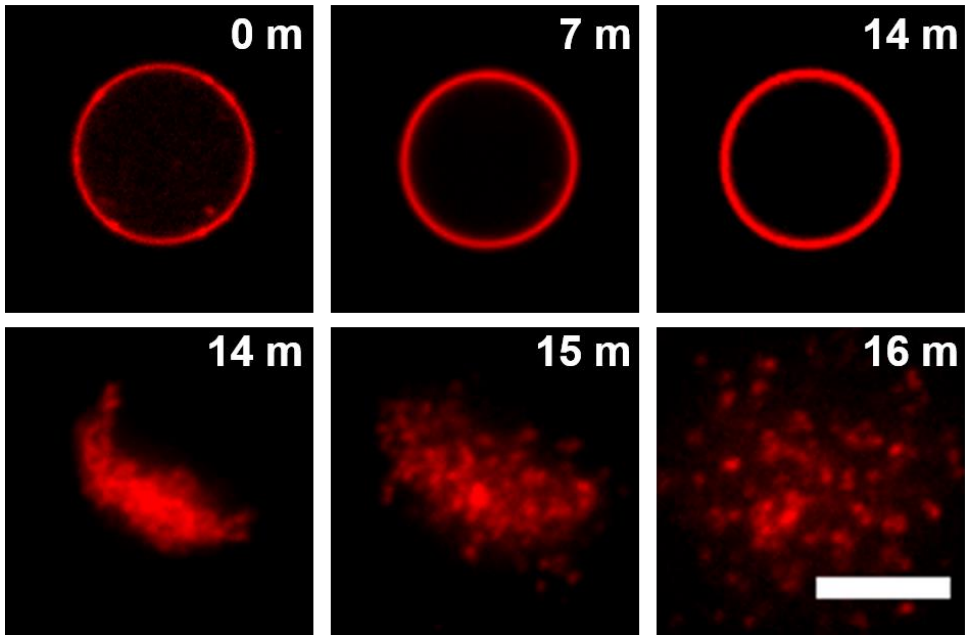

Figure 5. 8 1% HLM-GUV collapse induced by 5 µM AH peptide. Fluorescence micrographs were captured by SDCM measurements. Note that each indicated time scale corresponds to the peptide injection time. Scale bar indicates 10 µm.

Next, we increased the amount of HLM to 5%. GUVs containing 5% HLM were subjected to the same experimental conditions as for pure DOPC and 1% HLM-DOPC lipid mixtures. From the recorded time scales of each event, it indicates that higher concentrations of AH peptide reduce the membrane stability as the concentration of HLM is increased. From the fluorescence micrographs as shown in the below Figure 5. 9, it is observed that addition of small amount of peptide (0.5 µM) did not affect membrane stability significantly. At a slightly higher concentration (1 µM), the stability increases almost in a HLM concentration dependent manner. At the highest HLM concentration of 5 %, the vesicles were intact for more than 90 minutes. The trend, however, reverses at higher AH peptide concentrations where the vesicles containing 5 µM HLM ruptured fastest at a maximum of 5 µM of AH peptide used in the current study.

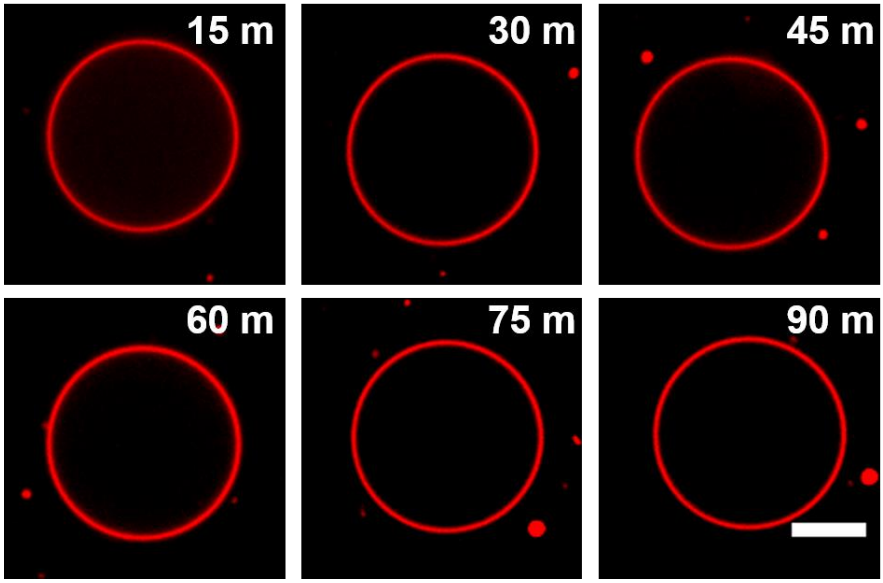

Figure 5. 9 Interaction between 5% HLM-GUV with 0.5 µM AH peptide. Spinning disc confocal microscopy images of GUVs consisting of 5 mol % of HLM, 98 mol % of DOPC doped with 1mol % of Rho-B DPPE upon interaction with 0.5µM AH peptide in 300mM glucose. Each labeled time corresponds to the peptide injection time. Scale bar is 10 µm.

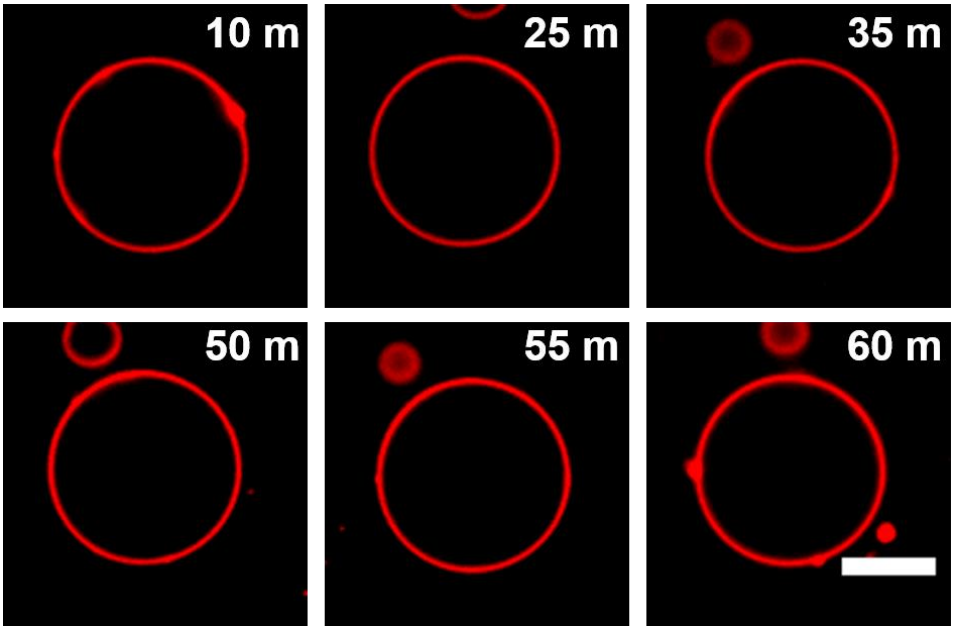

Figure 5. 10 Monitoring an interaction between 5% HLM-GUV and 1 μM AH peptide. Fluorescence micrographs were captured by SDCM measurements. Each indicated time scale corresponds to the AH peptide injection time. Scale bar indicates 10 μm.

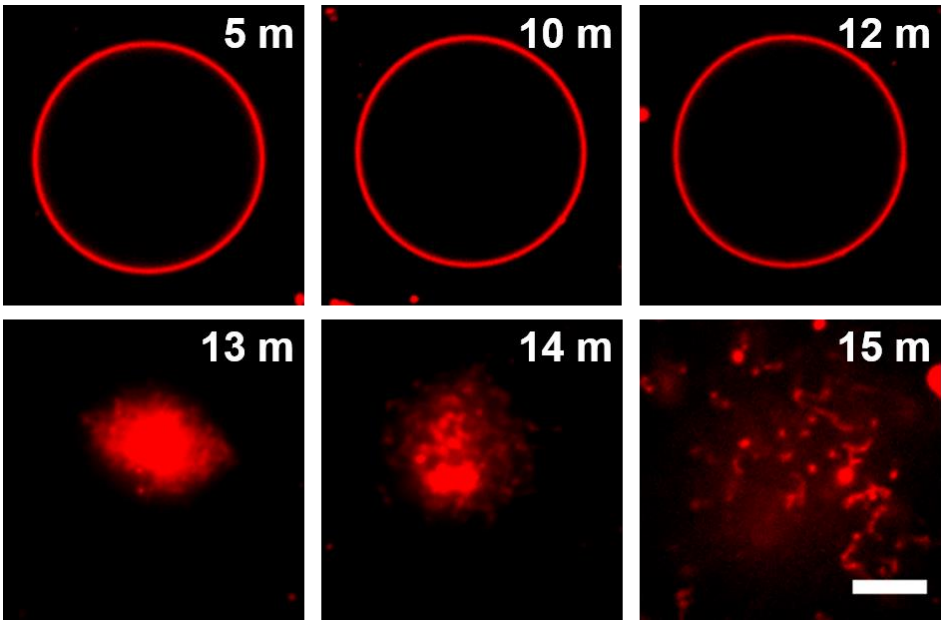

Figure 5. 11 Vesicular collapse of 5% HLM-GUV induced by 2.5 µM AH peptide. Fluorescence micrographs were captured by SDCM measurements. Note that each indicated time scale corresponds to the AH peptide injection time. Scale bar is 10 µm.

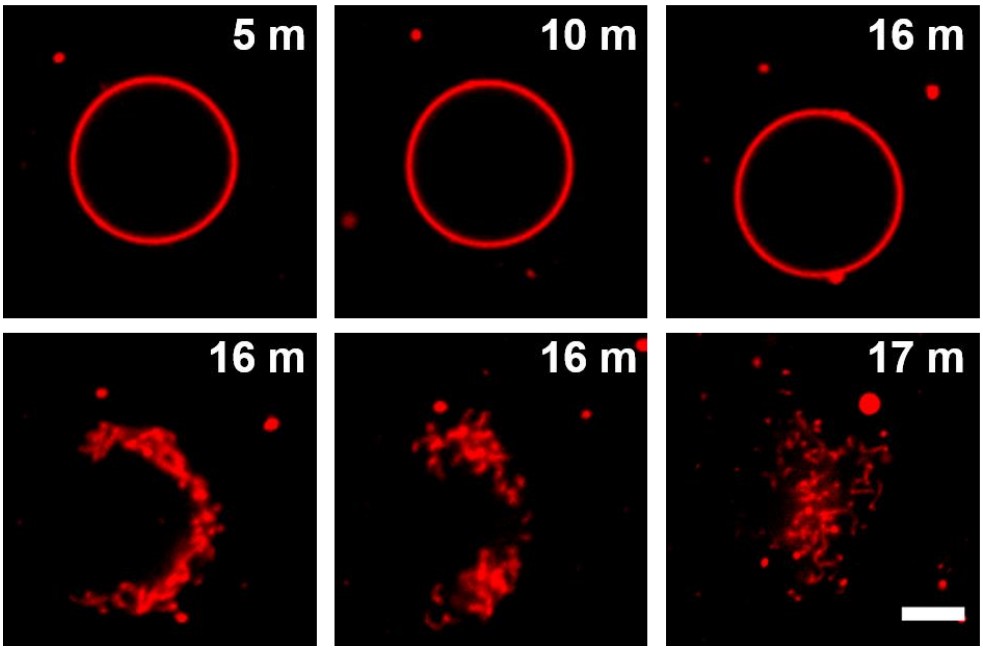

Figure 5. 12 Collapse of 5% HLM-GUV induced by injection of 5 µM AH peptide. Fluorescence micrographs were captured by SDCM measurements. Note that each indicated time scale corresponds to the AH peptide injection time. Scale bar represents 10 µm.

Even though these time-scales are not absolute values for each GUV measurement, the time kinetic information can be used as a supportive measure indicating that amount of HLM incorporated into bilayers of GUV prevented or delayed membrane deformation. The details of the fluorescence assay in presented in the next section.

Circularity of vesicles

As mentioned in the above discussion, smaller amount of AH peptide induced deformation of vesicles. We measured the circularity of the vesicles for each of the three cases of bilayers containing 0%, 1% and 5% of HLM. The amount of deformation upon addition of 0.5 µM of AH peptide was measured using ImageJ

program's roundness measurement. Here the vesicle edge is detected and the values are obtained through the ImageJ software's inbuilt based on fluorescence intensity threshold and contrast measurement algorithm that calculates the circularity of selected object. The results are shown in the following Figure 5. 13. For a perfect circle, the value of circularity is 1. As seen from the figure, the vesicles with 1% and 5% HLM membranes do not show a significant deviation from 1 upon addition of the peptide. DOPC vesicle however, is only 40% circular upon addition of AH peptide. This indicates that addition of small amounts HLM inhibits membrane deformation upon addition of peptide.

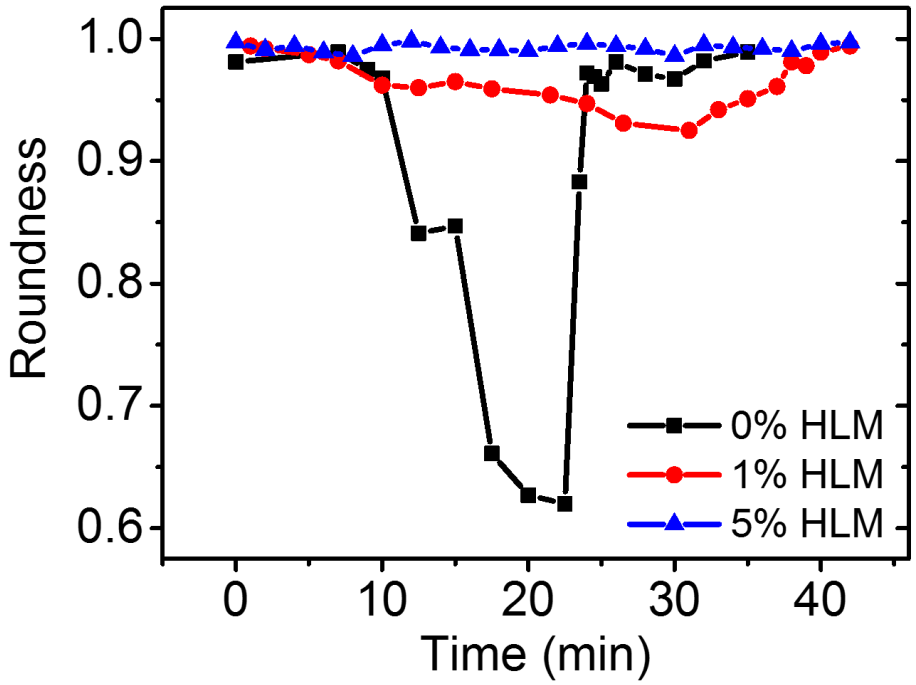

Figure 5. 13 AH peptide induces shapte deformations of vesicles. Circularity of monitoring vesicles were measured based on roundness measurements using ImageJ software.

5.3.3. Membrane stabilization by HLM against peptide interaction

Adsorption of AH peptide on GUVs was examined by adding fluorescently labeled AH peptide (TAMRA-AH) in unlabeled GUVs made of three different concentrations of HLM 0%, 1% and 5% in DOPC lipid (see below Figure 5. 14). The TAMRA-AH peptide adsorbs well on the GUV surface and can be visualized by observing the increase in the intensity of the initially non-fluorescence vesicles. For this, the average intensity of the vesicle is obtained within ROI at t = 0. Keeping the same ROI, the average intensity as a function of time is calculated for each vesicle. At least 10 vesicles of radius up to 20 microns were used to obtain statistical data. Each vesicle-intensity is also background subtracted and normalized to the initial intensity. From the plot, if the saturation point is taken, as the point after which there was not any changes in the intensity of the GUV membrane boundary, the following observations can be made (see Figure 5. 14C). For GUVs made from pure synthetic DOPC lipid, the intensity of the vesicles increases throughout the experiment. However, the rate of change of intensity is much slower after about 40 min. Up to 40 minutes the intensity increases almost linearly at a rate 0.164. If total intensity of fully adsorbed peptide is 1, where every lipid is interacting with AH peptide, one can see that about 70% of AH peptide is interacting with DOPC lipid of the GUV. As the amount of HLM is increased to 1%, the increase in the intensity shows multiple regions. Initially the intensity increases linearly at the rate of 0.07 for about 20 minutes. After 20 mins, the increase in the intensity is not linear for up to 60 minutes. The intensity stabilizes after 60 min. For 1% HLM case, the total intensity is around 50% when no further increase in intensity is observed. In comparison to pure DOPC, the adsorption of AH peptide is much lower in 1% HLM membranes. This further lowers to 38% for 5% HLM-GUV case. The increase in the intensity was also non-linear at an overall rate of 0.05 indicating that addition of HLM reduces AH-membrane interaction in a concentration dependent manner.

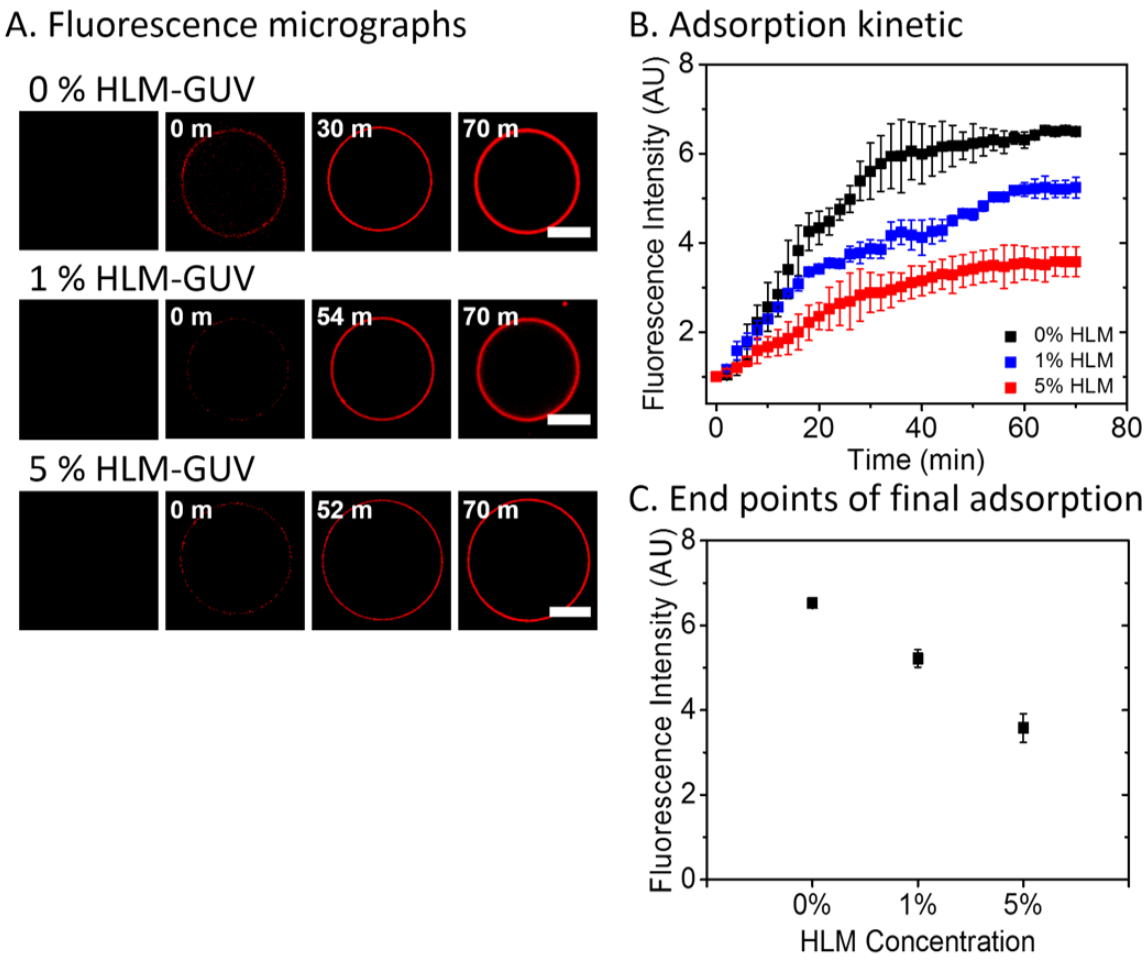

Figure 5. 14 Adsorption kinetic measurements using fluorescence labeled AH peptide against HLM containing and non-containing GUVs. (A) TAMRA-AH peptide was utilized to monitor adsorption kinetics with 0%, 1% and 5% HLM-GUV platforms. Scale bars indicate 10 μm. (B) From each corresponding time-lapse image from TAMRA-AH interaction measurements, average fluorescence intensities of each monitored vesicle were normalized to the initial values and plotted. (C) End point values of normalized fluorescence intensities of three GUV platforms were plotted.

From the florescent data (Figure 5. 14), it is observed that AH peptide adsorbs differently on bilayers of varying HLM concentration. To understand the membrane behavior upon the addition of HLM to membrane before and after the addition of AH peptide, electrical impedance measurements were performed. The primary motivation of this study was to check if membrane becomes leakier when HLM is

included and subsequently subjected to AH peptide interaction. We utilized 2.5 and 5µm of AH peptide on 1% and 5% HLM membranes. For this study, tethered bilayer membrane platform was employed where the tethered supported lipid bilayer membrane was formed using the kit provided from SDx Tethered Membranes.

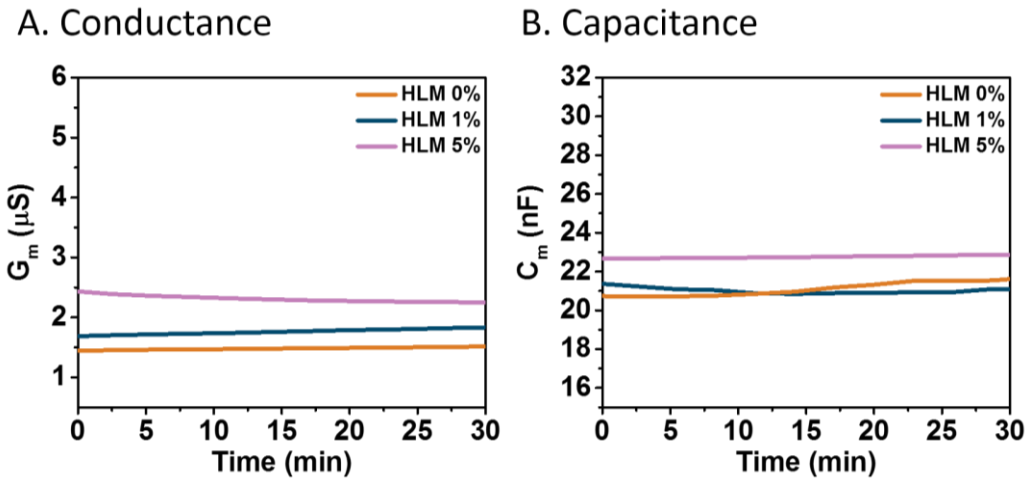

Figure 5. 15 Initial quality of tethered lipid bilayer (tLB) using 0%, 1% and 5% of HLM. Stabilized (A) conductance and (B) capacitance values of formed tLBs were measured and plotted.

Tethered membranes are lipid bilayers that are used as model cell membranes for a wide range of biophysical and physiological research. Here, a tethering foundation is chemically attached to a thin gold film that acts as an inert base and electrode. Bilayer can be formed on this substrate through solvent exchange technique[31]. Specifically, lipids are initially dissolved in ethanol and incubated for about 5 minutes. The ethanol is quickly exchanged with the buffer of choice which leads to the formation of stable supported bilayer. Using this technology, membrane capacitance and conductance values can be measured as shown in the above Figure 5. 15. tSLB platform has been widely used in ion channel, toxin and membrane studies using electrical and fluorescent data[32-34].

The plots of conductance and capacitance as a function of time for bilayers containing varying amounts of HLM are shown in Figures 5.15. The conductance

of membranes with HLM and without HLM is not significantly different before the addition of peptide. After the addition of 2.5 µM of AH peptide, the conductance of the membrane increases with increase in HLM concentration. The capacitance however decreases with HLM concentration. Increasing the amount of AH peptide to 5% shows the conductance increases almost linearly for both 1% and 5% HLM containing bilayers. The capacitance however decreases with concentration of HLM.

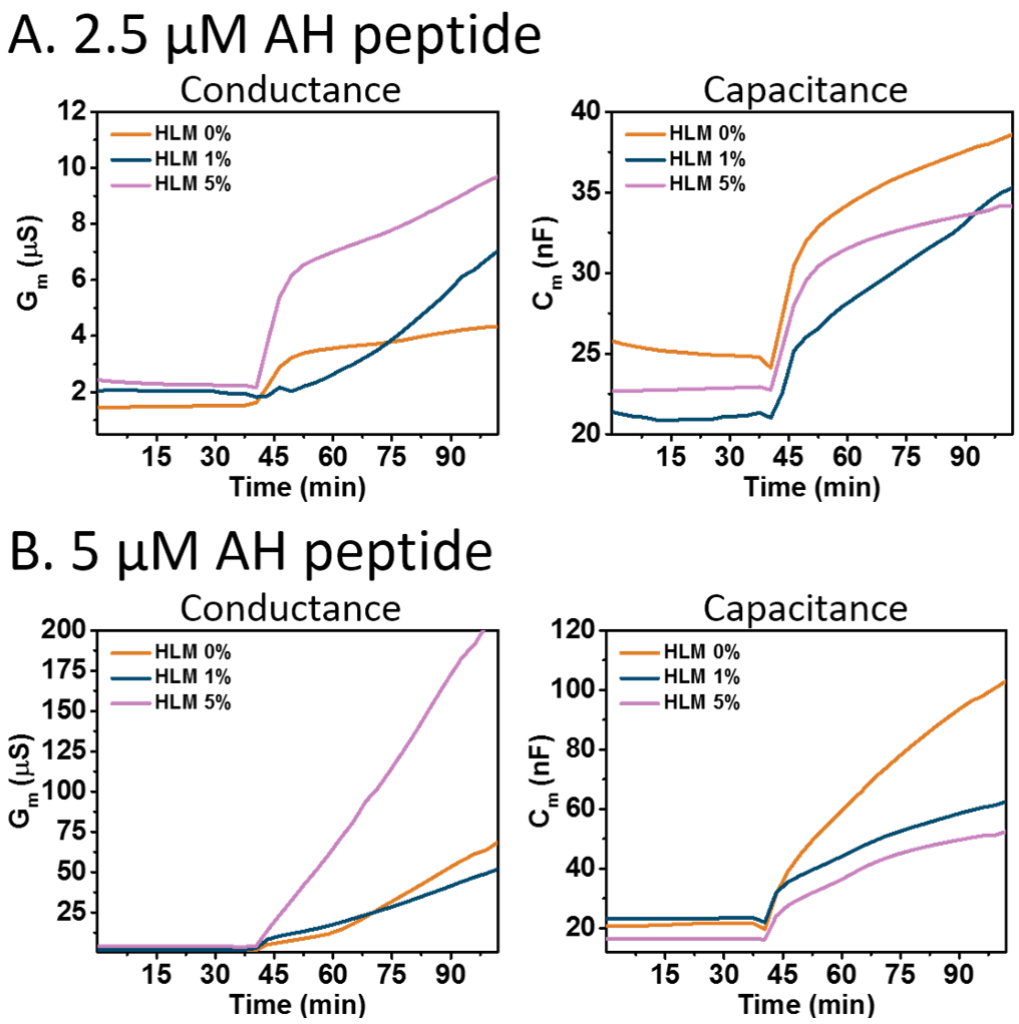

Figure 5. 16 Impedance spectroscopy measurements on varied HLM amount in tSLB platforms after the addition of AH peptide. Conductance and capacitance measurements before and after the additions of (A) 2.5 µM and (B) 5 µM of AH peptide were recorded.

5.4. Discussion

From the florescence measurement studies of GUVs in the result section (Figure 5. 14), two regions can be extracted. At lower concentrations of AH peptide (up to 1 µM), HLM membranes become more stable with the increased in stability as amount of HLM increases. At 2.5 and 5 µM of AH, the membrane is highly unstable and ruptures. Comparing the results obtained from the impedance measurements (Figure 5. 16), the membrane capacitance increases upon the addition of AH peptide to 1% and[32] 5% HLM bilayers. If bilayer is considered as a parallel plate capacitor, the thickness of the hydrocarbon chain region of the bilayer is inversely proportional to the capacitance[35]. Based on this, the following observations can be made: a) each bilayer is thinning over time upon the addition of AH peptide. The rate of thinning of pure DOPC membrane being fastest in both 2.5 and 5 µM AH peptide. b) At any given time after the addition of AH peptide, HLM containing membranes are thicker than pure DOPC membrane. c) The behavior of membranes with concentration for AH peptide is not linear. d) In all the membranes addition of AH peptide increases the conductivity.

First, we will look at pure DOPC membranes. When 2.5 µM AH peptide is added, the membrane becomes thinner (showing higher capacitance) as shown in Figure 5. 16A, while presence of HLM does not seem to alter the thickness of the bilayer. This is depicted as similar changes in capacitance upon addition of 2.5 µM AH peptide to HLM bilayers and the control experiment on DOPC bilayers as well. The addition of 5% AH peptide however causes a dramatic increase in capacitance of the control DOPC bilayer indicating a faster rate of membrane thinning as shown in Figure 5. 16B. On the other hand, HLM containing membrane shows stable thinning, highly similar with the 2.5 µM AH peptide addition case. It has been previously shown that peptides can cause membrane thinning in supported bilayer systems[36]. Drawing parallels from the systems in literature, one possible explanation is that upon the interaction with the peptide the head groups of lipids become spread, forcing the hydrocarbon chains to reorganize to fill the space which causes

membrane thinning, and reduction in dielectric barrier thereby increasing the conductance. This result explains the instability of pure DOPC bilayer upon addition of AH peptide as observed in the florescence experiments. Since the membrane is thinning at a faster rate at higher concentrations of AH peptide, the membrane becomes leakier eventually disintegrating as confirmed by both capacitance and fluorescence measurements.

Next, we investigated the conductance behavior of the three different membrane compositions as presented in Figure 5. 16. Comparing the rate of change of conductance of bilayers upon addition of 2.5 μM AH peptide with 5 μM AH peptide case, the following observations can be made: a) The conductivity increases with increase in peptide concentration, and b) the presence of HLM vary conductance in a concentration (of HLM) dependent manner.

The increase in conductivity indicates an increase in membrane permeability, which could be due to either membrane thinning, the presence of defects, or the presence of pores in the membrane. Addition of lower concentration of peptide although not altering the membrane thickness, it increases the conductance as shown in Figure 5. 16A. This could be attributed to the interaction of AH peptide with HLM in the bilayer, presumably because AH peptide binding can induce membrane thinning through its intercalation in the lipid bilayer or cause pore formation—either scenario is consistent with the observed increase in conductance[37-38]. These defects are more pronounced as the amount of HLM is increased to 5% as presented in Figure 5. 16B. Further, as HLM is increased to 5 %, the defects increased significantly upon the addition of higher amount of AH peptide indicating that AH peptide interacts with HLM. Lastly, it is worth noting that at higher AH peptide concentration (see Figure 5. 16B), HLM containing membranes are thicker than the membranes composed of pure synthetic DOPC lipid.

These observations indicate that AH peptide causes instability in bilayers. The instability can be caused by two factors that are not synergistic. AH peptide causes membrane thinning in pure DOPC membranes and makes them unstable. However,

in the presence of HLM, the membrane thinning is not a significant factor, but the instability is caused due to defects created upon interaction with HLM in the bilayer. Both conductance and capacitance measurements support observations made using fluorescence studies. One possible application of such mixed lipid membrane systems is in therapeutic applications. We have previously shown that AH peptide interacts differently with Huh 7 cell line, which is a human liver tumor derived cell line, in comparison to the synthetic lipid bilayers[18]. In these studies, it was observed that AH peptide binding (adsorption) was stronger in the case of Huh 7 cells. The study suggested the development of AH binding inhibitors for potential clinical applications. In this thesis, it has been shown that the incorporation of small amounts of HLM can potentially disrupt peptide adsorption onto lipid membranes in line with the suggestions.

Finally, we investigated the adsorption efficiency of AH peptide on HLM membranes as shown in Figure 5. 14. For this purpose, we investigated dye adsorption kinetics by employing 5 µM of TAMRA dye labeled AH peptide. The amount of TAMRA-AH adsorbed on bilayer of GUVs was measured with time, from which the adsorption reaction order and reaction constant is evaluated. For the given experimental conditions, following approximations can be made: first, the concentration of the adsorbate (TAMRA-AH) does not change in the bulk solution throughout the experiment. In other words, the measurements were recorded in equilibrium conditions, and the measured fluorescence intensities are directly proportional to the concentration of peptide. Second, the temperature for all the experiments is kept constant. Lastly, since the size of GUVs is too large to be assumed as a small spherical model, the assumption was made that the model platform is an infinite bilayer

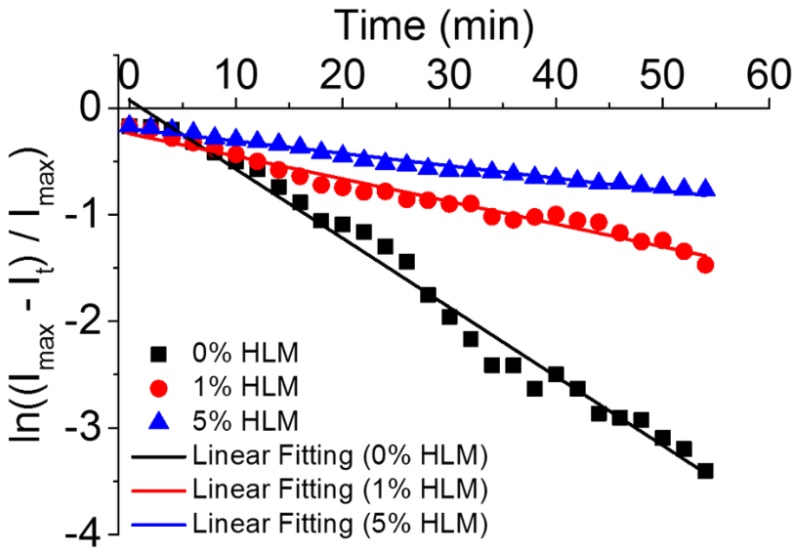

Figure 5. 17 Adsorption kinetics of AH peptide binding to GUVs based on pseudo-first-order reaction showing linear relationship over measured time. Based on the changes in fluoroscence intensity measurments from the different GUV platforms including 0 %, 1 % and 5 % HLM upon the addition of 5 μM of TAMRA dye labeled AH peptide, the relative linear fitting of adsorption points were plotted.

From the Figure 5. 17, our initial attempt was to test a simple pseudo first order adsorption reaction model. Adsorption reaction models originate from chemical kinetics and are modeled as a pseudo first-order system. The rate of fluorescent intensity changes upon addition of TAMRA-AH peptide based on the adsorption capacity can be given as:

$$\frac{\mathrm{d}I_t}{\mathrm{dt}} = k\,(I_{max} - I_t)$$

Where, I_t is the intensity at any given time t on the vesicle arising from adsorption of TAMRA-AH on vesicle, I_{max} is the amount of TAMRA-AH adsorbed at equilibrium and k is the first order rate constant. From the initial conditions when the intensity on the vesicle is 0 (I_t =0 at t = 0), the above equation can be written as

$$\ln(I_{max} - I_t) = \ln(I_{max}) - kt$$

Plotting $\left[\frac{ln(I_{max}-I_t)}{\ln(I_{max})}\right]$ against the time t and fitting a linear plot will give the rate constant from slope. The values of the rate constants (slope) for pure DOPC bilayer, 1% and 5% of HLM membranes are 0.06 min^{-1}, 0.02 min^{-1} and 0.01 min^{-1}, respectively. Each linear fitting resulted in R-square values of 0.98, 0.97 and 0.98, respectively for 0%, 1% and 5% of HLM. The intercept values are -0.07, -0.1 and -0.2, respectively. The intercept values are close to zero indicating that the first order approximation is valid for the current study. From the rate constants, it is evident that TAMRA-AH adsorbs on pure DOPC membranes faster than in the case of HLM–DOPC membranes. The interaction however is significantly reduced for higher HLM membrane (5% HLM). As observed in the impedance studies, addition of HLM increases the thickness of the bilayer when subjected to AH peptide. From the adsorption kinetic studies, it is observed that higher HLM containing membranes also inhibits AH adsorption on the membrane. From these observations, one can safely conclude that membrane can be stabilized with the inclusion of small amount of HLM into pure DOPC lipid bilayers. At higher concentrations of HLM, the behavior is rather complex. On one hand, the conductivity measurements show a significant increase in the conductivity that is usually ascertained to defects and pores or membrane thinning while the adsorption kinetic result shows less adsorption upon increase in the amount of HLM. Hence, the effects of HLM on membrane-peptide interactions exhibit a strong dependence on HLM fraction and corresponding membrane structural properties (*e.g.,* permeability/molecular packing).

5.5. Conclusion

In conclusion, in this chapter, we investigated the interaction of AH peptide with a natural membrane extract in artificial bilayer systems. We show that artificial membrane bilayer assemblies can be formed using small amounts of HLM membrane into DOPC lipids. Further, both adsorption kinetics and impedance

spectroscopy show significant effects of addition of HLM to pure DOPC membrane when interacting with AH peptide. Addition of HLM causes membrane thickening and less binding of AH peptide to the vesicles. These results show promising applications of blending natural and synthetic lipid mixtures in GUV platforms in order to study interactions involving biomacromolecules such as amphipathic peptides and higher-order protein assemblies (*e.g.*, membrane attack complex). Indeed, the above experiments emphasize the importance of natural extracts for biophysical studies which are otherwise performed on simple one component/two component synthetic lipid mixtures. In future, investigation of the impedance properties and relation to the binding behavior of AH peptide and other membrane-active compounds will be explored in detail.

References

1. Cho, N.-J.; Dvory-Sobol, H.; Xiong, A.; Cho, S.-J.; Frank, C. W.; Glenn, J. S., Mechanism of an Amphipathic α-Helical Peptide's Antiviral Activity Involves Size-Dependent Virus Particle Lysis. *ACS Chemical Biology* **2009,** *4* (12), 1061-1067.

2. Hanson, J. M.; Gettel, D. L.; Tabaei, S. R.; Jackman, J.; Kim, M. C.; Sasaki, D. Y.; Groves, J. T.; Liedberg, B.; Cho, N.-J.; Parikh, A. N., Cholesterol-Enriched Domain Formation Induced by Viral-Encoded, Membrane-Active Amphipathic Peptide. *Biophysical Journal* **2016,** *110* (1), 176-187.

3. Hardy, G. J.; Nayak, R.; Zauscher, S., Model cell membranes: Techniques to form complex biomimetic supported lipid bilayers via vesicle fusion. *Current opinion in colloid & interface science* **2013,** *18* (5), 448-458.

4. Kim, M. C.; Gunnarsson, A.; Tabaei, S. R.; Höök, F.; Cho, N.-J., Supported lipid bilayer repair mediated by AH peptide. *Physical Chemistry Chemical Physics* **2016,** *18* (4), 3040-3047.

5. Cho, N.-J.; Pham, E. A.; Hagey, R. J.; Lévêque, V. J.; Ma, H.; Klumpp, K.; Glenn, J. S., Reconstitution and Functional Analysis of a Full-Length Hepatitis C

Virus NS5B Polymerase on a Supported Lipid Bilayer. *ACS central science* **2016,** *2* (7), 456-466.

6. Menger, F. M.; Angelova, M. I., Giant vesicles: imitating the cytological processes of cell membranes. *Accounts of chemical research* **1998,** *31* (12), 789-797.

7. Walde, P.; Cosentino, K.; Engel, H.; Stano, P., Giant vesicles: preparations and applications. *ChemBioChem* **2010,** *11* (7), 848-865.

8. Lee, M.-T.; Hung, W.-C.; Chen, F.-Y.; Huang, H. W., Mechanism and kinetics of pore formation in membranes by water-soluble amphipathic peptides. *Proceedings of the National Academy of Sciences* **2008,** *105* (13), 5087-5092.

9. Tamba, Y.; Yamazaki, M., Single giant unilamellar vesicle method reveals effect of antimicrobial peptide magainin 2 on membrane permeability. *Biochemistry* **2005,** *44* (48), 15823-15833.

10. Ambroggio, E. E.; Separovic, F.; Bowie, J. H.; Fidelio, G. D.; Bagatolli, L. A., Direct visualization of membrane leakage induced by the antibiotic peptides: maculatin, citropin, and aurein. *Biophysical Journal* **2005,** *89* (3), 1874-1881.

11. dos Santos Cabrera, M. P.; Alvares, D. S.; Leite, N. B.; Monson de Souza, B.; Palma, M. S.; Riske, K. A.; Ruggiero Neto, J. o., New insight into the mechanism of action of wasp mastoparan peptides: lytic activity and clustering observed with giant vesicles. *Langmuir* **2011,** *27* (17), 10805-10813.

12. Lee, J.; Hwang, J.-S.; Hwang, B.; Kim, J.-K.; Kim, S. R.; Kim, Y.; Lee, D. G., Influence of the papiliocin peptide derived from Papilio xuthus on the perturbation of fungal cell membranes. *FEMS microbiology letters* **2010,** *311* (1), 70-75.

13. Park, C.; Lee, D. G., Fungicidal effect of antimicrobial peptide arenicin-1. *Biochimica et Biophysica Acta (BBA)-Biomembranes* **2009,** *1788* (9), 1790-1796.

14. Hwang, B.; Hwang, J.-S.; Lee, J.; Lee, D. G., Antifungal properties and mode of action of psacotheasin, a novel knottin-type peptide derived from Psacothea hilaris. *Biochemical and biophysical research communications* **2010,** *400* (3), 352-357.

15. Huang, H. W., Free energies of molecular bound states in lipid bilayers: lethal concentrations of antimicrobial peptides. *Biophysical Journal* **2009,** *96* (8), 3263-3272.

16. Henriksen, J.; Rowat, A. C.; Ipsen, J. H., Vesicle fluctuation analysis of the effects of sterols on membrane bending rigidity. *European Biophysics Journal* **2004,** *33* (8), 732-741.

17. Loftus, A. F.; Noreng, S.; Hsieh, V. L.; Parthasarathy, R., Robust measurement of membrane bending moduli using light sheet fluorescence imaging of vesicle fluctuations. *Langmuir* **2013,** *29* (47), 14588-14594.

18. Cho, N.-J.; Cheong, K. H.; Lee, C.; Frank, C. W.; Glenn, J. S., Binding dynamics of hepatitis C virus' NS5A amphipathic peptide to cell and model membranes. *Journal of virology* **2007,** *81* (12), 6682-6689.

19. Tabaei, S. R.; Rabe, M.; Zhdanov, V. P.; Cho, N.-J.; Höök, F., Single vesicle analysis reveals nanoscale membrane curvature selective pore formation in lipid membranes by an antiviral α-helical peptide. *Nano Letters* **2012,** *12* (11), 5719-5725.

20. Tabaei, S. R.; Cho, N., Lamellar sheet exfoliation of single lipid vesicles by a membrane-active peptide. *Chemical Communications* **2015,** *51* (51), 10272-10275.

21. Jackman, J. A.; Saravanan, R.; Zhang, Y.; Tabaei, S. R.; Cho, N. J., Correlation between Membrane Partitioning and Functional Activity in a Single Lipid Vesicle Assay Establishes Design Guidelines for Antiviral Peptides. *Small* **2015,** *11* (20), 2372-2379.

22. Maurer, N.; Fenske, D. B.; Cullis, P. R., Developments in liposomal drug delivery systems. *Expert opinion on biological therapy* **2001,** *1* (6), 923-947.

23. Samad, A.; Sultana, Y.; Aqil, M., Liposomal drug delivery systems: an update review. *Current drug delivery* **2007,** *4* (4), 297-305.

24. Tamba, Y.; Ohba, S.; Kubota, M.; Yoshioka, H.; Yoshioka, H.; Yamazaki, M., Single GUV method reveals interaction of tea catechin (−)-epigallocatechin gallate with lipid membranes. *Biophysical Journal* **2007,** *92* (9), 3178-3194.

25. Inaoka, Y.; Yamazaki, M., Vesicle fission of giant unilamellar vesicles of liquid-ordered-phase membranes induced by amphiphiles with a single long hydrocarbon chain. *Langmuir* **2007,** *23* (2), 720-728.

26. Peterlin, P.; Arrigler, V.; Kogej, K.; Svetina, S.; Walde, P., Growth and shape transformations of giant phospholipid vesicles upon interaction with an aqueous oleic acid suspension. *Chemistry and physics of lipids* **2009,** *159* (2), 67-76.

27. Shaklee, P. M.; Semrau, S.; Malkus, M.; Kubick, S.; Dogterom, M.; Schmidt, T., Protein incorporation in giant lipid vesicles under physiological conditions. *ChemBioChem* **2010,** *11* (2), 175-179.

28. Fenz, S. F.; Sachse, R.; Schmidt, T.; Kubick, S., Cell-free synthesis of membrane proteins: Tailored cell models out of microsomes. *Biochimica et Biophysica Acta (BBA)-Biomembranes* **2014,** *1838* (5), 1382-1388.

29. Angelova, M. I.; Dimitrov, D. S., Liposome electroformation. *Faraday discussions of the Chemical Society* **1986,** *81*, 303-311.

30. Rodriguez, N.; Pincet, F.; Cribier, S., Giant vesicles formed by gentle hydration and electroformation: a comparison by fluorescence microscopy. *Colloids and Surfaces B: Biointerfaces* **2005,** *42* (2), 125-130.

31. Tabaei, S. R.; Choi, J.-H.; Haw Zan, G.; Zhdanov, V. P.; Cho, N.-J., Solvent-Assisted Lipid Bilayer Formation on Silicon Dioxide and Gold. *Langmuir* **2014,** *30* (34), 10363-10373.

32. Terrettaz, S.; Mayer, M.; Vogel, H., Highly electrically insulating tethered lipid bilayers for probing the function of ion channel proteins. *Langmuir* **2003,** *19* (14), 5567-5569.

33. Wallin, M.; Choi, J.-H.; Kim, S. O.; Cho, N.-J.; Andersson, M., Peptide-induced formation of a tethered lipid bilayer membrane on mesoporous silica. *European Biophysics Journal* **2015,** *44* (1-2), 27-36.

34. Jackman, J. A.; Knoll, W.; Cho, N.-J., Biotechnology applications of tethered lipid bilayer membranes. *Materials* **2012,** *5* (12), 2637-2657.

35. Raguse, B.; Braach-Maksvytis, V.; Cornell, B. A.; King, L. G.; Osman, P. D.; Pace, R. J.; Wieczorek, L., Tethered lipid bilayer membranes: formation and ionic reservoir characterization. *Langmuir* **1998,** *14* (3), 648-659.

36. Sokolov, Y.; Kozak, J. A.; Kayed, R.; Chanturiya, A.; Glabe, C.; Hall, J. E., Soluble amyloid oligomers increase bilayer conductance by altering dielectric structure. *The Journal of general physiology* **2006,** *128* (6), 637-647.

37. Cho, N.-J.; Cho, S.-J.; Hardesty, J. O.; Glenn, J. S.; Frank, C. W., Creation of lipid partitions by deposition of amphipathic viral peptides. *Langmuir* **2007,** *23* (21), 10855-10863.

38. Wang, J.; Liu, K.-W.; Biswal, S. L., Characterizing α-Helical Peptide Aggregation on Supported Lipid Membranes Using Microcantilevers. *Analytical chemistry* **2014,** *86* (20), 10084-10090.

Chapter 6

Controlling Membrane Compartmentation *via* Glycerol Monoglyceride-Induced Fission and Fusion

In an effort to reveal evolution of phospholipid membranes from early cells, single-chain lipids including fatty acids have been gaining attentions. There have been several studies employing giant unilamellar vesicles (GUV) as a cell membrane-mimetic platform to observe interactions against various fatty acids. Herein, I present an experimental study of interaction between GUVs and glycerol monolaurate (GML) which has never been utilized with GUV model platforms. Based on the experimental results acquired with both micellar and monomeric states of GML, vesicle fission and fusion behaviors were observed from confocal fluorescence microscopy time-lapse measurements regardless of GUV lipid compositions. In contrast, structurally similar compounds such as 1-O-dodecyl-rac-glycerol (DDG) did not show any fusion or fission behaviors in both high and low concentrations. The presented results can provide important cue for further understanding the molecular evolution of cellular membrane from single-chain fatty acids to modern phospholipids.

6.1. Introduction

It is most likely presumed that the very first cellular membranes were risen from single-chain lipids including single or triple glycerides and their derivatives which have been already existed in the prebiotic environment[1-4]. Simple lipid chains comprise cellular membranes which are highly permeable to nucleotides representing dynamic features of spontaneous division processes leading to cell growth[5-7]. It has been reported that the modern cells synthesize phospholipids, which is a key building block of membrane, with having hydrophobic tails in a prevention of unregulated influx of materials including ions and any polar molecules[8-11]. In this way, the cell metabolic processes can be regulated through controlling of influx and efflux of essential cellular nutrients. Therefore, cell membranes have been evolved from a simple membrane consisted of single chain lipids to a more complex one composed of phospholipids to have more efficiently regulations over membrane transportation systems[12-15]. The evolution or simply a transition from single lipid-chains or fatty acids evolved into phospholipids can lead us significant insights of origin of life, a very beginning model of cell.

It has been reported that glycerol esters are able to self-assemble into bilayer forms[16-18]. Since the glycerol head group does react with hydrogen ions, glycerol esters or monoglycerides can be spontaneously formed into bilayer forms at various ranges of pH[4]. In contrast, depending on melting points, most fatty acids do not spontaneously form into bilayered vesicle at low pH ranges. Even though there is no direct evidence that the monoglycerides were found in the pre-biotic environment, it is presumed that the monoglycerides were synthesized from the esterification of natural carboxylic acids[3]. This also lead us to take it as a first step of chemical evolution transiting from simple carboxylic form of molecules into self-assembled amphiphiles. The resistant feature of monoglycerides against various ranges of pH strongly supports that the natural esterification was conducted for the better evolution[19]. In addition, most phospholipids share the same glycerol backbone with esterified fatty acids[20].

Among many, compartmentalization is the most essential stage in forming the very first cells or protocells in the evolution period of prebiotic chemical environment[21-25]. As briefly mentioned above, it is important to note that the building blocks of modern cellular membranes, phospholipids, utilize glycerol as a main backbone structure. This indicates that the ester bond of glycerol has been the one of the strong candidates responsible for the evolution that has led into current form of phospholipid layers[26]. In fact, Simoneit et al reported that the monoglycerides were able to spontaneously assemble into membrane like structures featuring multi-lamellarity along with budding of small liposomes[26]. In addition, it is importantly to note that C-10 and C-12 monoglycerides have been reported to self-assemble into vesicle format which are originally budded from multilamellar structures, but any longer carbon chains of monoglycerides have not been observed to form any spontaneously produced liposomes[27].

Among various cell membrane mimetic model platforms as listed in Chapter 2 (Literature Review) to study interactions between foreign materials at the cellular membrane interface, giant unilamellar vesicle (GUV) is the only model platform that can provide microscopy optical resolution of morphological dynamics allowing one to observe new changes which is not achievable with small unilamellar vesicles or lipid bilayer platforms[28-30]. In fact, numerous new findings have been reported employing the GUV platforms against fatty acids or their derivatives. Some of the representative key information obtained from the reported studies includes vesicle fission behavior induced by lysophosphatidylcholine (lyso PC 16:0)[31-32] and sodium dodecyl sulfate (SDS)[31], octylglucoside[31], shape transformations induced by lyso PC 16:0[31], burst of vesicles caused by oleic acid[33] and tea catechin (EGCg)[34], and vesicle budding, invagination and evagination phenomena were observed from various concentrations of oleic acid[33, 35]. However, among the listed fatty acids, monoglycerides surprisingly never have been tested against GUV model platforms, albeit it is one of the key materials that can lead us to reveal the cellular membrane origins. Hence, it is necessary to conduct experimental study to observe the interactions between GUVs with single-chain monoglycerides.

In this chapter, in order to study membrane interactions of various single monoglycerides including glycerol monolaurate (GML), 1-O-dodecyl-rac-glycerol (DDG) and lauric acid against cell sized GUV model membrane platforms, 20-30 μm diameters of GUVs were employed. From the experiments based on confocal fluorescence microscopy measurements, we find that interactions with the single monoglycerides induced significant changes of vesicle morphology including the first time reporting of fission and fusion behaviors based on critical micelle concentration (CMC) effects of GML. Hence, exact assessment of micelle forming concentrations of each tested single chain monoglycerides were measured by fluorescence spectroscopy. Further quantitative analyses were conducted by obtaining changes of membrane stiffness and vesicle area derived from recorded fluorescence micrographs. Taken together, the presented results herein reported dynamic membrane morphological responses from the interactions between GUVs and monoglycerides which have never been reported.

6.2. Materials & Experimental Methods

6.2.1. Materials

1,2-Dioleoyl-*sn*-glycero-3-phosphocholine (DOPC), 1,2-dioleoyl-*sn*-glycero-3-phosphoethanolamine-N-(lissamine rhodamine B sulfonyl) (Ammonium salt) (Rhod-PE fluorophore), cholesterol and sphingomyelin were purchased from Avanti Polar Lipids, Inc. (Alabaster, AL). Lauric acid, glucose, and sucrose were obtained from Sigma-Aldrich (St Louis, MO). Glycerol monolaurate (GML) was obtained from Abcam (Cambridge, U.K.), and 1-O-dodecyl-rac-glycerol (DDG) was obtained from Angene International Limited. All solutions were prepared with Milli-Q-treated water (>18 MΩ·cm) (Millipore, Billerica, MA).

6.2.2. Giant unilamellar vesicle electroformation

Giant unilamellar vesicles (GUV) were prepared using the electroformation method[36]. Stock solutions of lipid mixtures based on defined molar ratios were prepared at a mass concentration of 1 mg/ml in chloroform. 20 µL of the stock solution was spread onto an indium tin oxide (ITO)-coated glass slide within an area delimited by an O-ring and the deposited solution was allowed to dry in vacuum for at least 1 hr. Electroformation was performed in a 300 mM sucrose solution by using a commercial Vesicle Prep Pro instrument (Nanion, Munich, Germany). GUVs were spontaneously formed by applying an AC current at 5 Hz, 3 V and at 45°C for 120 min. Then, the GUVs were diluted in a 300 mM glucose solution for fluorescence microscopy imaging. For GUV microscopy imaging experiments, it is a common strategy to conduct electroformation of GUVs using sucrose solution[37-40]. Then, for the microscopy imaging purposes, very small amount of GUV solution (e.g. ~ 5 to 10 µL) is added to a well containing equimolar concentration of glucose solution (volume of 200 ~ 300 µL) in order to allow sedimentation of the vesicles to the bottom of the well (or imaging chamber) and to facilitate their localization for imaging purposes. Hence, due to a different gravity caused by a density gradient between sucrose (1.59 g/cm^3) and glucose (1.54 g/cm^3), GML, lauric acid and DDG were all dissolved in glucose solutions to not to disturb equimolar osmolarity pressure between inside and outside of GUVs throughout the measurements. Also, all employed fatty acids were initially obtained as powder forms which all have to be solubilized in the same solution used to image the GUVs.

6.2.3. Sample preparation of single-chain lipid amphiphiles

Stock solutions of GML and DDG were prepared by dissolving the appropriate mass of compounds in ethanol to a stock concentration of 200 mM. Before each experiment, an aliquot from the stock solution was diluted 1:100 (v:v) with 300 mM glucose solution. The concentration of the diluted compound was 5 mM. To increase

the solubility of all test samples, the dissolved samples were heated in a 70 °C water bath for 30 min and then allowed to cool before experiment. All samples were prepared immediately before experiment.

6.2.4. Spinning disc confocal microscopy measurements

Spinning disk confocal microscopy experiments were carried out using an inverted Eclipse Ti-U microscope (Nikon) fitted with an X-Light spinning-disk confocal unit (CrestOptics, Italy) and an Andor iXon+ EMCCD camera (Andor Technology, Northern Ireland). For measurements, a 60× oil immersion objective (NA 1.49) was employed and Rhod-DPPE (Ex/Em; 560/583 nm) was exposed with a 50 mW 532 nm laser line. A minimum of 5 GUVs were imaged for each experimental condition.

6.2.5. Vesicle fluctuation analysis

The bending modulus of GUV membranes were determined by analyzing membrane fluctuations from time-lapse recorded fluorescence micrographs. As mentioned in Chapter 3, the edge of a GUV was tracked and its motion was analyzed by using a previously reported MATLAB code[41]. From each selected range of micrograph slices, the average bending modulus was calculated for further analysis of membrane deformations that were induced by the addition of single-chain lipid amphiphiles.

6.2.6. Critical micelle concentration measurement

Measurements of critical micelle concentration (CMC) values for the single-chain lipid amphiphiles were conducted by employing a Cary Eclipse fluorescence spectrophotometer (Varian, Inc., Australia). 1-pyrenecarboxaldehyde in 300 mM

glucose solution was used as the probe for measurement of the fluorescence emission spectrum. For each prepared concentration of tested sample, 0.1 µM of probe was included. The fluorescence spectrum measurements were conducted a minimum of six times in order to compute the average value.

6.3. Principle Outcomes & Discussion

6.3.1. Shape transformation and fission of DOPC GUVs induced by GML

To investigate the effect of glycerol monolaurate (GML) and other related molecules on GUVs, rhodamine-doped zwitterionic DOPC GUVs were prepared and utilized as a cell membrane model platform. Throughout the measurements, spinning disk confocal fluorescence microscopy was employed to track and record any morphological changes of GUVs (~ 20-30 µm diameter) against, its fatty acid analogue lauric acid, or its ether-version -O-dodecyl-rac-glycerol (DDG). The chemical structures of all three compounds are presented in Figure 6. 1.

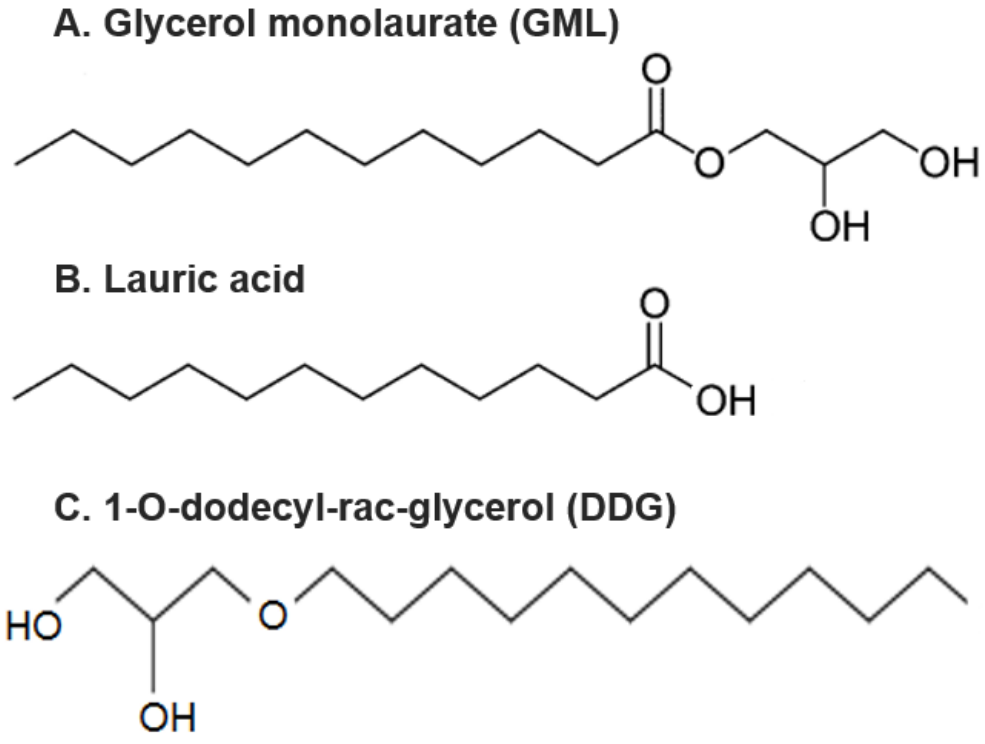

Figure 6. 1 Chemical structures of target antimicrobial lipids.

All three compounds have a saturated 12-carbon long primary alkyl chain as the main backbone. Both GML and DDG are attached to a glycerol backbone (a precursor component to form glycerophospholipids) *via* an ester or ether linkage, respectively, and are neutral compounds. By contrast, lauric acid has a carboxylic acid functional group and is an anionic molecule under typical solution conditions.

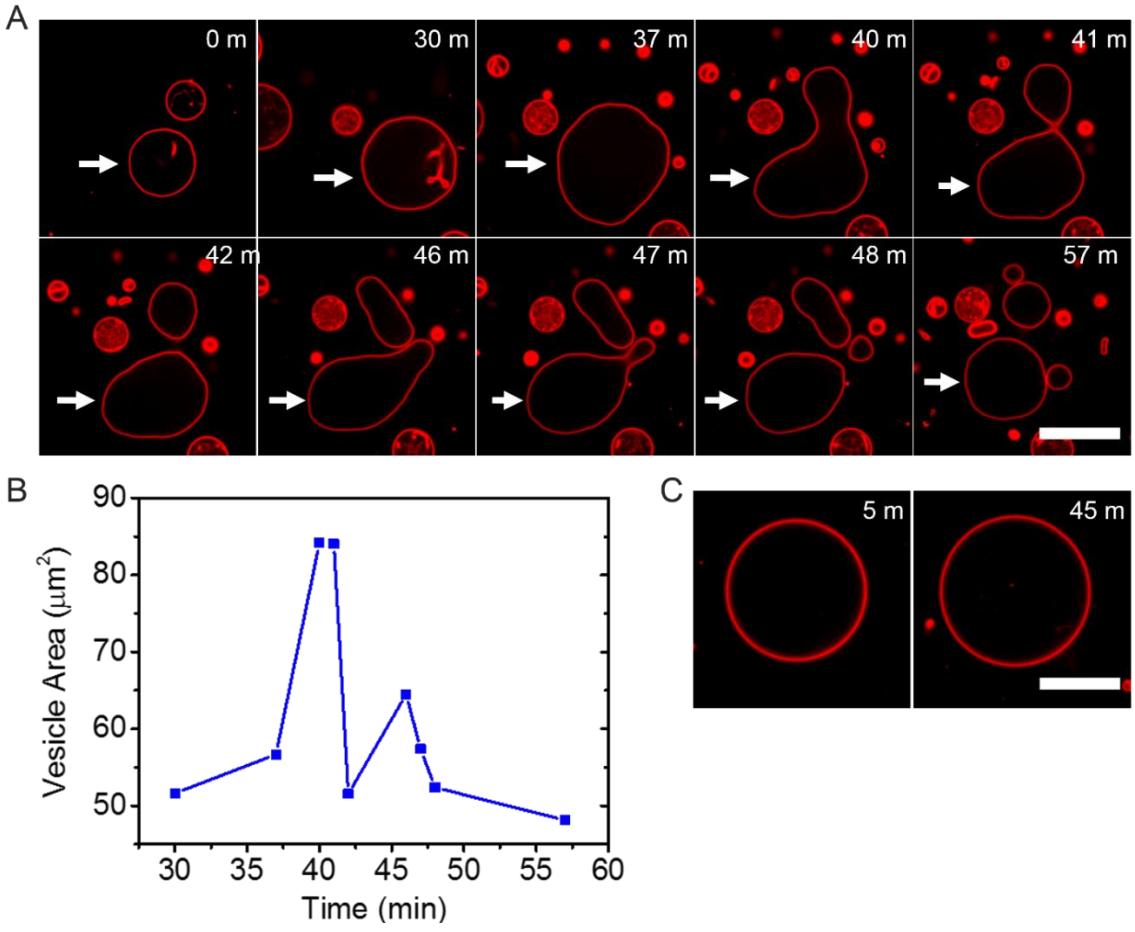

Figure 6. 2 GML-induced fission of DOPC GUVs. (A) Confocal fluorescence images of GUVs consisting of DOPC doped with Rho-B DOPE upon incubation with 200 μM glycerol monolaurate (GML) in 300 mM glucose. GUVs contain 300 mM of sucrose. (B) Enclosed area of selected GUV (indicated by white arrow in (A)) was measured based on image threshold analysis and plotted over time. (C) DOPC-GUV was incubated with 4 mM

of lauric acid. Each time corresponds to after the corresponding fatty acid injection time. Scale bar represents 20 μm.

In order to explore the interaction effects of GML on GUVs, a relatively high concentration of GML was first tested. Upon incubating DOPC-GUVs with 200 μM GML, morphological transformations and subsequent vesicle fission behaviors were observed in the confocal fluorescence microscopy measurements (Figure 6. 2A). Before fission occurred, various shape transformations such as elongated tubes, prolate and adjacent spheres connected by a narrow neck, were observed during an intermediate phase (Figure 6. 2A). As presented in Figure 6. 2B, the surface area changes of a selected GUV were estimated by utilizing a fluorescence intensity threshold feature. It was determined that the vesicle went through a cycle of swelling and contraction after fission. Even though the initially monitored GUV (see white arrow in Figure 6. 2A) twice experienced the vesicle fission process resulting in the creation of two smaller daughter vesicles, the area of the selected GUV did not appear to significantly differ from the 1st swelling state (30 minutes after the interaction). As for control measurements, lauric acid was utilized to investigate whether it can also induce similar morphological changes against DOPC GUVs. As can be seen in Figure 6. 2C, even at 4 mM concentration of lauric acid, which is 20 times higher than the GML concentration used to induce fission (Figure 6. 2A), there was no induction of any morphological changes of the vesicle throughout the 1 hr period of fluorescence microscopy monitoring. Based on this observation, it can be concluded that GML exerts significantly more potent effects against DOPC GUVs than its fatty acid equivalent. Based on this result, I decided to test lower concentrations of GML in order to determine both the minimum GML concentration required to induce morphological effects as well as the dependence of the resulting morphological responses on the specific GML concentration.

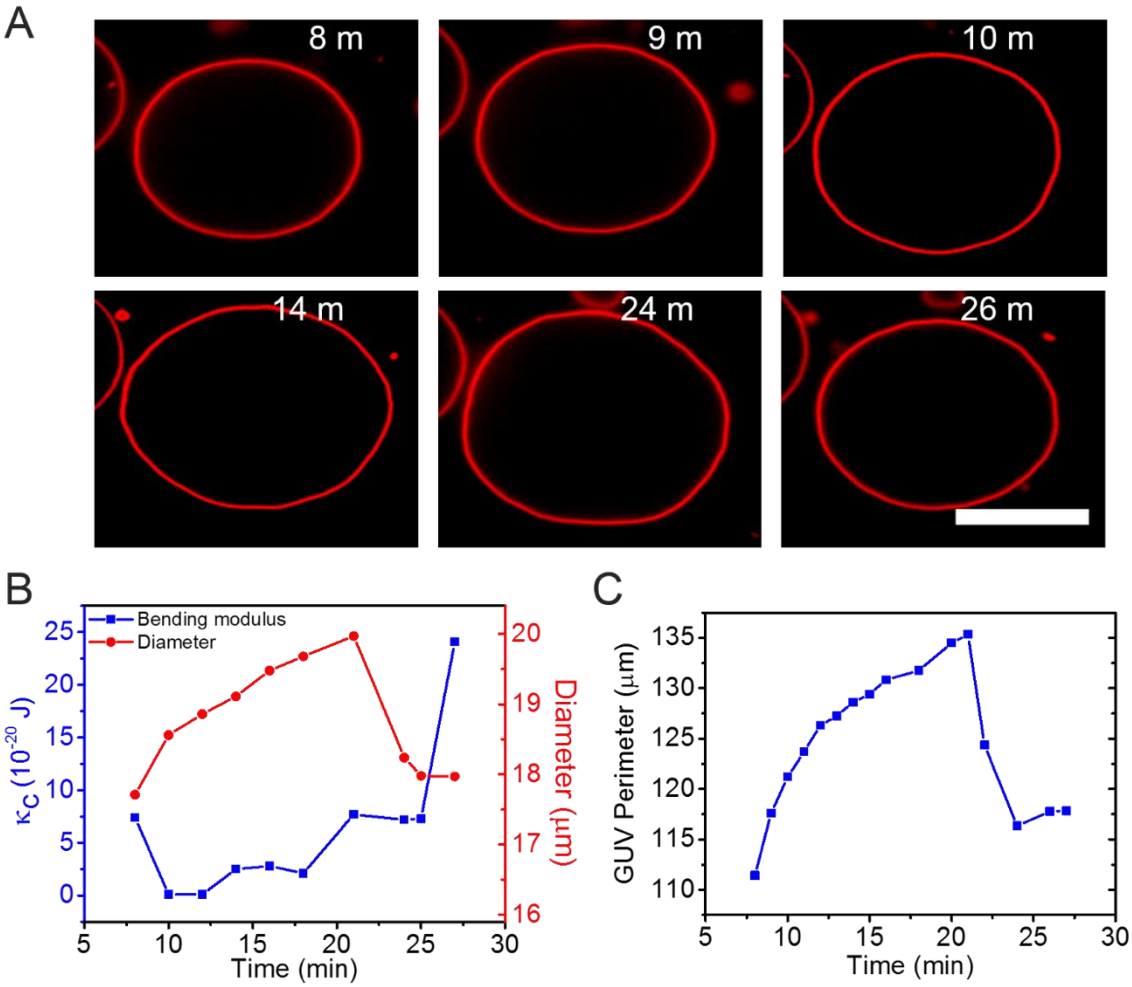

Figure 6. 3 GUV swelling and bursting induced by low concentration of GML. (A) Confocal fluorescence time-lapse images were recorded for DOPC-GUV upon incubation with 12 μM of GML. Each time corresponds to after the GML injection time. Scale bar indicates 20 μm. (B) Changes of GUV membrane softening of DOPC GUVs were measured during the incubation with 12 μM of GML, characterized by changes in the membrane bending rigidity along with its changes of vesicle diameter during the incubation. (C) Changes of the GUV perimeter is plotted showing dynamic size changes of the GUV in (A). Perimeter was measured based on fluorescence contrast change for each captured micrograph.

Interestingly, due to the interaction between 12 μM of GML and DOPC-GUV (Figure 6. 3A), similar fission behavior was not observed. At this low concentration of GML induced a large degree of membrane fluctuations decreasing the membrane's bending modulus from 7.4 to 0.1 x 10^{-20} J and the final state of the membrane was even more rigid (24.1 x 10^{-20} J) than before the interaction. The vesicle diameter (Figure 6. 3B) and perimeter (Figure 6. 3C) were also measured, and it fairly followed the trend of vesicle swelling and bursting cycle[42] that increased vesicular volume, which was reduced again near to the GUV's original size from about 20 minutes after the incubation began. Instead, vesicle swelling-bursting along with mild membrane fluctuations throughout the measurement period was observed from fluorescence microscopy monitoring. From the bending modulus analysis which allows to assess the rigidity of the GUV membrane throughout the incubation period (Figure 6. 3B), the results show similar trends with the bending modulus pattern from the GUV-antiviral peptide interaction caused by membrane thinning effects, as discussed in the previous chapter[43], exhibiting dynamic membrane flickering, confirming GML association with the lipid and preceding bilayer permeabilization. The interfacial association between GML and membrane locally increases the separation between polar lipid headgroups in the proximal monolayer creating both perturbation of chain packing[44] and area difference between the two membrane leaflets[45].

The observation of a cycle of vesicle swelling and bursting as reported by Mally et al[33] that lower concentrations of oleic acid induced very similar behavior where the GUV was going through swelling and burst. During the swelling, the membrane strain was increasing up to a critical value, after that the membrane was relaxed by a burst for its size dimensions to attain the initial value. This reported behavior is well matched with the observed result with a low concentration of GML interaction as shown in above Figure 6. 3. It can be concluded that the area of vesicle during the swelling stage increases due to the incorporation of the GML molecules into the membrane, and that at the burst all the GML molecules being accommodated during the growth phase due to membrane strain is dissolved, while all the phospholipid

remains in the membrane. The most plausible explanation of the bursting and swelling behavior, as described in Mally et al[33], the fatty acid partitioning into the phospholipid membrane depends on the stretching energy of the membrane. During the swelling stage, it is energetically favorable for the GML molecules in partition into the lipid membrane reducing the membrane stretching energy. During the burst moment, the required energy for the GML molecules in the lipid membrane disappears. Hence, the data show that 12 μM GML is sufficient to stiffen membranes without causing morphological transformations while 200 μM GML induces membrane budding and fission. The intermediate cases between these two GML concentrations were further observed.

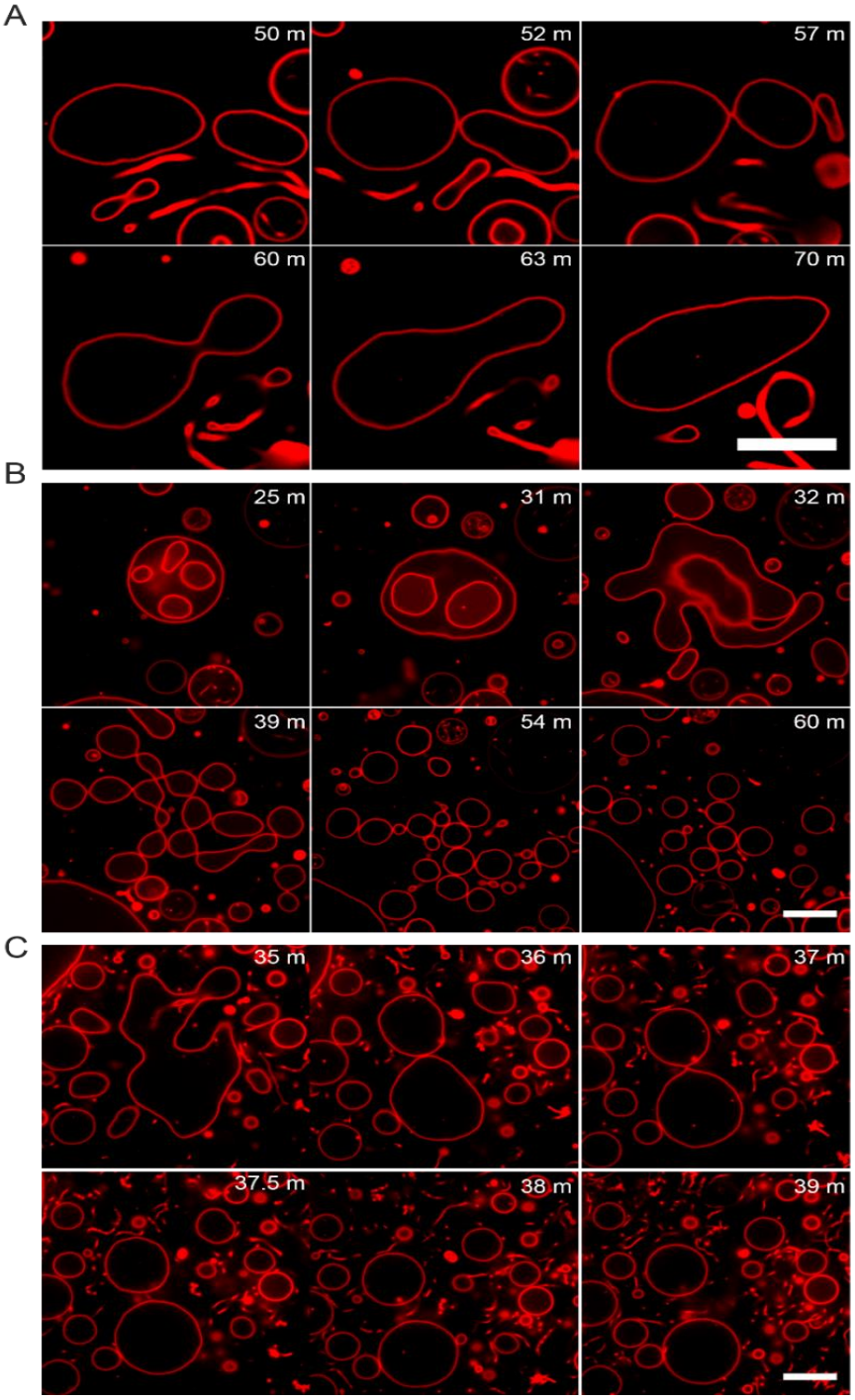

Figure 6. 4 Various morphological changes of DOPC-GUV induced by concentration-dependent effects of GML. Confocal fluorescence micrographs were recorded for DOPC-GUV upon incubation with (A) 25 µM, (B) 50 µM and (C) 100 µM of GML. Each time corresponds to after the GML injection time. Scale bar indicates 20 µm. Note that (A)

micrographs of 25 µM of GML case were enlarged from the original 136 µm x 136 µm image.

Next, three different concentrations of GML in the intermediate range were evaluated against DOPC GUVs (Figure 6. 4). Strikingly, at 25 µM GML, fusion between two neighboring GUVs occurred within approximately 70 minutes of GML introduction (Figure 6. 4A). The two vesicles initially underwent mild shape transformations and they were connected via a narrow neck after about 52 minutes. Then, the area of the neck became larger from 60 minutes onward, resulting in one final prolate shaped vesicle after 70 minutes of the GML-DOPC GUV interaction. By contrast, higher concentrations of GML, including 50 µM (Figure 6. 4B) and 100 µM (Figure 6. 4C), induced fission of vesicle creating multiple smaller daughter vesicles. Through comparison between these two different concentrations of GML, the length of time that it took to observe the fission behaviors was different depending on the GML concentration. While it took around 39 minutes for 50 µM GML to induce fission, only 30 minutes was needed for 100 µM GML to separate one large GUV into a number of daughter vesicles indicating that a higher concentration of GML can reduce the time scale to reach the vesicle fission state. Table 6.1. summarizes the experimental observations for the five different tested concentrations of GML.

Table 6.1 Summary of morphological changes of concentration-dependent GML interaction with DOPC-GUVs. The recorded times were estimated based on observations of the first morphological changes.

GML Concentration (μM)	Time (Fission or any morphological changes)	Final results
12	~ 10 min	GUV swelling & Bursting observed
25	~ 50 min	Fusion between neighboring GUVs
50	~ 39 min	Fission
100	~ 30 min	Fission
200	~ 20 min	Fission

As mentioned in the Introduction Chapter (Chapter 2), membrane-active surfactants such as oleic acid are known to induce GUV fission or fusion but there has never been a report of a compound that can induce both fission and fusion depending on the concentration.

6.3.2. DOPC GUVs treated by DDG

Given the unique membrane transformation conferred by GML, I next asked whether the combination of the primary alkyl chain and the glycerol head-group is sufficient or if the specific attachment chemistry matters. To answer this question, I investigated the effects of DDG against DOPC-GUVs as shown below in Figure 6. 5 and Figure 6. 6. While both GML and DDG have a saturated 12-carbon alkyl chain as the main backbone, the alkyl chain and glycerol moiety are connected by an ester linkage in GML and an ether group in DDG. Of note, like GML, DDG has also been explored as an antimicrobial agent with a similar level of biological activity.

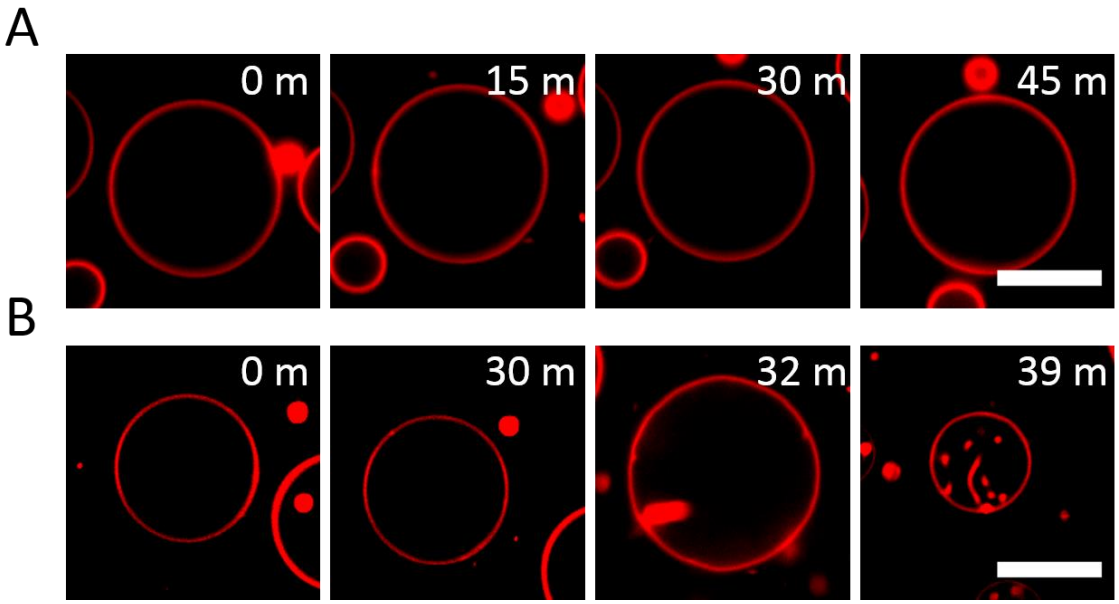

Figure 6. 5 GUV Interactions with below critical micelle concentrations of DDG. Confocal fluorescence micrographs were imaged for DOPC-GUV upon incubation with (A) 12 µM and (B) 25 µM of DDG. Each time corresponds to after the DDG injection time. Each scale bar indicates 20 µm.

Lower concentrations of DDG (12 µM and 25 µM) were administered against DOPC-GUV as presented in the above micrographs (Figure 6. 5). While 12 µM DDG concentration did not induce any morphological changes, 25 µM DDG induced swelling and bursting as observed with the 12 µM GML-DOPC GUV interaction.

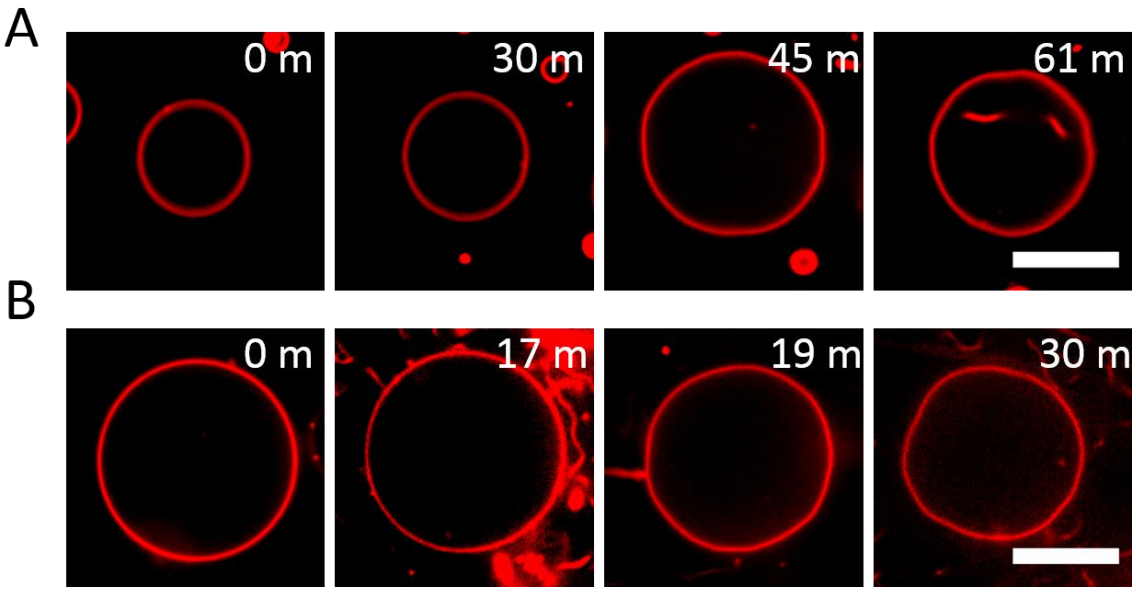

Figure 6. 6 GUV interactions with above critical micelle concentrations of DDG. Confocal fluorescence micrographs were imaged for DOPC-GUV upon interaction with above CMC of DDG, (A)100 µM and (B) 200 µM. Each time corresponds to after the DDG injection time. Each scale bar indicates 20 µm.

As shown in the above figure of micrographs (Figure 6. 6), higher concentrations of DDG (100 and 200 µM) were introduced to DOPC-GUVs. In marked contrast to GML, high DDG concentrations still did not induce any similar fission behaviors. Instead, swelling-bursting behaviors were observed showing vesicular volume and area changes. In addition, 200 µM DDG induced a network of lipid tubules around the vesicle after 17 minutes from the start of DDG introduction as shown in Figure 6. 6B. Hence, in this higher concentration range, GUVs underwent a mild degree of membrane fluctuations after going through tubular structure formation around its membrane. Based on the behaviors of GML and DDG, it appears both compounds exhibit concentration-dependent effects although the capability of inducing either fusion or fission is only exclusively found with GML. Therefore, to further explore the concentration-dependent effects of GML and DDG, I investigated the critical micelle concentration (CMC) of GML and DDG along with other two control tested samples were examined in the following section.

6.3.3. CMC effect of GML against DOPC-GUV

To further evaluate the tested compounds as surfactants dissolved in aqueous solution (300 mM glucose throughout the experiment), critical micelle concentrations (CMC) were examined as shown in the below concentration-dependent wavelength measurements (Figure 6. 7). From the fluorescence emission spectrum measurements of various concentrations of tested compounds dissolved in 300 mM glucose buffer solution which was also used to dilute GUV sample, it was determined that CMC of GML is about 50 µM (Figure 6. 7A). At higher concentrations, GML is in the micellar state while it is in the monomer state at lower concentrations. The CMC value is consistent with the trend in morphological transitions whereby fission occurs above the CMC and fusion occurs below the CMC. Furthermore, the CMC of DDG was determined to be approximately 40 µM (Figure 6. 7C), and the CMC of lauric acid (Figure 6. 7B) was above the tested range of concentrations. Taken together, the results demonstrate that GML exhibits unique possibilities for controlling the membrane morphological responses of GUVs based on inducing different degrees of membrane strain when partitioning in the micellar or monomeric state into the GUV membrane.

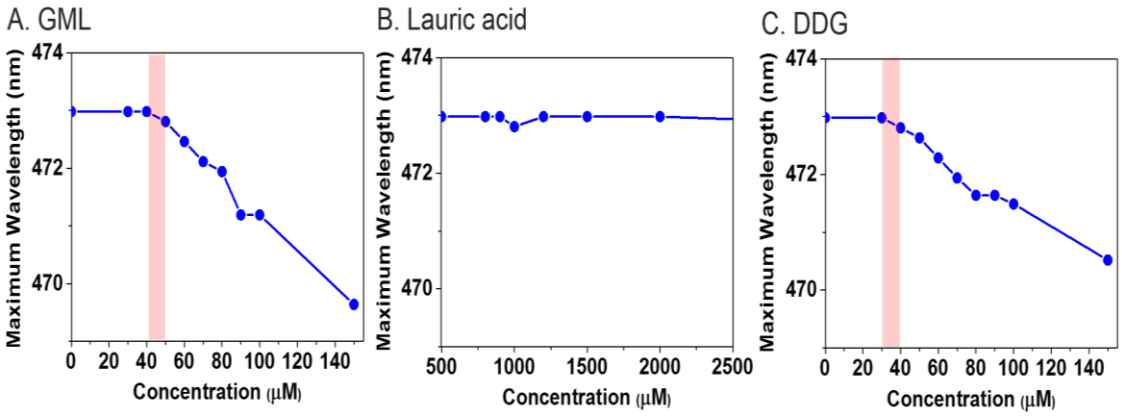

Figure 6. 7 Critical micelle concentration measurements of tested antimicrobial lipids in 300 mM glucose solution. CMC measurements of each tested compound, (A) GML, (B), lauric acid and (C) DDG, were conducted by employing fluorescence spectroscopy measurements. The pink-colored areas in the plots indicate where CMCs were estimated.

Hence, the CMC measurements of GML supports the result of GML-DOPC GUV interactions that the fission behaviors were only observed from above CMC cases as summarized in the Table 6. 1 (GML concentrations that were higher or equal to 50 μM). In other words, the concentrations of GML play a significant role determining the fate of interacting cell-sized vesicles.

To note that, the only molecular difference between GML and DDG is the existence of carbonyl group from the ester linkage in GML while ether linkage of DDG lacks the carbonyl center. The carbonyl group can participate in hydrogen bonding as hydrogen-bond acceptors so that it can be proposed that GML is able to intercalate into lipid membrane more freely inducing higher curvature effect of the external monolayer and increased packing-density as well compared to DDG. Because of the lack of carbonyl group in ether linkage of DDG molecule, it lacks the same degree of hydrogen bonding capacity compared to GML so that much less attractive interactions with phosphate groups of phospholipids which would decrease the residence time within the bilayer disabling the partitioning of a sufficient number of molecules at a given time to cause membrane strain and following membrane morphological response (e.g. vesicle fission observed from GML case). Interestingly, this factor along with a different packing parameter are the distinguishing features and the aggregation properties of GML vs. DDG are similar (nearly equivalent CMC values).

There was a study of CMC of self-assembly of amphiphilic molecules by Hadgiivanova et al[46] reported the another state of the amphiphilic aggregation called ‘premicellar aggregation’ which lies between monomeric and micellar states. Simply, the study added another state in between the monomer and micelle states re-established the CMC states into a sequence of three well separated concentrations: C_1, a metastable aggregated state starts to be observed but at well below significant

amount, C_2, above which an appreciable amount of meta-stable aggregates appears, and lastly, C_3 at which the aggregated micellar state becomes quite stable and consistent. Hence, in the premicellar state, both monomer and less stable aggregated micelles are present. From the GML concentrations dependent study and its CMC measurement, while 50 µM concentration was determined as CMC where the vesicle fission started to appear, its 2-fold decreased concentration (25 µM) induced vesicle fusion. Hence, at this 25 µM concentration, the coexistence of monomer and pre-micellar aggregates of GML induced vesicle fusion between two close neighboring GUVS.

6.3.4. Effect of lipid compositions of GUV against GML

In order to explore the lipid composition specificity of GML inducing vesicle fission behavior, different lipid compositions of GUVs were prepared. Against the AH peptide, it has been reported that multi-phases of lipid compositions of GUVs resulted in totally different peptide binding results[43], as also discussed in Chapter 5. Hence, the same set of GUVs was tested to determine if GML exhibits differential activity against various lipid compositions (phase) when inducing fission or fusion behavior. The tested composition is a raft-forming lipid composition containing GUV which is composed of an equimolar ratio of sphingomyelin, cholesterol and DOPC (both sphingomyelin and cholesterol are liquid-ordered phase).

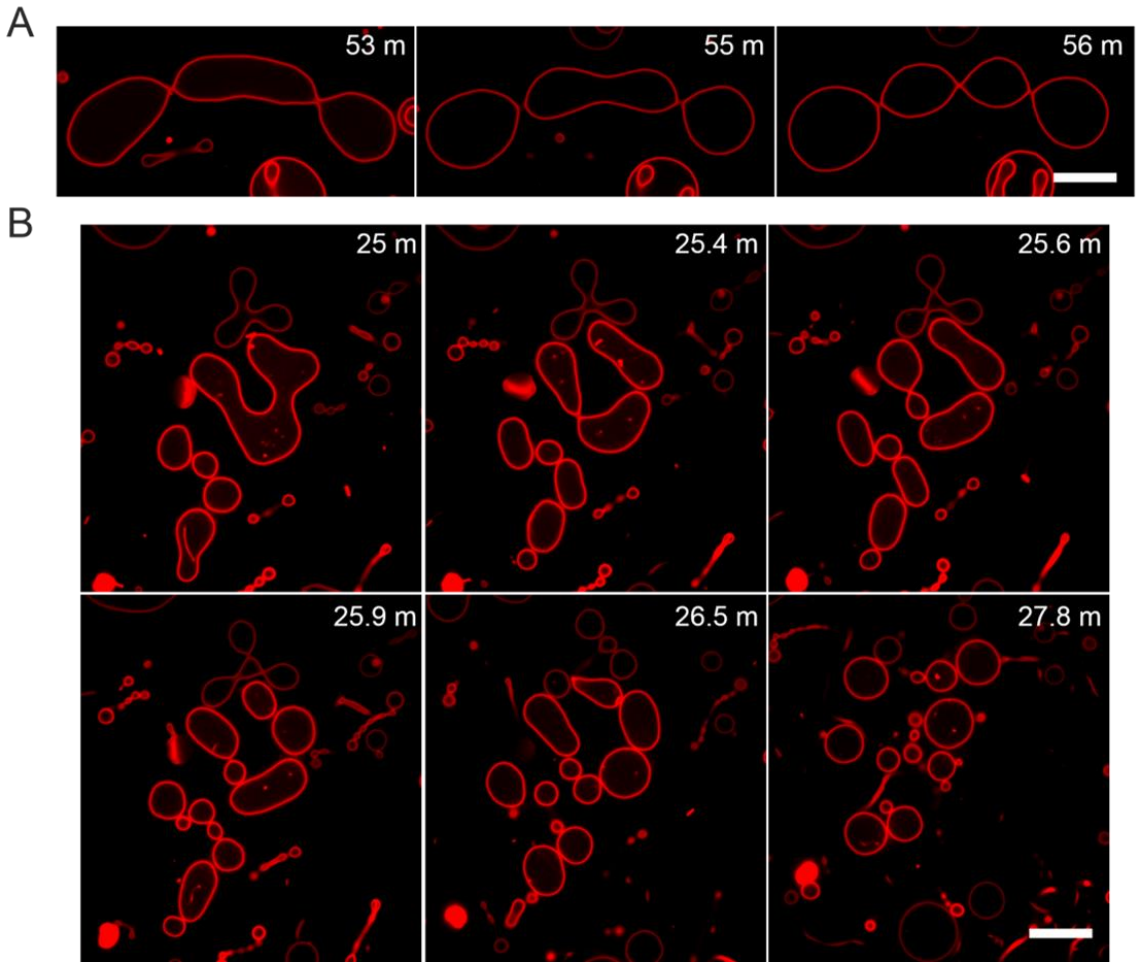

Figure 6. 8 GML-induced fission on raft-forming GUVs. Fluorescence micrographs of raft-forming GUVs consisting of equimolar concentrations of DOPC, Sphingomyelin and cholesterol were presented upon incubation with (A) 25 µM and (b) 200 µM of GML. Each time corresponds to after the GML injection time. Scale bars indicate 20 µm.

As presented in the above figure (Figure 6. 8), below (25 µM) and above (200 µM) CMCs of GML were introduced against raft-forming GUVs (raft-GUV). Sub-CMC concentrations of GML induced shape transformation of GUVs within 56 minutes, changing the original spherical shaped vesicle into multiple spherical structures connected via narrow necks. By contrast, supra-CMC concentrations of GML against raft-GUV, it surprisingly induced the same vesicle fission behavior resulting in one large GUV being separated into multiple, daughter vesicles. This indicates

that GML is a potent agent for inducing vesicle fission or fusion regardless of phase states of lipid membranes highlighting that the attachment chemistry is also important because monoglycerides (e.g. ester-linked ones including GML) possess such capacity but DDG (ether-linked equivalents) does not induce such morphological changes.

6.4. Discussion

6.4.1. Mechanism of vesicle fission induced by GML

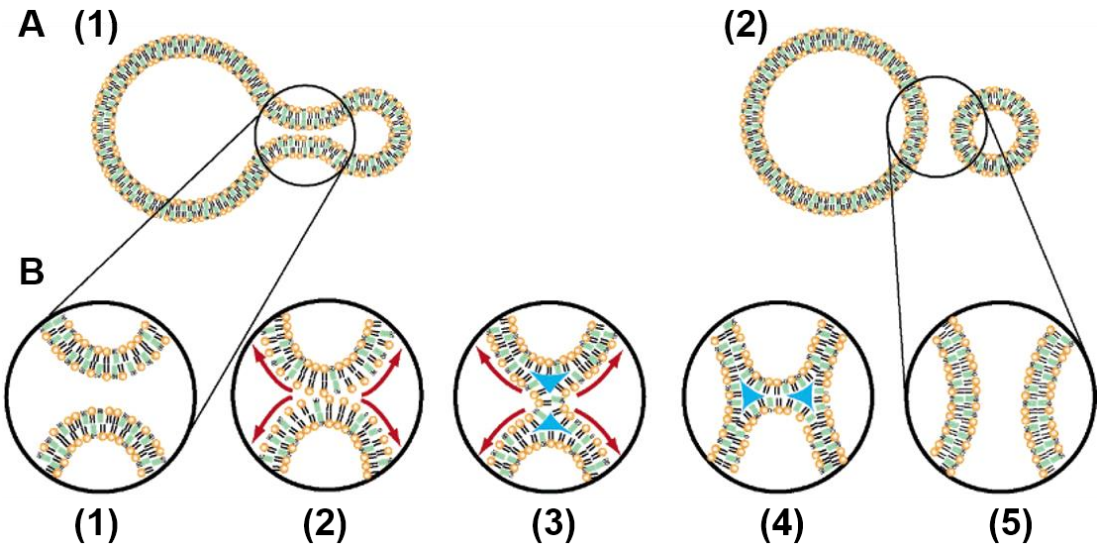

Figure 6. 9 Schematic diagram of proposed mechanism of GML induced vesicle fission. While blue triangels refer to the interstitial hydrocarbon region in which the free energy of chain packing is very large. Red arrows indicate the lateral pressure of the internal membranes induced by vesiclular shape changes. Schematic is reproduced from Tanaka et al[32].

In order to explain the observation of vesicle fission induced high concentrations of GML (above CMC), I discussed a molecular-level mechanism as first proposed by Tanaka et al[32]. As GML molecules intercalates into the external monolayer of GUV, the Gibbs free energy of the total system decreases. Then, until the elastic energy of the GUV becomes minimum, the GUV shape becomes the two spheres connected via a neck structure as it can be observed in various figures presenting fluorescence

micrographs of GUV fission induced by GML (Figure 6. 2A, 6. 4B-C), and above schematic diagram of fission (Figure 6. 9A(1)) also depicts the narrow neck structure. The shape change induces stretching of the internal monolayer allowing further intercalation of GML molecules into the external monolayer. Hence, at the narrow neck region, its stretching becomes quite significant because of the large curvature of the membrane as described in above Figure 6. 9B (2). As the GML molecules interact with the external monolayer, the distance between the hydrocarbons of neighboring DOPC lipids becomes increased. The resulting instability may bring out the linking of the opposing two bilayers at the neck area and they become resealed to reduce the high curvature of the internal monolayers (see Figure 6. 9B (3)). By lowering the elastic energy of the high curvature region, the dimension of neck becomes very narrow with a low-curvature internal monolayer as described in Figure 6. 9B (4). Hence, the rearrangement of the membranes finally occurs resulting in the vesicle fission. To note that Tanaka et al[32] reported the vesicle fission induced by lysophophatidylcholine (lyso-PC) against GUV composed of liquid-ordered phase lipids (e.g. large amount of cholesterol or gel-phase lipid of dipalmitoylphosphatidylcholine (DPPC)). However, in this Chapter, the main novelty is that depending on the aggregation state of GML, it can induce the universal lipid vesicle fission or fusion regardless of lipid phases (e.g. in both liquid disordered and ordered phases).

6.4.2. Proposed mechanism of fusion induced by premicellar state of GML

To complement and propose a possible mechanism of the fusion of GUVs, one of the famous ‘fusion stalk’ model can be applied[47]. Indeed, as it was captured in the Figure 6. 4A, formation of ‘stalk’ or a narrow neck between the two neighboring GUVs was the first step. For the aggregation of two external monolayers forming the stalk, the two monolayers need to become partially dehydrated to prevent a possible strong repulsion from the bound water molecules. For this reason, we can predict that the premicellar state of GML acts to provide the dehydration near the

surrounding GUVs. Hence, the deformation of the two GUVs induced the localized rearrangement of bilayers causing the full fusion between the giant vesicles. There have been a large number studies reported that divalent cations, especially calcium ion, playing a great role inducing the membrane fusion against negatively charged lipids[48-51]. Therefore, the novelty of current chapter is that the premicellar state of GML can induce the vesicle fission on two closely located GUVs composed of only zwitterionic lipids. However, its further experimental and theoretical rationales of fission or fusion inducing mechanism need to be further elucidated for the future work. For now, it is clear that a single-chain amphiphile compound can induce both membrane fission and fusion, the two morphological transformations depend on the aggregation state, either micellar or monomeric state.

6.4.3. Platform design approaches between SLB and GUV

As referenced in Chapter 2 (literature review), the same lauric acid and GML molecules have been tested against SLB platform composed of same DOPC lipid which was employed to form GUV in this current chapter[52]. Surprisingly, primarily due to the confined structural features of SLB (2-dimensional structure), above CMC of GML (500 μM) induced morphological changes of SLB creating nucleation sites from which entangled tubular structures grow and form spherical caps during the course of GML injection. The reported mechanism of this morphological transformation of bilayer was that the confined and essentially flat structural features of SLB passively regulate the given stress by nucleating and evolving protrusions of either tubular or circular shapes[53]. Hence, the asymmetric insertion of GML brings about the increased monolayer curvature strain[54] which ultimately leading to have a mechanical failure which caused the morphological changes of membrane as shown in the below comparison figure with GUV case. Because of the 3-dimensional structure of GUV, it is able to freely expand and contract which can provide new discoveries of overall physical changes of vesicle as it was confirmed in the GML-GUV interactions in this chapter. Therefore, the different structural

feature of GUV produced totally different morphological changes upon interaction with above CMC of GML inducing vesicle fission which is not possible to observe with SLB model membrane platform.

6.5. Conclusions

In conclusion, the presented experimental results and quantitative analyses were the first study investigating the interactions between monoglycerides and GUV platforms including DOPC only and raft compositions. The study specifically identified that GML can induce fission or fusion behavior depending on the concentration. In contrast, few fatty acids including lyso PC, SDS and octylglucoside were observed to induce fission against gel or liquid-ordered phase GUVs, but none of any compounds have been reported to induce both fusion and fission. Surprisingly, structurally similar compounds such as DDG did not induce same fusion/fission behaviors in both micellar and monomeric states. Such obtained information is highly important for understanding the molecular evolution of membrane components from fatty acids to glycerophospholipids.

References

1. Hanczyc, M. M.; Fujikawa, S. M.; Szostak, J. W., Experimental models of primitive cellular compartments: encapsulation, growth, and division. *Science* **2003,** *302* (5645), 618-622.

2. Black, R. A.; Blosser, M. C.; Stottrup, B. L.; Tavakley, R.; Deamer, D. W.; Keller, S. L., Nucleobases bind to and stabilize aggregates of a prebiotic amphiphile, providing a viable mechanism for the emergence of protocells. *Proceedings of the National Academy of Sciences* **2013,** *110* (33), 13272-13276.

3. Apel, C. L.; Deamer, D. W., The formation of glycerol monodecanoate by a dehydration condensation reaction: increasing the chemical complexity of

amphiphiles on the early Earth. *Origins of Life and Evolution of Biospheres* **2005,** *35* (4), 323-332.

4. Apel, C. L.; Deamer, D. W.; Mautner, M. N., Self-assembled vesicles of monocarboxylic acids and alcohols: conditions for stability and for the encapsulation of biopolymers. *Biochimica et Biophysica Acta (BBA)-Biomembranes* **2002,** *1559* (1), 1-9.

5. Mansy, S. S.; Schrum, J. P.; Krishnamurthy, M.; Tobé, S.; Treco, D. A.; Szostak, J. W., Template-directed synthesis of a genetic polymer in a model protocell. *Nature* **2008,** *454* (7200), 122-125.

6. Zhu, T. F.; Szostak, J. W., Coupled growth and division of model protocell membranes. *Journal of the American Chemical Society* **2009,** *131* (15), 5705-5713.

7. Hanczyc, M. M.; Szostak, J. W., Replicating vesicles as models of primitive cell growth and division. *Current Opinion in Chemical Biology* **2004,** *8* (6), 660-664.

8. Singer, S.; Nicolson, G. L., The fluid mosaic model of the structure of cell membranes. *Membranes and Viruses in Immunopathology; Day, SB, Good, RA, Eds* **1972**, 7-47.

9. SKou, J. C., Enzymatic basis for active transport of Na+ and K+ across cell membrane. *Physiological Reviews* **1965,** *45* (3), 596-618.

10. Rothman, J. E., Mechanisms of intracellular protein transport. **1994**.

11. Ikonen, E., Roles of lipid rafts in membrane transport. *Current opinion in cell biology* **2001,** *13* (4), 470-477.

12. Hargreaves, W.; Mulvihill, S.; Deamer, D., Synthesis of phospholipids and membranes in prebiotic conditions. *Nature* **1977,** *266*, 78-80.

13. Budin, I.; Szostak, J. W., Physical effects underlying the transition from primitive to modern cell membranes. *Proceedings of the National Academy of Sciences* **2011,** *108* (13), 5249-5254.

14. Hargreaves, W. R.; Deamer, D. W., Liposomes from ionic, single-chain amphiphiles. *Biochemistry* **1978,** *17* (18), 3759-3768.

15. Deamer, D.; Dworkin, J. P.; Sandford, S. A.; Bernstein, M. P.; Allamandola, L. J., The first cell membranes. *Astrobiology* **2002,** *2* (4), 371-381.

16. Deamer, D.; Singaram, S.; Rajamani, S.; Kompanichenko, V.; Guggenheim, S., Self-assembly processes in the prebiotic environment. *Philosophical Transactions of the Royal Society of London B: Biological Sciences* **2006,** *361* (1474), 1809-1818.

17. Jensen, T. R.; Jensen, M. Ø.; Reitzel, N.; Balashev, K.; Peters, G. H.; Kjaer, K.; Bjørnholm, T., Water in contact with extended hydrophobic surfaces: direct evidence of weak dewetting. *Physical review letters* **2003,** *90* (8), 086101.

18. Garti, N.; Aserin, A.; Spernath, A.; Amar, I., Nano-sized self-assembled liquid dilutable vehicles. Google Patents: 2007.

19. Engström, K.; Nyhlén, J.; Sandström, A. G.; Bäckvall, J.-E., Directed evolution of an enantioselective lipase with broad substrate scope for hydrolysis of α-substituted esters. *Journal of the American Chemical Society* **2010,** *132* (20), 7038-7042.

20. Arouri, A.; Lauritsen, K. E.; Nielsen, H. L.; Mouritsen, O. G., Effect of fatty acids on the permeability barrier of model and biological membranes. *Chemistry and physics of lipids* **2016,** *200*, 139-146.

21. Oparin, A. I., *The origin of life*. Courier Corporation: 2003.

22. Dzieciol, A. J.; Mann, S., Designs for life: protocell models in the laboratory. *Chemical Society reviews* **2012,** *41* (1), 79-85.

23. Tang, D.; Rohaida Che Hak, C.; Thompson, A. J.; Kuimova, M. K.; Williams, D.; Perriman, A. W.; Mann, S., Fatty acid membrane assembly on coacervate microdroplets as a step towards a hybrid protocell model. *Nature chemistry* **2014,** *6* (6).

24. Maurer, S. E.; Monnard, P.-A., Primitive membrane formation, characteristics and roles in the emergent properties of a protocell. *Entropy* **2011,** *13* (2), 466-484.

25. Li, M.; Huang, X.; Tang, T. D.; Mann, S., Synthetic cellularity based on non-lipid micro-compartments and protocell models. *Current Opinion in Chemical Biology* **2014,** *22*, 1-11.

26. Simoneit, B. R.; Rushdi, A. I.; Deamer, D. W., Abiotic formation of acylglycerols under simulated hydrothermal conditions and self-assembly

properties of such lipid products. *Advances in Space Research* **2007,** *40* (11), 1649-1656.

27. Olasagasti, F.; Maurel, M.-C.; Deamer, D. In *Physico-chemical interactions between compartment-forming lipids and other prebiotically relevant biomolecules*, BIO Web of Conferences, EDP Sciences: 2014; p 05001.

28. Walde, P., Building artificial cells and protocell models: experimental approaches with lipid vesicles. *Bioessays* **2010,** *32* (4), 296-303.

29. Menger, F. M.; Angelova, M. I., Giant vesicles: imitating the cytological processes of cell membranes. *Accounts of chemical research* **1998,** *31* (12), 789-797.

30. Dimova, R.; Aranda, S.; Bezlyepkina, N.; Nikolov, V.; Riske, K. A.; Lipowsky, R., A practical guide to giant vesicles. Probing the membrane nanoregime via optical microscopy. *Journal of Physics: Condensed Matter* **2006,** *18* (28), S1151.

31. Inaoka, Y.; Yamazaki, M., Vesicle fission of giant unilamellar vesicles of liquid-ordered-phase membranes induced by amphiphiles with a single long hydrocarbon chain. *Langmuir* **2007,** *23* (2), 720-728.

32. Tanaka, T.; Sano, R.; Yamashita, Y.; Yamazaki, M., Shape changes and vesicle fission of giant unilamellar vesicles of liquid-ordered phase membrane induced by lysophosphatidylcholine. *Langmuir* **2004,** *20* (22), 9526-9534.

33. Mally, M.; Peterlin, P.; Svetina, S. a., Partitioning of oleic acid into phosphatidylcholine membranes is amplified by strain. *The Journal of Physical Chemistry B* **2013,** *117* (40), 12086-12094.

34. Tamba, Y.; Ohba, S.; Kubota, M.; Yoshioka, H.; Yoshioka, H.; Yamazaki, M., Single GUV method reveals interaction of tea catechin (−)-epigallocatechin gallate with lipid membranes. *Biophysical Journal* **2007,** *92* (9), 3178-3194.

35. Peterlin, P.; Arrigler, V.; Kogej, K.; Svetina, S.; Walde, P., Growth and shape transformations of giant phospholipid vesicles upon interaction with an aqueous oleic acid suspension. *Chemistry and physics of lipids* **2009,** *159* (2), 67-76.

36. Angelova, M. I.; Dimitrov, D. S., Liposome electroformation. *Faraday discussions of the Chemical Society* **1986,** *81*, 303-311.

37. Angelova, M. I.; Soléau, S.; Méléard, P.; Faucon, F.; Bothorel, P., Preparation of giant vesicles by external AC electric fields. Kinetics and applications. In *Trends in Colloid and Interface Science VI*, Helm, C.; Lösche, M.; Möhwald, H., Eds. Steinkopff: Darmstadt, 1992; pp 127-131.

38. Oglecka, K.; Sanborn, J.; Parikh, A. N.; Kraut, R. S., Osmotic gradients induce bio-reminiscent morphological transformations in giant unilamellar vesicles. *Frontiers in physiology* **2012,** *3*, 120.

39. Moscho, A.; Orwar, O.; Chiu, D. T.; Modi, B. P.; Zare, R. N., Rapid preparation of giant unilamellar vesicles. *Proceedings of the National Academy of Sciences* **1996,** *93* (21), 11443-11447.

40. Walde, P.; Cosentino, K.; Engel, H.; Stano, P., Giant vesicles: preparations and applications. *ChemBioChem* **2010,** *11* (7), 848-865.

41. Loftus, A. F.; Noreng, S.; Hsieh, V. L.; Parthasarathy, R., Robust measurement of membrane bending moduli using light sheet fluorescence imaging of vesicle fluctuations. *Langmuir* **2013,** *29* (47), 14588-14594.

42. Ho, J. C.; Rangamani, P.; Liedberg, B.; Parikh, A. N., Mixing Water, Transducing Energy, and Shaping Membranes: Autonomously Self-Regulating Giant Vesicles. *Langmuir* **2016,** *32* (9), 2151-2163.

43. Hanson, J. M.; Gettel, D. L.; Tabaei, S. R.; Jackman, J.; Kim, M. C.; Sasaki, D. Y.; Groves, J. T.; Liedberg, B.; Cho, N.-J.; Parikh, A. N., Cholesterol-Enriched Domain Formation Induced by Viral-Encoded, Membrane-Active Amphipathic Peptide. *Biophysical Journal* **2016,** *110* (1), 176-187.

44. Hristova, K.; Dempsey, C. E.; White, S. H., Structure, location, and lipid perturbations of melittin at the membrane interface. *Biophysical Journal* **2001,** *80* (2), 801-811.

45. Svetina, S.; Zeks, B., Bilayer couple as a possible mechanism of biological shape formation. *Biomedica biochimica acta* **1985,** *44* (6), 979-986.

46. Hadgiivanova, R.; Diamant, H., Premicellar aggregation of amphiphilic molecules. *The Journal of Physical Chemistry B* **2007,** *111* (30), 8854-8859.

47. Kozlov, M.; Markin, V., Possible mechanism of membrane fusion. *Biofizika* **1983,** *28* (2), 242-247.

48. Papahadjopoulos, D.; Poste, G.; Schaeffer, B.; Vail, W., Membrane fusion and molecular segregation in phospholipid vesicles. *Biochimica et Biophysica Acta (BBA)-Biomembranes* **1974,** *352* (1), 10-28.

49. Papahadjopoulos, D.; Nir, S.; Düzgünes, N., Molecular mechanisms of calcium-induced membrane fusion. *Journal of bioenergetics and biomembranes* **1990,** *22* (2), 157-179.

50. Chanturiya, A.; Scaria, P.; Woodle, M., The role of membrane lateral tension in calcium-induced membrane fusion. *Journal of Membrane Biology* **2000,** *176* (1), 67-75.

51. Pannuzzo, M.; De Jong, D. H.; Raudino, A.; Marrink, S. J., Simulation of polyethylene glycol and calcium-mediated membrane fusion. *The Journal of chemical physics* **2014,** *140* (12), 124905.

52. Yoon, B. K.; Jackman, J. A.; Kim, M. C.; Cho, N.-J., Spectrum of membrane morphological responses to antibacterial fatty acids and related surfactants. *Langmuir* **2015,** *31* (37), 10223-10232.

53. Staykova, M.; Arroyo, M.; Rahimi, M.; Stone, H. A., Confined bilayers passively regulate shape and stress. *Physical review letters* **2013,** *110* (2), 028101.

54. Monnard, P. A.; Deamer, D. W., Membrane self-assembly processes: Steps toward the first cellular life. *The Anatomical Record* **2002,** *268* (3), 196-207.

Chapter 7

Conclusion & Future Outlook

There is a great interest in understanding how membrane-active agents perturb cellular membranes from diverse origins, e.g., mammalian and bacterial, as well as other biological entities such as much smaller, enveloped viruses. The main objective of the thesis is to examine the biophysical interactions between membrane-active agents such as amphipathic peptides, fatty acids, and monoglycerides, and model membrane platforms in order to distinguish the corresponding membrane morphological responses. From the various observational studies employing the model membrane platforms, the findings in this thesis contribute to a fundamental understanding of how different classes of molecules including peptides, fatty acids, monoglycerides induce membrane morphological responses in biologically relevant model membranes and offer insights into the roles in which these morphological responses play in therapeutic applications as well as molecular evolution. In addition to the conclusions of presented work, reconnaissance studies are suggested as future work in this last chapter of thesis.

7.1. Conclusion

In this thesis dissertation, the interactions of various membrane active agents with two different model membrane platforms were investigated employing various experimental techniques. The specific objective was to study dynamic membrane morphological responses upon interaction with various membrane-active agents such as antiviral peptide and single chain monoglycerides. Under this specific objective, the overall hypothesis was that employing the artificial lipid membrane platforms provides useful model systems to interrogate changes of membrane morphologies upon interacting with membrane-active peptides and surfactants, thereby revealing unknown vesicle shape transformations as well as evaluate key membrane active agents. Among various artificial lipid membrane model platforms, giant unilamellar vesicle platform provides cell sized lipid vesicles that can be optically resolved by microscopy measurements. Hence, any morphological changes of GUVs upon interaction with membrane active agents can be easily followed and analyzed. Corresponding studies were conducted as follows:

In chapter 4, a new post-assembly repair method of supported lipid bilayer formed via vesicle fusion was presented. By employing AH peptide, it allows to create defect-free lipid bilayer by rupturing still unruptured lipid vesicles trapped on the bilayer. This new repair method enables one to form complete SLB using large size lipid vesicles which normally prevent complete rupture of adsorbed vesicles on the substrates. From the epifluorescence microscopy and QCM-D measurements, the AH peptide mediated repair reduced the amount of unruptured vesicles or defect of SLB to less than 1%.

In chapter 5, human liver microsome (HLM) incorporated GUV model platforms were prepared which has never been reported. The new HLM-GUV platform was used to study dynamic membrane morphological responses upon interaction with various concentrations of AH peptide. Even 1% or 5% amount of incorporated HLM significantly affected the stability of the membrane. It was revealed that the

incorporated HLM played a significant role in stabilizing the overall vesicle structure over susceptible vesicles composed of DOPC lipid only. The findings suggest how the stabilization induced from the liver microsome incorporated synthetic lipid model platform can be extended to interrogate mechanisms behind the viral peptide interactions against more complex cell membrane model platforms.

In chapter 6, in an effort to reveal evolution of phospholipid membranes from early cells, experimental study of interaction between GUVs and glycerol monolaurate (GML) which has never been utilized with GUV model platforms was conducted. The experimental results identified that GML can induce fission or fusion behavior depending on concentration, either in micellar or monomeric state. In the meantime, structurally similar compounds such as DDG did not induce same fusion/fission behaviors in both micellar and monomeric states. Such obtained information is highly important for understanding the molecular evolution of membrane components from fatty acids to glycerophospholipids.

Taken all together, the presented results in this thesis contribute to the fundamental understandings of membrane morphology dynamics of newly designed biological relevant GUV model platforms induced by key membrane active agents including antiviral AH peptide and single chain monoglycerides.

7.2. GUV-ECM Protein Platform Development

In the presented results from the previous chapters, various cell sized liposome models were presented, including simple synthetic lipids based GUV and human liver microsome incorporated GUV, to mimic the complex nature of cell membranes. This bottom-up engineering approach to develop ideal cell model platform can even be further extended to more complex platform by conjugating extracellular matrix (ECM) protein which is composed of a complex meshwork of proteins and polysaccharides which is secreted by animal cells into the spaces around them[1-2]. The ECM contains structural proteins such as collagen and elastin, specialized

proteins such as fibronectin and laminin, and proteoglycans[3]. Because of its diverse composition, the ECM serves various functions including providing support and anchorage for cells, regulation of cell to cell communication, and segregation of a variety of growth factors, acting as a depot for them[4-8]. This property of the ECM to act as a depot enables the rapid activation of cellular functions mediated by growth factors, without necessitating de novo synthesis[9-10]. The composition and physical properties of ECM proteins including elasticity and topography features largely influence a numerous cellular processes with changes in cell morphology and the actin cytoskeleton structures as well[11-13]. The presence of the ECM is essential for processes like cell growth, proliferation and wound healing[14-15]. Recently, there have been several studies trying to mimic the cell membrane attached with ECM proteins including collagen type I and fibronectin (FN) by employing supported lipid bilayer (SLB) platforms[16-17]. The ECM proteins conjugated SLB platforms are highly useful as a more membrane mimic cell culture platform. Since SLB model is 2-dimensional platform, it still has some limitations to be considered as a potential complete cell model platform in terms of monitoring its membrane dynamics against membrane-active agents. Hence, there is a strong potential for developing GUV based ECM protein conjugated cell-model platforms.

7.2.1. Fibronectin conjugated GUV platform

For the lipid functionalization by Huang et al[16], DOPC, 5 mol % of 1,2-Dipalmitoyl-sn-glycero-3-phosphoethanolamine-N-(glutaryl) (DP-NGPE), and 1 mol % Rh-DPPE based GUVs are prepared. Then, for the chemical conversion of carboxylic head group of DP-NGPE lipids to active ester group, N-(3-Dimethylaminopropyl)-N'-ethylcarbodiimide hydrochloride (EDC) and sulfo-N-hydroxysuccinimide (sNHS) were treated with GUV samples with appropriate Hepes buffer at pH 5.5. Then, the chemically activated head group containing GUVs were again treated with

FN for the protein conjugation. Following schematic figure (Figure 7. 1) briefly explains methodology of fibronectin conjugation onto GUVs.

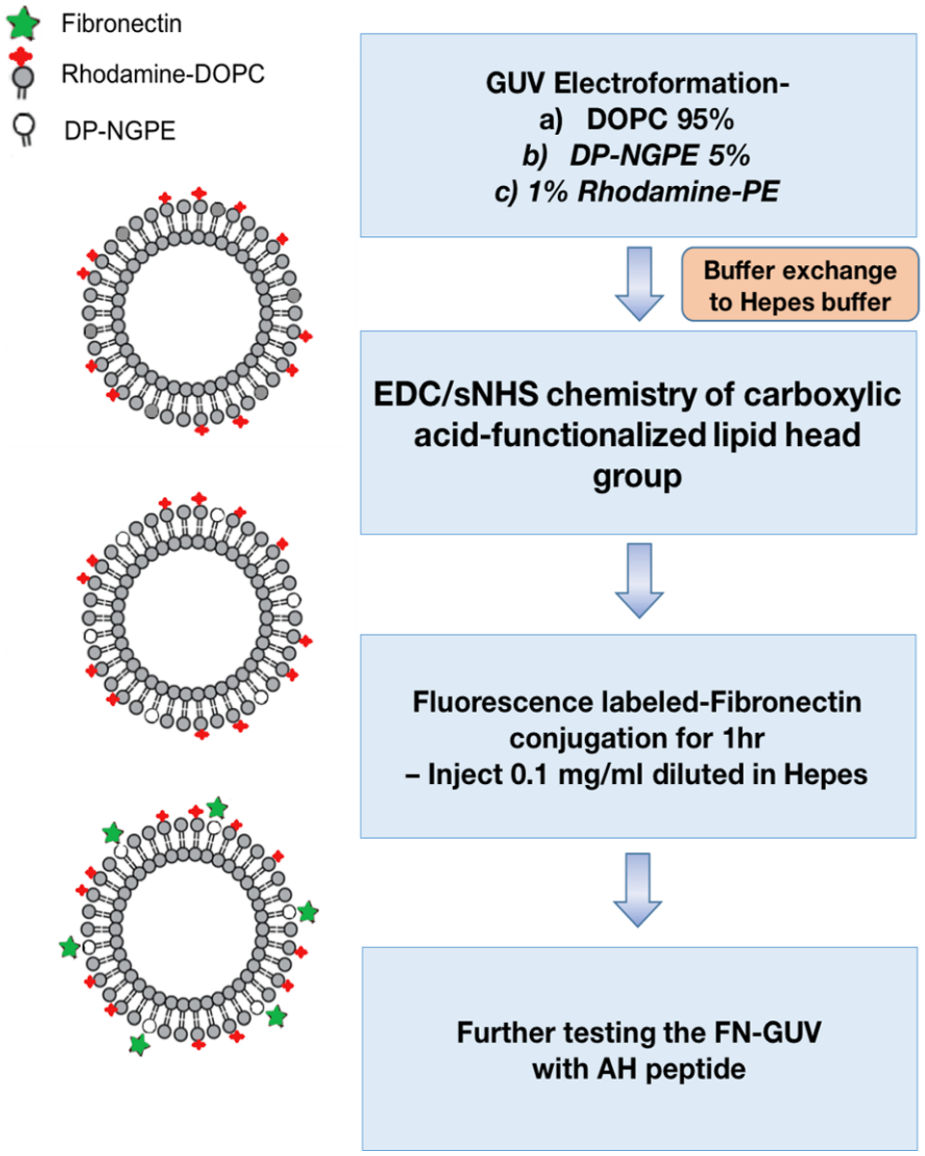

Figure 7. 1 Schematic representation fibronectin conjugated GUV model platform presented along with brief methodology of its preparation.

In order to confirm the successful conjugation of fibronectin onto GUV membrane, spinning disc confocal microscopy measurements were conducted as presented in the below representative fluorescence micrographs.

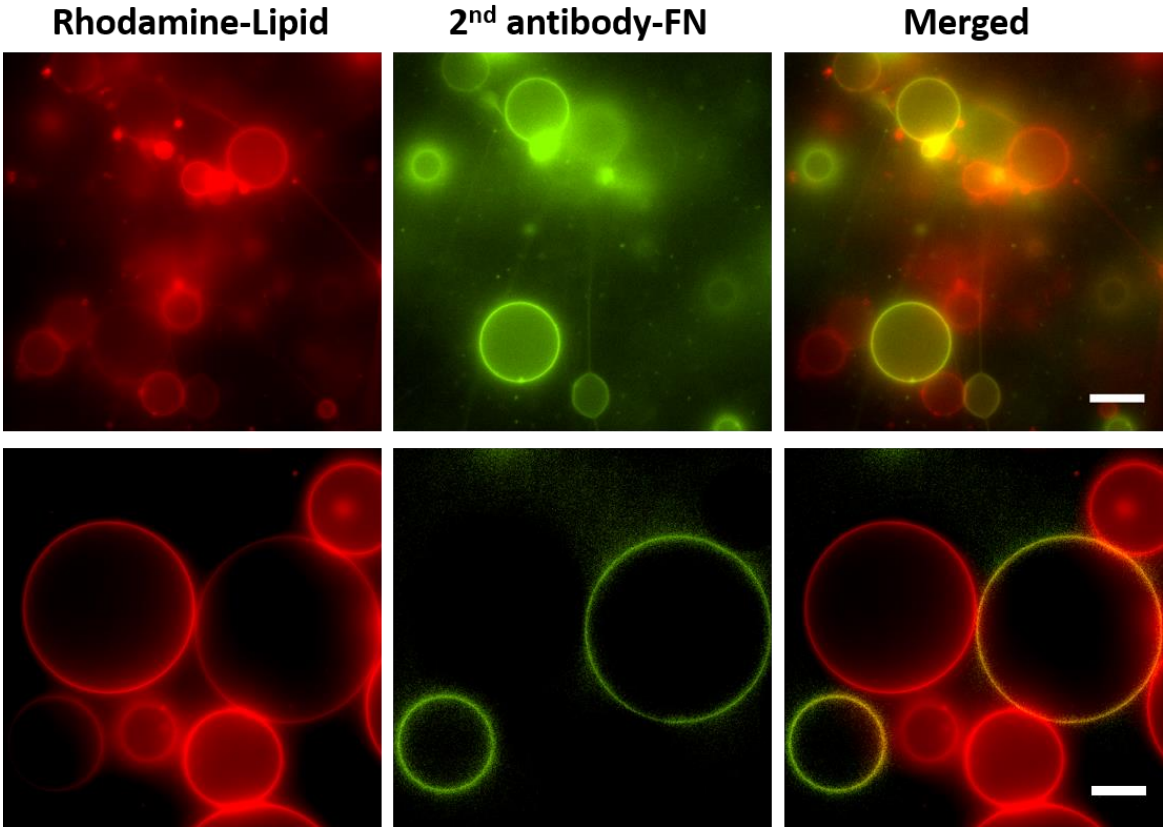

Figure 7. 2 Fibronectin conjugated synthetic lipid based GUV platforms. Fluorescence micrographs were captured by spinning disc confocal microscopy using 60x oil objective lens. While left column images (Rhodamine-Lipid) were recorded under TRITC filter used to image rhodamine labeled vesicles, center column images (2nd antibody-FN) captured secondary antibody bound onto fibronectins conjugated onto GUVs. Right column images represent merged images of both different fluorescence filtered micrographs. Each scale bar indicates 20 µm.

As presented in the above fluorescence micrographs, even though the efficiency of FN conjugation was not 100%, many of vesicles were confirmed to be hosting the FN proteins. This was the first approach of ECM protein conjugation onto the cell-sized vesicle model platform.

7.2.2. Antiviral peptide interaction with fibronectin conjugated GUV

In order to explore membrane interactions of AH peptide against fibronectin protein conjugated GUV model platforms, various concentrations of AH peptide were tested. For direct comparison with DOPC GUVs and HLM incorporated GUVs, same set of concentrations of AH peptide were administered.

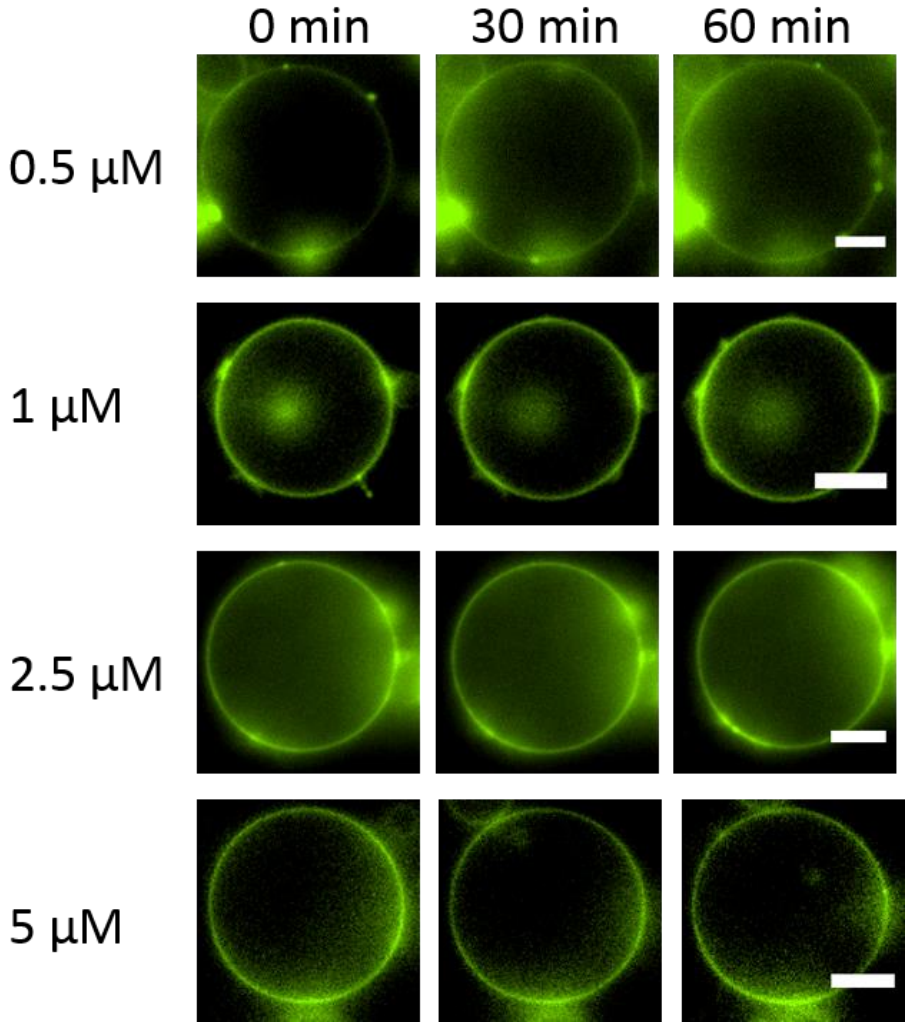

Figure 7. 3 Interaction between FN-GUV with various concentrations of AH peptide. Spinning disc confocal microscopy images of fibronectin conjugated GUVs consisting of 5 mol % of DP-NGPE, 94 mol % of DOPC doped with 1 mol % of Rho-B DPPE upon interaction with 0.5, 1, 2.5 and 5 µM AH peptide in 300 mM

glucose. Each labeled time corresponds to the peptide injection time. Scale bar is 10 μm.

Surprisingly, the tested concentrations of AH peptide did not induce any morphological changes on the fibronectin conjugated GUVs (FN-GUV). Throughout 1 hr of fluorescence microscopy measurements, the FN-GUVs stayed as intact regardless of the administered concentrations of AH peptide. These results were significantly different from the cases of DOPC GUVs and HLM-GUVs where membrane fluctuation and vesicular collapse were observed from the AH peptide interactions. The highly resistant feature of FN-GUV against the lipid membrane specific antiviral peptide could possibly due to the coating of fibronectin proteins over the membranes.

The new findings from the preliminary study of AH peptide interaction employing fibronectin conjugated GUVs suggests us the need of development of more complex model membrane platforms that can closely mimic the intricate nature of cellular membrane properties.

7.3. Future Outlook

Based on the main outcomes and conclusions presented in this thesis, the following new future directions can be suggested. As presented in Chapter 4, we showed a new capability of AH peptide as a SLB post-repair agent to form a complete defect-free SLB. This method can be further applied to more complex lipid compositions rather than using simple one-component lipid membrane platform employed in the chapter. For instance, liposomes composed of highly charged lipids usually result in incomplete rupture forming bilayer patches instead of creating a complete planar lipid bilayer on substrates[18-19]. To further validate potent vesicle rupturing capacity of AH peptide on various phases of lipids, utilizing new lipid composition of vesicle including gel-phase or liquid-ordered phase lipids (e.g., large amount of cholesterol or sphingomyelin) is suggested for broadening the application possibilities for

fabricating high-quality SLB platforms based on AH peptide treatment. Based on the results obtained with the HLM-incorporated GUV platform results as presented in Chapter 5, there is significant potential to develop more biologically relevant platforms using biological membrane components. Indeed, to mimic the more complex structural features of the cell membrane, the bottom-up approach employed in the study will allow us to add more membrane proteins along with other lipids components. With the more complex biologically relevant model platform, one can build up explicit kinetic profiles of pore formation and vesicle lysis. Also, employing single vesicle method using small unilamellar vesicle tethered platform[20] will be able to reveal more of the membrane stabilizing capacity by HLM especially against membrane-specific antiviral or antimicrobial peptide agents and comparative analysis across small and large vesicles can aid understanding of membrane curvature sensing and its potential utility for designing therapeutic agents. Also, for the single GUV model platform and its interactions against several single-chain amphiphiles as presented in Chapter 6, we can further develop the cell model platform by including more complex phospholipid compositions across different phase states to check GML's vesicle fission and fusion ability. Also, by adding physiologically significant amounts of cholesterol (up to or exceeding 40 mol %), it will be possible to study the effect of regulating membrane stress as governed by cholesterol in biological membranes, helping to build more detailed knowledge of membrane fusion and fission. The new inclusions will again help to add more biologically relevance. Lastly, the striking observation of vesicle fission or fusion induced by below and above CMC of GML presented in Chapter 6 reflects the strong importance of single-chain amphiphiles to understand compartmentalization of early protocell models. This will further contribute to the study of modeling of protocell functions in exploring the plausible role of fatty acid molecules in facilitating cellular compartmentalization and the emergence of organelles and other detailed cellular features. Also, the new results highlighting vesicle fission/fusion induced by GML may lead to prevail new insights into how the chemical evolution of self-assembled amphiphiles connect to biological evolution from primitive cells (or protocell systems) to current complex cells. While drawing such insights into

complex biological systems are outside the scope of the present study, it is known that, depending on membrane composition and environmental factors, lipid vesicles can be exposed to morphological transformations including fusion, fission, growth budding, and internal vesicle assembly (creating daughter vesicles)[21-24]. Therefore, the diverse range of membrane morphological responses induced by GML can further suggest empirical models of how primitive cellular growth and division might have occurred in response to chemical and physical environmental driving forces, and this will eventually provide cues to identify pre-biotic constituents of primitive cells.

References

1. Tensegrity, I., How structural networks influence cellular information processing networks, Donald E. Ingber. *Journal of Cell Science* **2003**.

2. Hinz, B.; Phan, S. H.; Thannickal, V. J.; Galli, A.; Bochaton-Piallat, M.-L.; Gabbiani, G., The myofibroblast: one function, multiple origins. *The American journal of pathology* **2007,** *170* (6), 1807-1816.

3. Hay, E. D., *Cell biology of extracellular matrix*. Springer Science & Business Media: 2013.

4. McDONALD, J. A.; Kelley, D. G.; Broekelmann, T. J., Role of fibronectin in collagen deposition: Fab'to the gelatin-binding domain of fibronectin inhibits both fibronectin and collagen organization in fibroblast extracellular matrix. *The Journal of cell biology* **1982,** *92* (2), 485-492.

5. Singhvi, R.; Kumar, A.; Lopez, G. P.; Stephanopoulos, G. N.; Wang, D. I.; Whitesides, G. M.; Ingber, D. E., Engineering cell shape and function. *SCIENCE-NEW YORK THEN WASHINGTON*- **1994**, 696-696.

6. Lukashev, M. E.; Werb, Z., ECM signalling: orchestrating cell behaviour and misbehaviour. *Trends in cell biology* **1998,** *8* (11), 437-441.

7. Beck, K.; Hunter, I.; Engel, J., Structure and function of laminin: anatomy of a multidomain glycoprotein. *The FASEB journal* **1990,** *4* (2), 148-160.

8. Badylak, S. F.; Freytes, D. O.; Gilbert, T. W., Extracellular matrix as a biological scaffold material: structure and function. *Acta biomaterialia* **2009,** *5* (1), 1-13.

9. Vlodavsky, I.; Folkman, J.; Sullivan, R.; Fridman, R.; Ishai-Michaeli, R.; Sasse, J.; Klagsbrun, M., Endothelial cell-derived basic fibroblast growth factor: synthesis and deposition into subendothelial extracellular matrix. *Proceedings of the National Academy of Sciences* **1987,** *84* (8), 2292-2296.

10. Clark, E. A.; Brugge, J. S., Integrins and signal transduction pathways: the road taken. *Science* **1995,** *268* (5208), 233.

11. Trappmann, B.; Gautrot, J. E.; Connelly, J. T.; Strange, D. G.; Li, Y.; Oyen, M. L.; Stuart, M. A. C.; Boehm, H.; Li, B.; Vogel, V., Extracellular-matrix tethering regulates stem-cell fate. *Nature materials* **2012,** *11* (7), 642-649.

12. Hynes, R. O., The dynamic dialogue between cells and matrices: implications of fibronectin's elasticity. *Proceedings of the National Academy of Sciences* **1999,** *96* (6), 2588-2590.

13. Klein, E. A.; Yin, L.; Kothapalli, D.; Castagnino, P.; Byfield, F. J.; Xu, T.; Levental, I.; Hawthorne, E.; Janmey, P. A.; Assoian, R. K., Cell-cycle control by physiological matrix elasticity and in vivo tissue stiffening. *Current biology* **2009,** *19* (18), 1511-1518.

14. Rho, K. S.; Jeong, L.; Lee, G.; Seo, B.-M.; Park, Y. J.; Hong, S.-D.; Roh, S.; Cho, J. J.; Park, W. H.; Min, B.-M., Electrospinning of collagen nanofibers: effects on the behavior of normal human keratinocytes and early-stage wound healing. *Biomaterials* **2006,** *27* (8), 1452-1461.

15. Schultz, G. S.; Wysocki, A., Interactions between extracellular matrix and growth factors in wound healing. *Wound repair and regeneration* **2009,** *17* (2), 153-162.

16. Huang, C.-J.; Cho, N.-J.; Hsu, C.-J.; Tseng, P.-Y.; Frank, C. W.; Chang, Y.-C., Type I collagen-functionalized supported lipid bilayer as a cell culture platform. *Biomacromolecules* **2010,** *11* (5), 1231-1240.

17. Huang, C.-J.; Tseng, P.-Y.; Chang, Y.-C., Effects of extracellular matrix protein functionalized fluid membrane on cell adhesion and matrix remodeling. *Biomaterials* **2010,** *31* (27), 7183-7195.

18. Zan, G. H.; Jackman, J. A.; Cho, N.-J., AH peptide-mediated formation of charged planar lipid bilayers. *Journal of Physical Chemistry B* **2014,** *118* (13), 3616-3621.

19. Tabaei, S. R.; Vafaei, S.; Cho, N.-J., Fabrication of Charged Membranes by the Solvent-Assisted Lipid Bilayer (SALB) Formation Method on SiO2 and Al2O3. *Physical Chemistry Chemical Physics* **2015**.

20. Tabaei, S. R.; Rabe, M.; Zhdanov, V. P.; Cho, N.-J.; Höök, F., Single vesicle analysis reveals nanoscale membrane curvature selective pore formation in lipid membranes by an antiviral α-helical peptide. *Nano Letters* **2012,** *12* (11), 5719-5725.

21. Hanczyc, M. M.; Fujikawa, S. M.; Szostak, J. W., Experimental models of primitive cellular compartments: encapsulation, growth, and division. *Science* **2003,** *302* (5645), 618-622.

22. Hanczyc, M. M.; Szostak, J. W., Replicating vesicles as models of primitive cell growth and division. *Current Opinion in Chemical Biology* **2004,** *8* (6), 660-664.

23. Maurer, S. E.; Monnard, P.-A., Primitive membrane formation, characteristics and roles in the emergent properties of a protocell. *Entropy* **2011,** *13* (2), 466-484.

24. Zhu, T. F.; Szostak, J. W., Coupled growth and division of model protocell membranes. *Journal of the American Chemical Society* **2009,** *131* (15), 5705-5713.

List of Publications

Journal Papers

1. Kolahdouzan K, Jackman JA, Yoon BK, **Kim MC**, Johal M, Cho NJ. Optimizing the Formation of Supported Lipid Bilayers from Bicellar Mixtures. Langmuir 2017. Accepted.

2. Yorulmaz S, Jackman JA, **Kim MC**, Hunziker W, Cho NJ. Immobilization Strategies for Functional Complement Convertase Assembly at Lipid Membrane Interfaces. Langmuir 2017. Accepted.

3. **Kim MC**, Jackman JA, Cho NJ. Controlling Membrane Compartmentation via Glycerol Monoglyceride Induced Fission and Fusion. Manuscript in preparation.

4. Yoon, BK, Jackman JA, **Kim MC**, Sut TN, Cho NJ. Correlating Membrane Morphological Responses with Micellar Aggregation Behavior of Capric Acid and Monocaprin. Langmuir 2017; 33, (11), pp 2750-2759.

5. **Kim MC**, Gunnarsson A., Tabaei SR, Höök, F. and Cho NJ. Supported Lipid Bilayer Repair Mediated by AH Peptide. Physical Chemistry Chemical Physics 2016, 18, 3040-3047

6. Jackman JA, **Kim MC**, Zhdanov, V, Cho NJ. Relationship between Vesicle Size and Steric Hindrance Influences Vesicle Rupture on Solid Supports. Physical Chemistry Chemical Physics 2016; 18, 3065-3072

7. Tabaei SR, Gillissen JJ, **Kim MC**, Ho JCS, Liedberg B, Parikh AN, Cho NJ. Brownian Dynamics of Electrostatically Adhering Nano-Vesicles on a Membrane Surface Induces Domains and Probes Viscosity. Langmuir 2016.

8. Hanson, JM, Gettel, DL, Tabaei SR, Jackman JA, **Kim MC**, Sasaki, DY, Groves, JT, Liedberg B, Cho NJ and Parikj AN. Cholesterol-enriched microdomain formation induced by viral-encoded, membrane active amphipathic peptide. Biophysical Journal 2016, 110, 176-187
9. **Kim MC**, Gillissen, J. J., Tabaei SR, Zhdanov V. and Cho NJ. Spatiotemporal Dynamics of Solvent-Assisted Lipid Bilayer Formation. Physical Chemistry Chemical Physics 2015; 17, 31145-31151

10. Jeong JH*, Choi JH*, **Kim MC***, Park JH, Herrin JS, Kim SH, Lee H, Cho NJ. (2015). Elucidating How Bamboo Salt Interacts with Supported Lipid Membranes: Influence of Alkalinity on Membrane Fluidity. European Biophysics Journal 2015; 44(5), 383-391.
*__Denotes shared first authorship__

11. Yoon BK, Jackman JA, **Kim MC**, Cho NJ. Spectrum of Membrane Morphological Responses to Antibacterial Fatty Acids and Related Surfactants. Langmuir 2015; *31* (37), 10223–10232

12. Tabaei SR, Jackman JA, **Kim MC**, Yorulmaz S, Vafaei S, Cho NJ. Biomembrane Fabrication by the Solvent-Assisted Lipid Bilayer (SALB) Method. Journal of Visualized Experiments 2015;

13. Jackman JA, Špačková B, Linardy E, **Kim MC**, Yoon BK, Homola J, Cho NJ. Nanoplasmonic Ruler to Measure Lipid Vesicle Deformation. Chemical Communications 2015